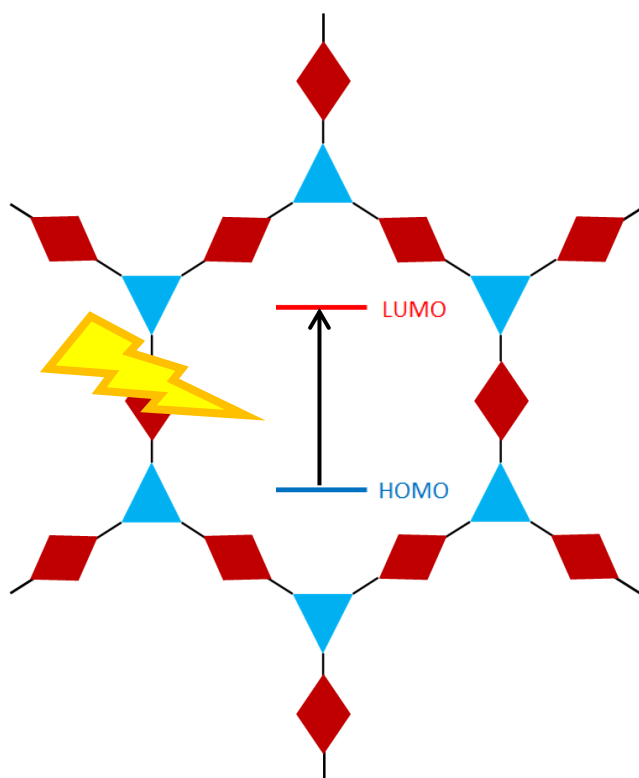# Conjugated microporous polymers for visible-light driven photocatalysis

-Diploma thesis-
in chemistry

Written by Kim Garth
Handed in at 29.01.2015

Table of content

Table of abbreviations

BET .... *Brunauer-Emmet-Teller*
BG .... *Band gap*
CMP .... *Conjugated microporous polymer*
COF .... *Covalent organic framework*
CP .... *Conjugated polymer*
dba .... *Dibenzylidenaceton*
DCM .... *Dichloromethane*
DMF .... *Dimethylformamid*
DRS .... *diffuse reflectance spectroscopy*
EPR .... *Electron paramagnetic resonance*
eq .... *equivalent*
FT .... *Fourier transform*
HCP .... *Hyper-crosslinked polymer*
HOMO .... *Highest occupied molecular orbital*
LUMO .... *Lowest unoccupied molecular orbital*
MMA .... *Methylmethacrylate*
MOF .... *metal-organic framework*
NMR .... *nuclear magnetic resonance*
PC .... *photocatalyst*
PIM .... *Polymer of intrinsic microporosity*
PMMA .... *Poly(methylmethacrylate)*
RT .... *Roomtemperature*
SA .... *Surface area*
Selectfluor ...... *1-Chloromethyl-4-fluoro-1,4-diazoniabicyclo[2.2.2]octane bis(tetrafluoroborate)*
SOMO .... *singly occupied molecular orbital*
THF .... *Tetrahydrofuran*
Xphos .... *2-Dicyclohexylphosphino-2',4',6'-triisopropylbiphenyl*

1. Introduction

Renewable, environmental-friendly and economical energy sources such as solar energy have gained a lot of attention over the past decades. It is of great interest for chemists to utilize the power of sunlight for chemical processes by mimicking nature, where chromophores or photocatalysts have been used for visible-light driven photo-redox processes for millions of years.[1-8]

Tremendous effort has been made for the development of photochemistry in the last decades. Transition metal based systems are widely studied and used in the area of visible-light driven photocatalysis due to their excellent photo-redox properties and good stability,[7,9-12] especially in fields such as water splitting, solar energy storage or photovoltaics.[7,11-13] However, the disadvantages of these materials are toxicity and high cost due to their limited availability in nature. From this point of view, metal-free, organic compounds such as organic dyes arose as photocatalysts and found a broad interest during the last decade.[14-17] Nevertheless, there are still some intrinsic drawbacks associated with these materials, for example, they are usually affected by the reaction medium due to the so-called photo-bleaching effect, which can be troublesome for catalyst recycling and long-term usage. To provide better stability, recyclability and an easy separation for the catalysts, heterogeneous catalytic systems are thus of great interest in our research.[18]

Conjugated porous polymers, combining a photoactive, conjugated polymer backbone and high porosity, have been used as heterogeneous visible-light active photocatalysts in organic synthesis in the past years.[19-25]

In this work, conjugated microporous polymers (CMPs) will be designed and synthesized as metal-free, heterogeneous photocatalysts. The developed CMPs either consist of a known organic catalyst embedded into a conjugated framework or the entire CMP network will function as a photocatalyst utilizing its photoactive conjugated backbone. Different photocatalytic reactions, which usually are catalyzed by metal-containing catalysts, such as free radical polymerization[26], C-H activation[27,28] and photo-oxidation[29] will be performed to test the feasibility of the CMPs as photocatalysts. Furthermore, the optical and electronic properties of the CMPs will be modified by incorporation of various electron donor- and electron acceptor-type monomers into the conjugated polymer backbone, in order to understand the influence of the structural and energetic characteristics of the CMPs on the photocatalytic efficiency.

2. Theoretical Part

2.1. Nanoporous polymers

According to IUPAC[30] there are different classifications of porosity defined by the pore sizes. Macroporous materials have pore widths larger than 50 nm, while microporosity contains pores smaller than 2 nm. Mesoporous pores have diameters between 2 and 50 nm.

The term "nanoporous polymer" has been used to mostly describe porous polymers with pore sizes in the nanometer range, i.e. micro- and mesoporous polymers. In the past decade, nanoporous polymers have gained much attention due to their broad application possibilities such as gas sorption[31-41], gas storage[42-65], catalysis or catalyst support[66-71]. Very recently, semiconductive porous polymers have also found use in photocatalysis.[28,72-76]

Defined by the morphology, they can be divided into two main classes, crystalline porous polymers, which includes metal-organic frameworks (MOFs)[44-47,77-79] and covalent organic frameworks (COFs)[52,70,71,80,81], and amorphous materials, to which hyper-crosslinked polymers (HCPs)[36,50,61,69,82-84], polymers of intrinsic microporosity (PIMs)[85-90] and conjugated microporous polymers (CMPs)[19,22,25,91-93] belong to.

Figure 2.1 shows an overview over the different types of nanoporous polymers that were in the focus of research.

Nanoporous polymers

Crystalline

Amorphous

Metal-organic
frameworks
(MOFs)

Covalent-organic
frameworks
(COFs)

Polymers of
intrinsic
microporosity
(PIMs)

Hyper-crosslinked
polymers
(HCPs)

Conjugated
microporous
polymers
(CMPs)
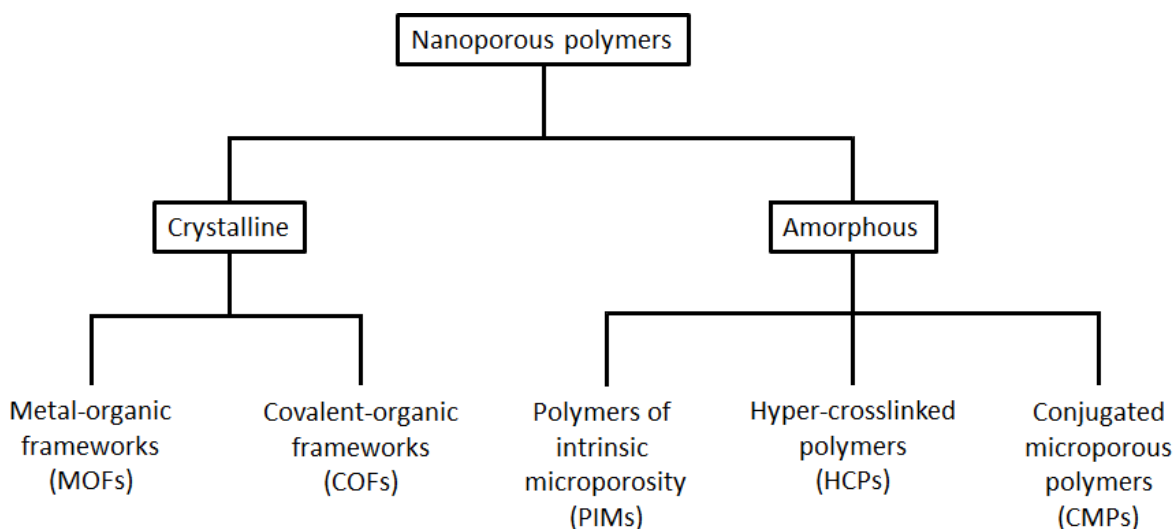
Figure 2.1 Overview over the different types of nanoporous materials.

MOFs consist of metal atoms or metal-containing clusters that possess coordinative bonds with multidentate ligands to achieve an well-ordered crystalline network.[44] Not only the porous nature but also the metal coordination gives these materials good properties for selective gas separation or storage[38,40,44-46,53,57,60,77] and heterogeneous catalysis[74,77,94,95].

COFs are formed by strong covalent bonds of lighter elements such as B, C, N, and O. COFs have therefore lower densities and are more stable to humidity and oxygen than their metal-containing equivalents.[96] Another advantage is the wide synthetic range of organic materials. COFs also possess high surface areas and porosity which can be used for gas storage.[49,52,54] With heteroatoms in the rigid framework also metal atoms for catalysis can be coordinated.[71,73,97-101]

In the class of amorphous nanoporous materials, HCPs were found as the first microporous, organic polymers.[82-84] They consist of precross-linked polymers which are then treated by further cross-linking reactions to hyper-cross-link. These materials are mostly used for gas storage purpuses[36,50,61], but also as metallic catalyst support by incorporation.[69] HPCs are not conjugated and do not allow a good mass transport due to the very high crosslinking degree.[69]

PIMs are usually soluble linear polymers, which observe microporosity in solid, i.e. dried state. [33,85-90,102,103] Their porosity results from a contortion of the backbone monomer due to a tetrahedral carbon, which leads to inefficient packing of the polymer chains and therefore free volume. Their linear nature makes them soluble and processable, which is a major problem for other porous materials. They are however commonly not conjugated, although recently conjugated PIMs were explored by the Cooper group.[87]

Conjugated microporous polymers (CMPs) combine conjugation throughout the polymer backbone with the advantage of microporosity. They are typically synthesized via metal-based coupling reactions like Suzuki[68,74,75,91,104-108], Yamamoto[105,109-116], and Sonogashira cross-[92,114,117-123] or homo-coupling[117,124,125], and recently also by a metal-free synthetic method[126]. Due to the rigidity caused by the aromatic building blocks inside the network permanent meso- and micropores are formed. First discovered by Cooper *et al.* in 2007[120] these materials give a versatile tool for different applications like gas storage[55,91,127,128], chemical entrapping[92,115,116,118,125], light-harvesting[75,127], chemo-sensing[112,113,126], and heterogeneous catalysis[28,29,66,67,72-74,76,106,129-135]. In the last few years, photocatalysis using CMPs, which is intensely developed in our research group,[26,132,133] has gained a lot of attention. The most recent development in this field will be discussed in detail in chapter 2.2.2 in this work.

2.2. Conjugated microporous polymers

CMPs combine the features of microporosity with semiconductivity due to the charge transfer ability of the conjugated system under light irradiation. Like conjugated polymers (CPs), they mostly consist of aromatic monomers, which have high rigidity and cause poor solubility. The solubility of CPs can be improved by adding bulky side groups, which lead to inefficient packing. This offers a good processability and makes them interesting materials for a variety of electronic and optical applications, such as organic, light-emitting devices, photovoltaic cells, or polymer field-effect transistors.[136-140] In comparison, CMPs are organic cross-linked networks, which are typically insoluble in all kinds of common solvents. The strategy of bulky side groups for enhanced solubility was also recently used for synthesizing soluble CMPs.[91,141]

CMPs are amorphous polymer networks, and show no long-range order.[120] They are usually built of different building blocks, i.e. cross-linkers and comonomers, where cross-linkers contain three or more functional groups for cross-linking, while the comonomers contain at least two functional groups.[142] These building blocks are usually π-electron-containing aromatic compounds. CMPs mostly have a low density and are very stable due to strong covalent bonds such as C-C, C-N or C-O.[127]

The first CMPs reported were poly(aryleneethynylene) networks, consisting only of carbon and hydrogen bonds.[120] The pore size and surface area (SA) were controlled by varying the strut length systematically.[119] Later a diversity of monomers and also other methods occurred for

defining the pore sizes[51,93,110,120,128,135,143,144] and also the surface area[93,104,111,120,121,128,135,143,144] for example by varying the reaction solvent[111,144] or using templating methods[135]. The highest SA found for a CMP is in the best of knowledge 5640 m^2g^{-1}.[145]

To use a CMP as a metal-free heterogeneous catalyst there are multiple strategies available: the incorporation of organic homogeneous catalysts as monomers into the polymer[28,66,67,72,76] and the use of the network itself by defined energetic levels[29,131,132,135].

The incorporation of organic dyes or other homogeneous catalysts into CMP networks makes them insoluble. In this case, the photocatalyst is stabilized and can be used in a heterogeneous fashion. This strategy was used in this work for the fluorination of ethylbenzene.

For the use of the entire CMP network as a photocatalyst, it should offer a specific energetic level, i.e. the (highest occupied molecular orbital) HOMO and (lowest unoccupied molecular orbital) LUMO levels and the resulting band gaps, which is suitable for activating specific chemical reaction. To reach the specific activation energy, the CMP network should be built of defined electron donor and acceptor combinations. This concept is comparable to the linear conjugated, donor–acceptor type copolymers.[146] In this case donor means an electron-rich molecule, while an acceptor is an electron-deficient one. The donor moiety is influencing the HOMO level of the polymer and the acceptor moiety dictates the LUMO level.[146] In Figure 2.2, this designing concept for CMPs is displayed. In contrast, homopolymers usually have a fixed band gap.
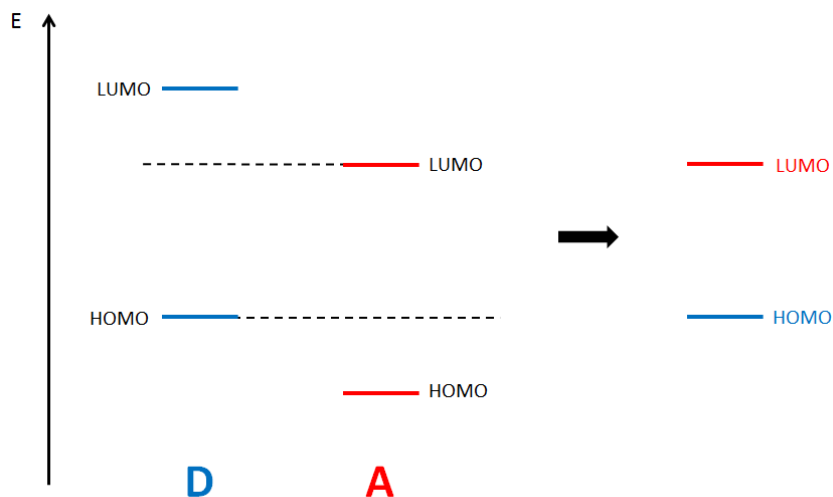
Figure 2.2 HOMO and LUMO levels in a donor – acceptor based system.

2.2.1. Mechanism of the CMP formation

In this work only Sonogashira coupling was used for the CMP synthesis,[19,22,25] in order to form a stable and large surface area. It is very important to take control over the exact reaction conditions, given the fact that they influence the surface area and therefore the porosity of the CMP. The Sonogashira-Hagihara coupling was developed in 1975.[147] In particular, terminal alkynes are coupled with halogen arylenes under the catalysis of a Pd(0)-catalyst and a CuI co-catalyst in the presence of a base, often amines. The first CMPs were synthesized by Songashira cross-coupling. As an example, the reaction equation is displayed in Figure 2.3.[120]
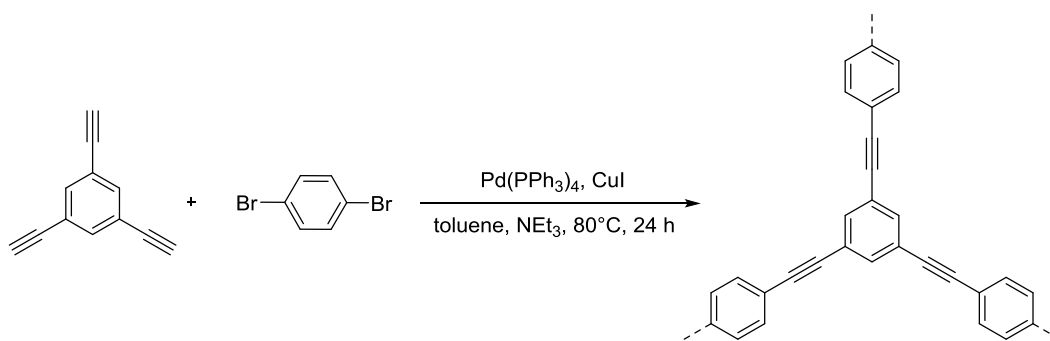
Figure 2.3 Synthesis of CMP-1 via Sonogashira coupling.[120]

The reaction mechanism is shown in Figure 2.4 and was suggested like this from Sonogashira *et al.*[123,147]
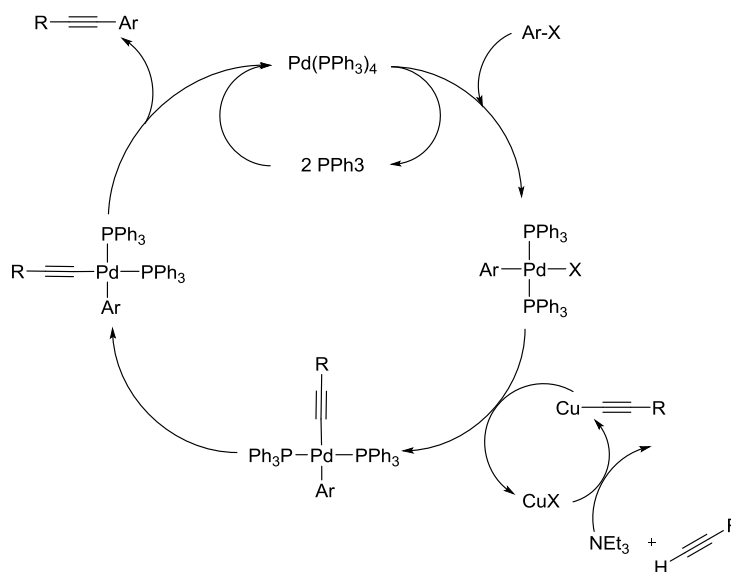
Figure 2.4 Reaction mechanism for the Sonogashira-Hagihara cross-coupling.[123,147]

A variety of different monomers as building blocks for CMPs can be used with this reaction mechamism.[66,108,127,128,143] The reaction however needs to be carried out under inert gas atmosphere to prevent it from termination via oxygen and side reactions like homo-coupling.[120,148] By only using alkynes as building block, CMPs can be synthesized via homo-coupling.[124,125] Also Laybourn *et al.* suggested a network formation mechanism where homo-coupling occurred after longer reaction times (Figure 2.5).[117]
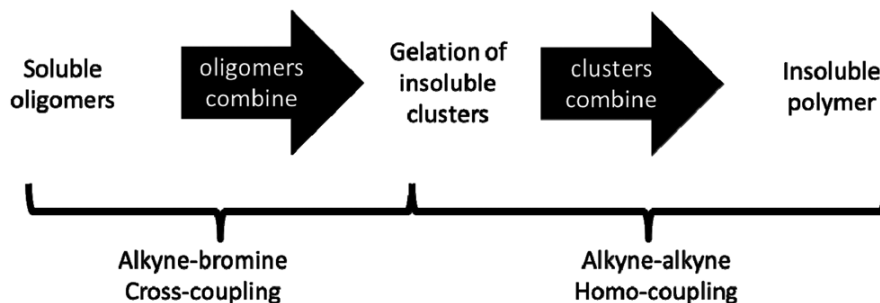
Figure 2.5 Network formation mechanism for CMPs via the Sonogashira coupling.[117]

As stated before, different strut lengths give different pore sizes,[119] and hence a different surface area, but also the choice of monomers[92,121] and solvent[118,144,148] is important. As solvent, DMF was found to give the best results regarding the SA.[144] Also the solvents are influencing the morphology of the CMP.[118] The phase behavior (like the solubility of oligomers at lower coupling degrees) is an important factor for good conversions and high surface areas.[121] As Jiang *et al.* stated, another influence on the SA is the ratio of comonomer to cross-linker.[117,120] They

claim that the SA is increased, if the empirical ratio 1:1 of an A_3+B_2-system (Figure 2.6) is used instead of the stoichiometric ratio of 1:1.5 although the reasons for this behavior are not fully explored yet.[117,120]
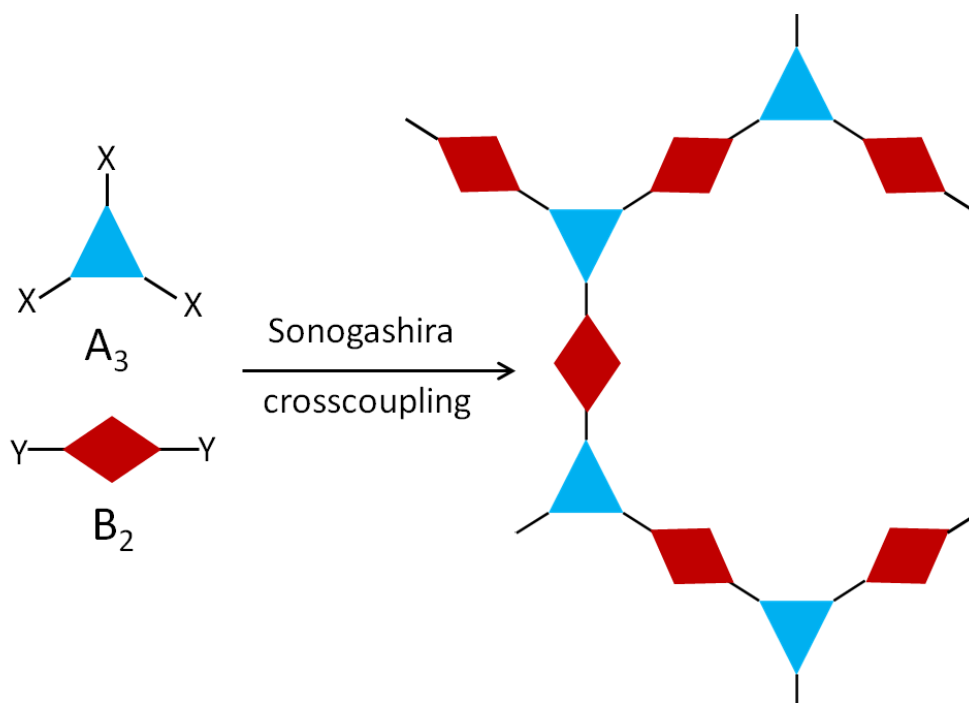
Figure 2.6 Scheme of an A_3+B_2 shaped acceptor-donor based CMP.

All these facts show that it is important to understand the Sonogashira coupling in order to gain control over the structural properties of the CMPs. In this work, the influence of the synthetic control of an A_3+B_2-system CMP will be studied regarding the photocatalytic efficiency.

2.2.2. CMPs as visible-light photocatalysts

As before-mentioned, photocatalysis is mainly predominated by transition-metal based catalysts, although there are other photocatalysts such as organocatalysts[6], i.e. organic dyes[14,17,149], salts[150] or even linear polymers[151]. Generally, in the process of photocatalysis (Figure 2.7), there is a photocatalyst (PC) which can transfer into an excited state PC* via the absorption of a photon with the energy hv. The energy of PC* can be transferred onto a reagent R_1, forming an active species R_A and the photocatalyst in the deactivated state PC_D.[6] R_A then reacts further with a second reagent R_2, resulting into the intermediate R_B.[6] The intermediate R_B reacts with PC_D, yielding in the product P and the photocatalyst PC is recovered in the ground state.[6]
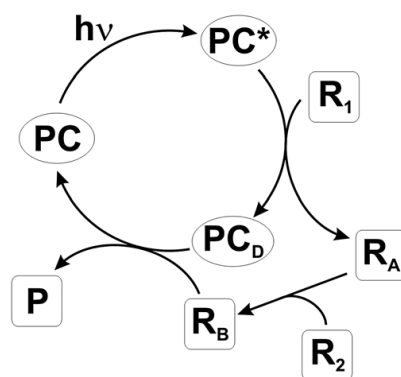
Figure 2.7 General process of photocatalysis.[6]

To transfer an electron to the excited state, it must overcome the bandgap energy of the PC. Thus the energy of the light must be high enough to do so. If that is the case, an electron-hole pair, a so-called exciton, is produced (Figure 2.8) which can then oxidize or reduce a reagent, respectively. By a oxidative reaction, the oxidation potential E_{ox} of the reagent should be energetically higher but in the same range as the HOMO level of the PC, so that an electron of the to be oxidized reactant can be transferred to the hole in the valence band of the PC. If the reaction is a reductive process, the LUMO level of the PC must be higher than the reduction potential E_{red} of the reagent, so that an excited electron can be transmitted to the reagent.
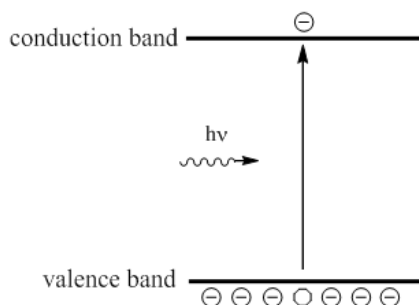
Figure 2.8 Light induced excitation.

If the organocatalyst is incorporated into the polymer network, it gets insoluble, which makes it recyclable and easy to remove, with its catalytic activity remaining.[28,67]

If an entire CMP network is used as a photocatalyst[29,131,132,135] the extended π-network is favorable. Due to high conjugation and its absorption band in the visible range, the photocatalysis can be initiated via visible light. Another advantage via synthetic methods is the aforementioned incorporation of defined donor- and acceptor-type building blocks in order to fine-tune the HOMO/LUMO levels and therefore the energy levels of the polymers for desired reaction.[146,152]

2.3. Methods

Several methods were used to characterize the CMPs in this work. Due to their insolubility, all methods need to be adaptive for the solid state.

2.3.1. Analysis of the porosity

For analyzing the pore sizes and the surface area of porous materials, gas sorption will be examined. Nitrogen will be adsorbed and desorbed on the polymer networks at 77 K, and the amount of nitrogen adsorbed is measured. The so-called adsorption isotherms can be differentiated into six different shapes to define the porosity type (Figure 2.9).[30]

Type I indicates microporosity as it approximates a limit value at the relative pressure whereas Type II exposes macro- or even non-porous materials.[30] For Type III and Type V, the isotherms are uncommon. The adsorbate-adsorbent interactions are weak while adsorbate-adsorbate interactions become more important. Type IV isotherm can be assigned to mesoporous materials. Type VI characterizes a stepwise adsorption onto a uniform non-porous surface.

Hysteresis usually appears due to capillary condensation in mesopores.[30] There are four different types of hysteresis (Figure 2.10). H1 hysteresis indicates that the pore size distribution is narrow and the material consists of uniform spheres or agglomerates, while H2 hysteresis shows not well-defined shapes and pore size distributions. H3 hysteresis appears, if the material has slit-shaped pores due to plate-like particles. For hysteresis H4 the pores are also slit-shaped, but the material has a microporous character.
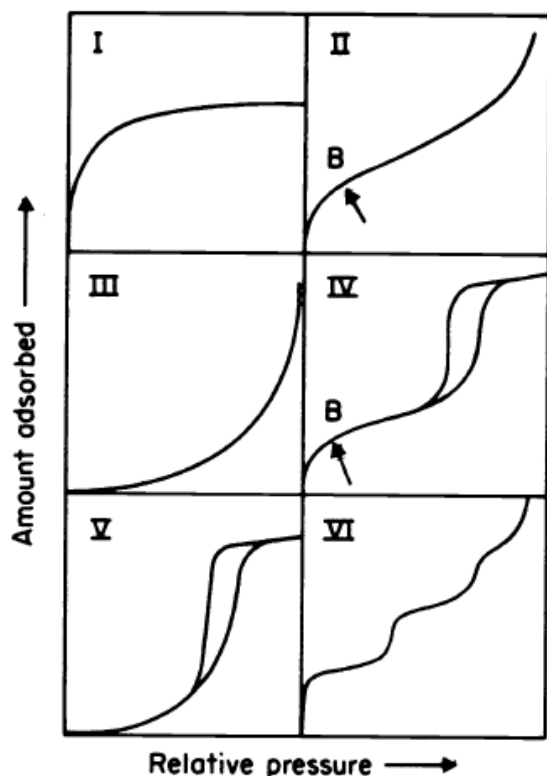
Figure 2.9 Types of adsorption isotherms.[30] Type I: microporosity; type II: macroporous; type III: adsorbate-adsorbate interactions; type IV: mesoporous; type V: adsorbate-adsorbate interactions; type VI: non-porous.
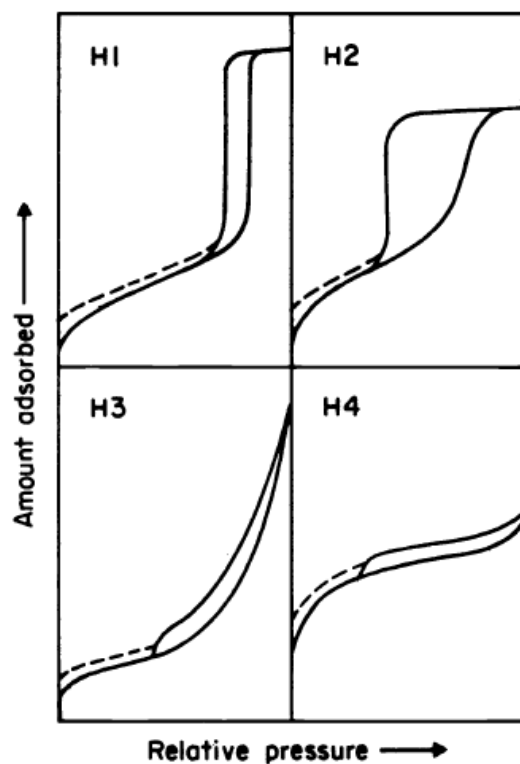
Figure 2.10 Types of Hysteresis.[30] Type H1: uniform spheres, mesoporous; H2: no defined shape; H3: slit-shaped pores, plate-like particles; slit-shaped pores, microporous.

For determining the SA of a material the Brunauer-Emmet-Teller (BET) or the Langmuir method is used.[153] Since the BET method is based on multilayer adsorption, it has found a higher prevalence than the monolayer theory of Langmuir. Both theories suffer of oversimplification, but they give comparable results which are quite repeatable. The BET theory applies a linear equation and therefore usually the points between 0.05 and 0.30 of P/P_0 are taken into account, where P/P_0 is the relative pressure.[30] In this work only points up to 0.25 were considered.

With different simulation methods pore size distributions can be calculated. They describe the incremental pore volume over the pore diameter. The density functional theory (DFT) is an often used instrument for that cause.[154]

2.3.2. Determination of HOMO/LUMO levels and the band gaps

The band gap (BG) and the HOMO and LUMO levels are important properties for photocatalytic applications of CMPs.

The BG can be determined using UV/Vis spectroscopy or cyclic voltammetry. The values that are obtained by the particular methods often differ from each other, so the one found with UV/Vis spectroscopy is further called "optical" BG, while the one determined via cyclic voltammetry is named "electrochemical" BG. To assign the optical BG an absorbance spectrum must be recorded. The band gap energy E_{BG} is equal to the equation

$$E_{BG} = \frac{hc}{\lambda}, \tag{1}$$

where h = 6.626 J·s is Planks constant, c = 3.0 · 10^8 m/s is the speed of light and λ is the wavelength of the absorption edge. At that wavelength the electrons will start to overcome the bandgap using the energy of the photons. It can be obtained from an absorbance spectrum as shown in Figure 2.11.
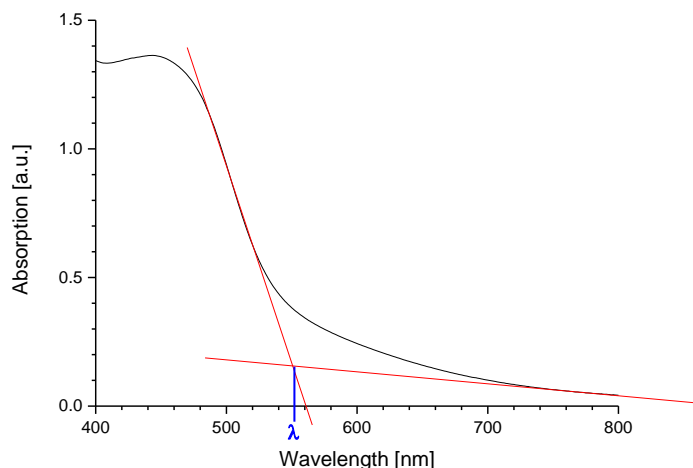
Figure 2.11 Absorbance spectrum of CMP-B-FN$_3$ for determining the absorption edge λ.

The electrochemical BG and the HOMO/LUMO levels of a CMP can be gained from a cyclic voltammogram. The HOMO and the LUMO level can be calculated from the oxidation, respectively reduction potential onset (E'$_{ox}$ or E'$_{red}$) (Equations (2) and (3)).

$$HOMO\ level = -(E'_{ox} + 4.4)\ eV \tag{2}$$

$$LUMO\ level = -(E'_{red} + 4.4)\ eV \tag{3}$$

The value - 4.4 eV in this case represents the energy difference of the vacuum level to the reference of a saturated calomel electrode (SCE).[155] The electrochemical BG can be obtained as the difference between the HOMO and the LUMO level.

2.3.3. Reaction conversion via NMR spectroscopy

The conversion of reactions can be determined by taking a NMR (nuclear magnetic resonance) spectrum of the reaction mixture. The formula which was used for calculations from ^{1}H-NMR spectra without using an internal standard is:

$$X\,\% = \left[\frac{\frac{1}{N_p}\cdot\frac{A_p}{A_{St}}}{\left(\frac{1}{N_p}\cdot\frac{A_p}{A_{St}}\right)+\left(\frac{1}{N_e}\cdot\frac{A_e}{A_{St}}\right)}\right]\cdot 100\,\% \tag{4}$$

X: Conversion
N_p: Amount of protons of the product peak
N_e: Amount of protons of the peak of the starting compound
A_p: Integral of the product peak
A_e: Integral of the peak of the starting compound
A_{St}: Integral of an outstanding peak as standard for one proton

By comparison of a separated signal of the product and the starting compound with an internal standard, the conversion and yield of the reaction can be determined. To note, the internal standard must not take part in the reaction. The internal standard is usually added in a molar 1:1 ratio to the starting compound and hence the conversion could be easily determined by setting the standard signal as 100%.

3. Aim of the project

The aim of the project is to study how the porosity and the electronic structure of acceptor-donor-type CMPs with an A_3+B_2 geometry (Figure 2.6) influence the photocatalytic behavior. A new synthetic method will be developed to enhance the porosity and surface area tremendously. Also the electronic structure of the acceptor unit will be varied to fine-tune HOMO/LUMO levels and band gap in order to give an in-depth understanding of the influence of the building blocks on the energetic structure and hence on the photocatalytic activity.

For the synthesis of CMPs via Sonogashira cross-coupling reaction, three different methods will be employed in order to take control over the surface area and porosity and the influence of the surface area on the photocatalytic activity will be investigated.

Two different strategies for the CMP synthesis will be examined: a) the embedding of a known homogeneous photocatalyst into the CMP backbone; and b) using the conjugated nature of a donor-acceptor based CMP network to generate electron-hole pairs for photocatalytic processes. As examples of the photocatalytic reactions, CMPs obtained by strategy a) will be utilized for reactions based on a C-H bond activation cycle. CMPs obtained by strategy b) will be applied for photo-redox reactions such as the aerobic oxidation of various amines.

4. Results and Discussion

In this chapter, synthesis and characterization of a series of new conjugated microporous polymers (CMPs) are described. Different synthetic methods are developed in order to control the porosity of the CMPs. Furthermore, the photocatalytic activity of the CMPs is tested. A special emphasis is paid to the influence of the energetic levels and the HOMO/LUMO band gaps of the CMPs on the photocatalytic efficiency.

4.1. Porosity control of the CMPs via synthetic methods

Several CMPs of the structures below were produced via Sonogashira coupling (Figure 4.1).

In heterogeneous catalysis, materials with highly porous structures can offer a high surface area and therefore a large reactive interface. This is of great importance for a catalytic reaction with high efficiency. In this work, it is in our desire to develop a synthetic method in order to gain CMPs with large surface areas. As examples for the synthetic development for CMPs, the following series of CMPs were chosen. Triethynylbenzene was used as cross-linker for the series. As comonomers, biphenyl (BP) and fluorenone (FN) were incorporated into the polymers CMP-B-BP$_3$ and CMP-B-FN$_3$. To study the structural effect of the comonomers on the porosity of the CMP, BP and FN were used in a ratio of 50:50 as comonomers to obtain a mixed copolymer CMP-B-BP$_{1,5}$-FN$_{1,5}$. The structures are displayed in Figure 4.1.

CMP-B-BP$_3$ CMP-B-FN$_3$ CMP-B-BP$_{1.5}$-FN$_{1.5}$
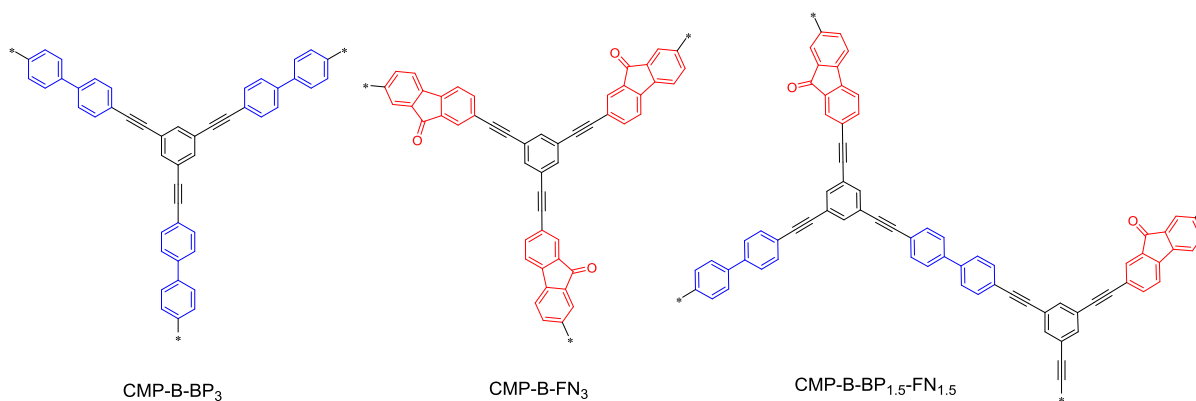
Figure 4.1 Structures of CMP-B-BP$_3$, CMP-B-FN$_3$ and CMP-B-BP$_{1,5}$-FN$_{1,5}$.

For this series, all the building blocks were used with stoichiometric cross-linker/monomer ratio according to their functional groups. The three CMPs were obtained as solid powders, which were insoluble in common organic solvents such as DCM, methanol, acetone, THF, or

chloroform. N_2 gas sorption experiments showed different surface areas and porosities for the CMPs. In Table 4.1, the synthetic and morphological properties of the CMPs are listed.

Table 4.1 Synthetic and morphological properties of the synthesized CMPs.

CMPs	Yield [%]	Surface area S_{BET} [m²/g]	Pore size [nm]	Pore volume [cm³/g]
CMP-B-BP$_3$ (St)	106	568	1.5	0.704
CMP-B-FN$_3$ (St)	72	60	13.9	0.122
CMP-B-BP$_{1.5}$-FN$_{1.5}$ (St)	88	8	2.6	0.025

St: stoichiometric cross-linker:monomer ratio.

CMP-B-BP$_3$ exhibited a high BET surface are of 568 m^2g^{-1} with a total pore volume of 0.704 m^3g^{-1}, while CMP-B-FN$_3$ possessed a much lower surface are of 60 m^2g^{-1} with a smaller pore volume of 0.122 m^3g^{-1}. The mixed polymer CMP-B-BP$_{1,5}$-FN$_{1,5}$ only exhibited a surface area of 8 m²/g with a pore volume of 0.025 m^3g^{-1}. The results indicate that the incorporation of FN as comonomer into the polymer backbone lead to a huge decrease of porosity of the polymer. One of the reasons could be the lower solubility of dibromo fluorenone, which leads to a lower polymerization degree. Another reason could be that the π–π stacking between the fluorenone units was tremendous, so that the polymer was rather obtained in a more flat morphology than a 3-dimensional cross-linked structure.

The corresponding sorption isotherms and pore size distributions of CMP-B-BP$_3$ and CMP-B-FN$_3$ are shown in the figures below (Figure 4.2 to Figure 4.5).
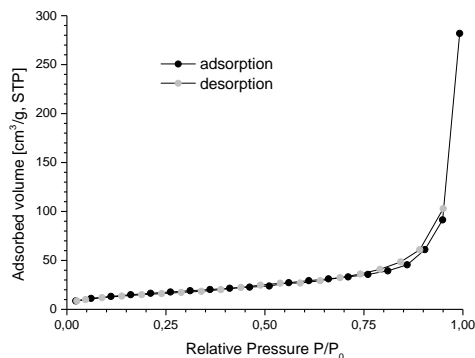
Figure 4.2 Adsorption isotherm of CMP-B-FN$_3$.
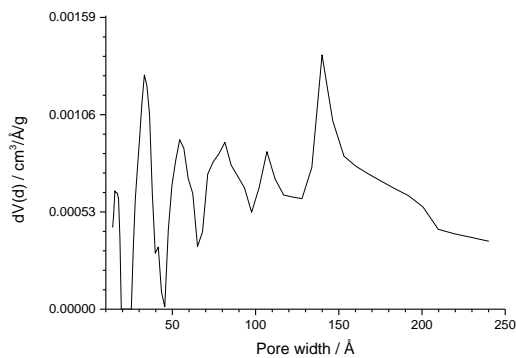
Figure 4.3 Pore size distribution of CMP-B-FN$_3$.
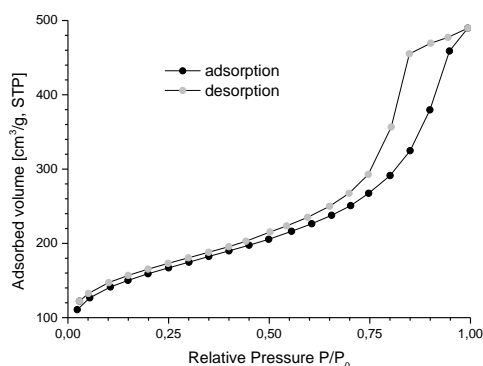
Figure 4.4 Adsorption isotherm of CMP-B-BP$_3$.
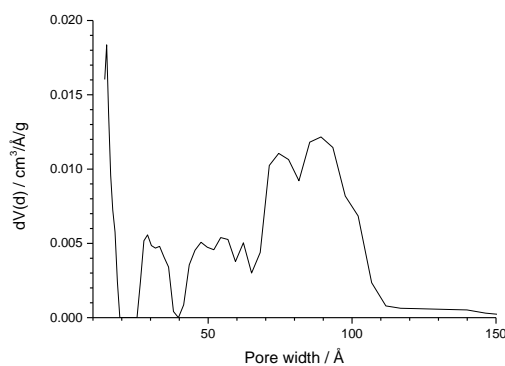
Figure 4.5 Pore size distribution of CMP-B-BP$_3$.

CMP-B-FN$_3$ shows a very flat type II or even a type III behavior which indicates non- or macroporosity. It possesses only a small volume of micro- and mesopores regarding to its pore size distribution. These results fit with the low surface area.

CMP-B-BP$_3$ has a type IV isotherm suggesting mesoporosity due to the hysteresis loop H1. The pore size distribution supports that most of the pore volume is resulting from mesopores and only a few micropores are observed.

SEM images support the results of the sorption measurements (Figure 4.6 and Figure 4.7). While the surface of CMP-B-BP$_3$ looks rough and porous the surface of CMP-B-FN$_3$ is more bulky. Both look like merged spheres, but for CMP-B-FN$_3$ those spheres are bigger, which results in the lower surface area.
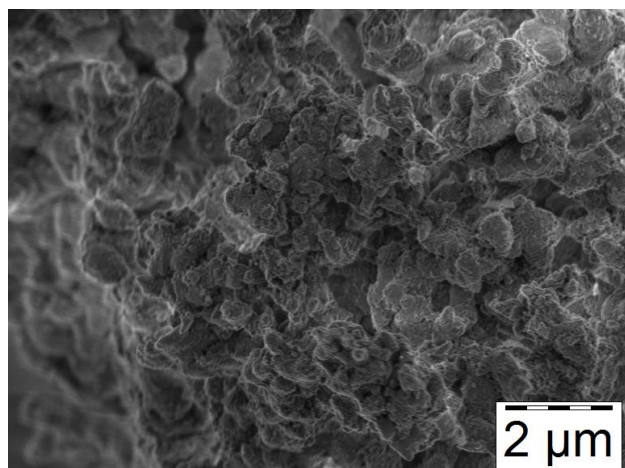
Figure 4.6 SEM image of CMP-B-FN$_3$.
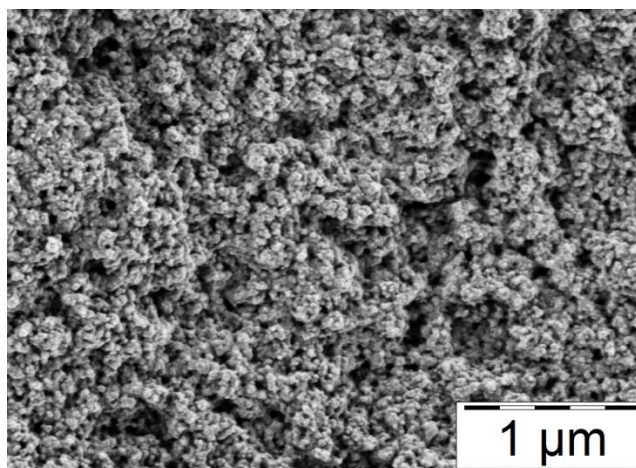
Figure 4.7 SEM image of CMP-B-BP$_3$.

As can be seen in Figure 4.8 the different morphologies and porosity of the CMPs do not influence the thermal stability.
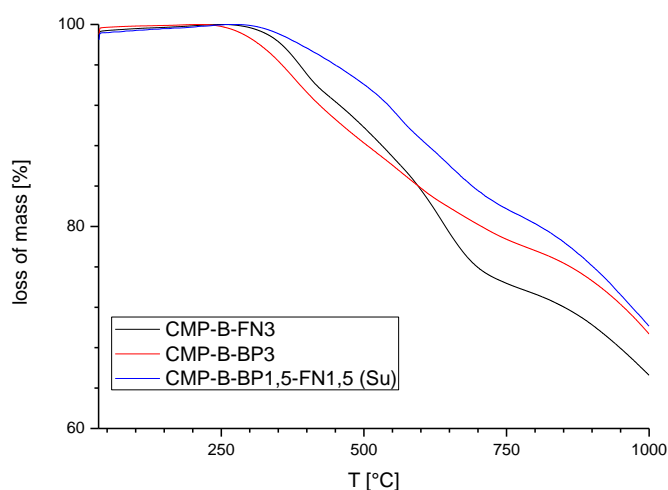
Figure 4.8 TGA curves of CMP-B-FN$_3$ (black), CMP-B-BP$_3$ (red) and CMP-B-BP$_{1.5}$-FN$_{1.5}$ (blue).

The three CMPs have a similar stability despite their different chemical composition and porosity. They are stable until 250-300 °C. The combined CMP-B-BP$_{1.5}$-FN$_{1.5}$ starts decomposing the latest.

The chemical composition was checked via FT-IR and ss-^{13}C-NMR spectroscopy. The IR spectra display the typical signals for terminal and internal alkynes at around 3300 cm^{-1}, respectively 2200 cm^{-1}. Also the strong –C=O signal can be found for CMP-B-FN$_3$ and CMP-B-BP$_{1.5}$-FN$_{1.5}$ at 1700 cm^{-1}.
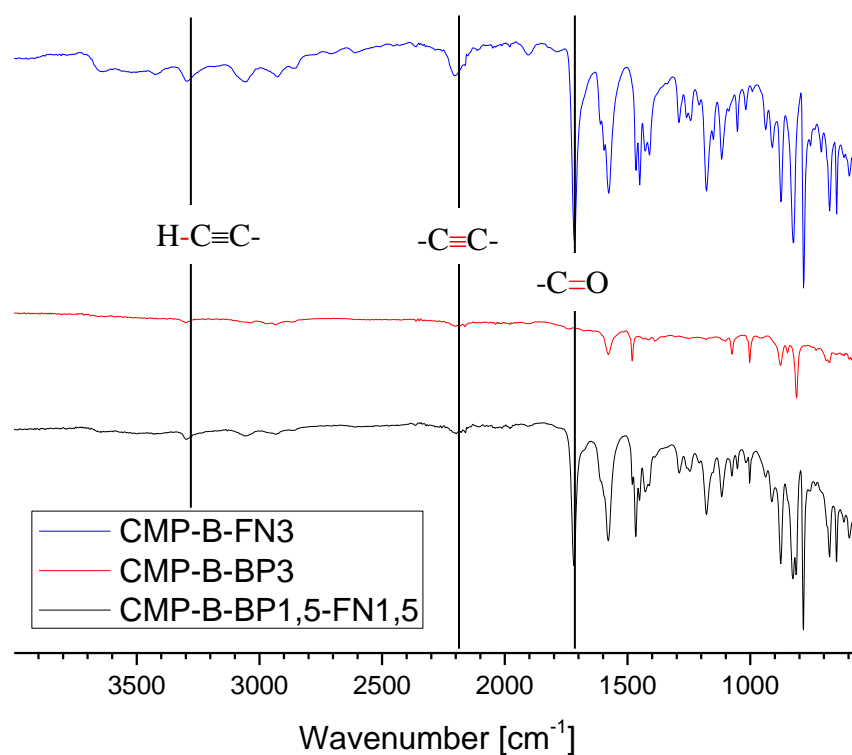
Figure 4.9 Stacked IR spectra of CMP-B-BP$_{1.5}$-FN$_{1.5}$ (black), CMP-B-FN$_3$ (blue) and CMP-B-BP$_3$ (red).

Looking closer at the fingerprint area of the IR spectra of the different compositions (Figure 4.10) it can clearly be seen that CMP-B-BP$_{1.5}$-FN$_{1.5}$ contains both biphenyl and fluorenone units. The spectrum of CMP-B-BP$_{1.5}$-FN$_{1.5}$ displays signals of both other spectra.
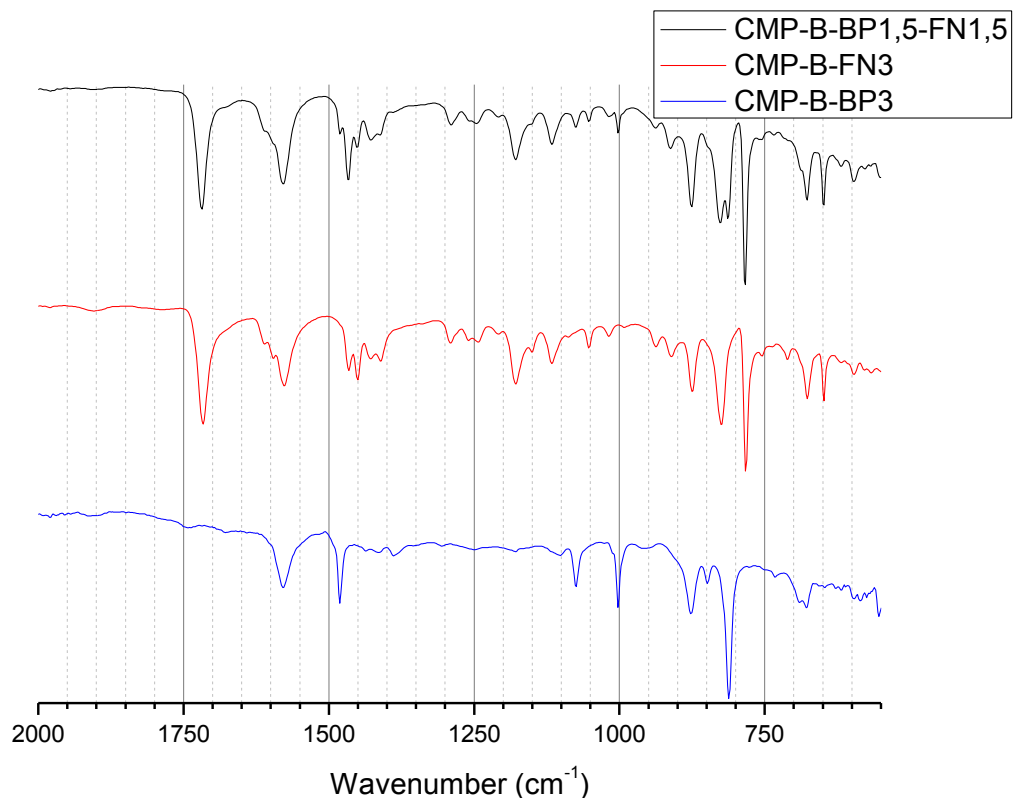
Figure 4.10 Fingerprint area of the IR spectra of CMP-B-BP$_{1.5}$-FN$_{1.5}$ (black), CMP-B-FN$_3$ (red) and CMP-B-BP$_3$ (blue).

In the ss-^{13}C-NMR spectra these results are reflected (Figure 4.11). CMP-B-BP$_{1.5}$-FN$_{1.5}$ possesses mostly the signals like CMP-B-FN$_3$ but in the aromatic region the signal around 132 ppm seems to originate from the biphenyl unit in the backbone. So the copolymerized structure of CMP-B-BP$_{1.5}$-FN$_{1.5}$ is confirmed by these results.
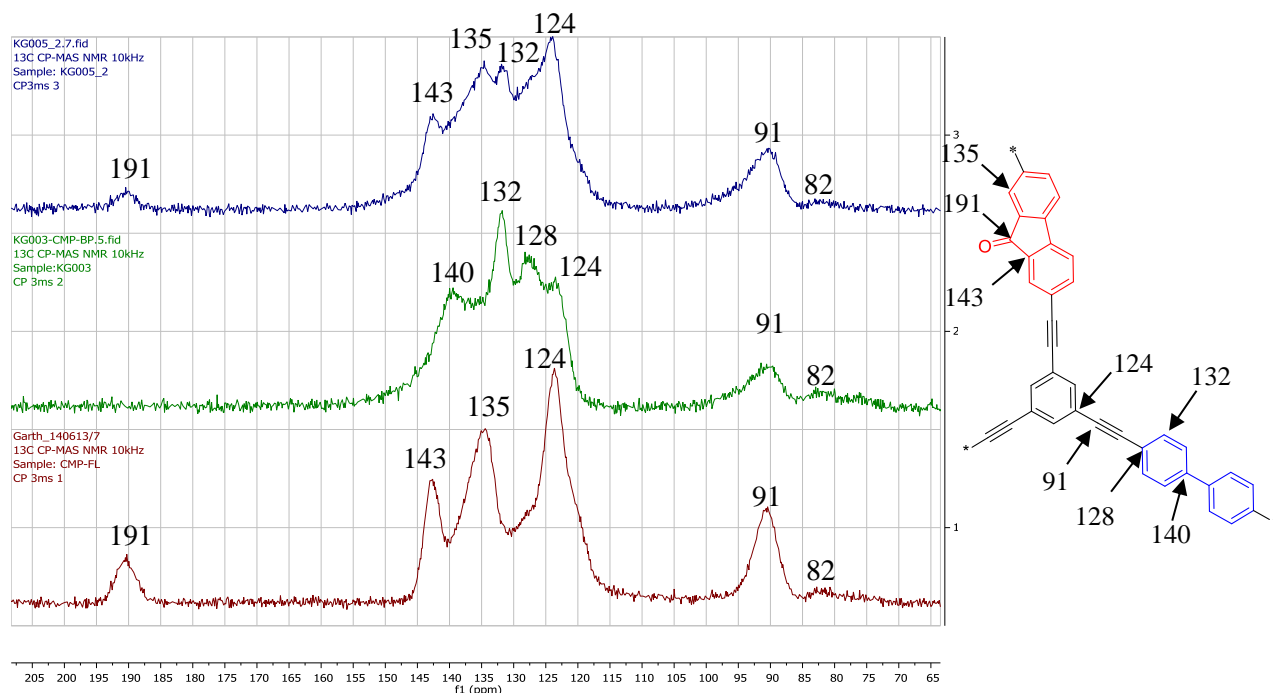
Figure 4.11 Solid state ^{13}C-NMR of CMP-B-FN$_3$ (red), CMP-B-BP$_3$ (green) and CMP-B-BP$_{1.5}$-FN$_{1.5}$ (blue).

UV/Vis diffuse reflectance spectroscopy (DRS) was used to measure spectra of the insoluble, solid samples. The spectra were compared (Figure 4.12) and optical band gaps were calculated (Table 4.2).

Table 4.2 Calculated optical band gaps for the different CMPs.

CMP	Optical BG / eV
CMP-B-FN$_3$	2.26
CMP-B-BP$_3$	1.59
CMP-B-BP$_{1.5}$-FN$_{1.5}$	2.24
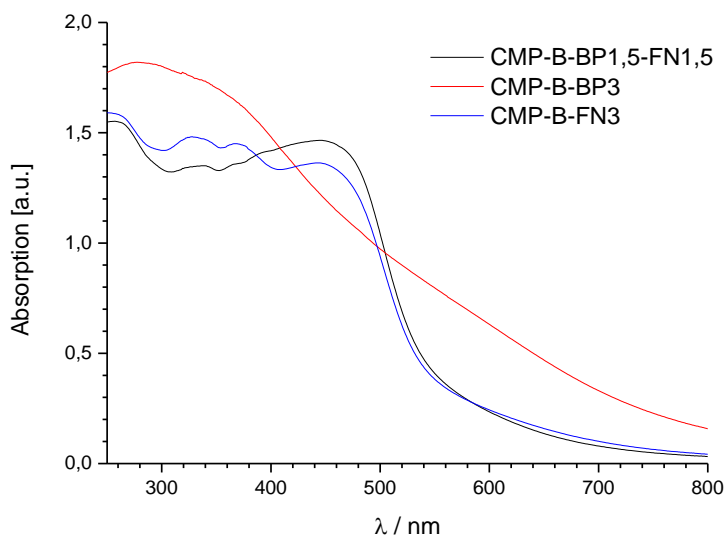
Figure 4.12 UV/Vis DRS spectra of CMP-B-FN$_3$ (blue), CMP-B-BP$_3$ (red) and CMP-B-BP$_{1.5}$-FN$_{1.5}$ (black).

The mixed polymer CMP-B-BP$_{1.5}$-FN$_{1.5}$ showed similar UV/Vis absorption bands as CMP-B-FN$_3$, indicating similar energetic levels for both polymers. CMP-B-BP$_3$ has the lowest optical BG with 1.59 eV, which is not expected since it does not possess any acceptor units.

In order to weaken the aforementioned comonomer effect and therefore to gain highly porous polymer backbone structures, a number of synthetic methods were developed.

Three different synthetic mechanisms were used during the coupling reaction. As displayed in Scheme 4.1, different ratios of cross-linker and dibromo monomer were taken.

1. Stoichiometric cross-linker:monomer ratio (1:1.5 ratio) (St)
2. Empiric cross-linker:monomer ratio (1:1 ratio) (E)
3. Successive monomer addition (1:1.5 ratio) (Su)

The stoichiometric method was used to synthesize the first series of CMPs at the beginning of this chapter. It would be expected to yield the best result since the Sonogashira coupling is a step-growth polymerization. But according to the works of Cooper *et al.*[120], a ratio of 1:1 between the cross-linker and dibromo monomer should lead to larger surface areas of the CMP than the stoichiometric ratio of 1:1.5. This so-called empiric method was tested as well.

Additionally, another method, the so-called successive addition of the dibromo monomers was developed in our group and applied here. In this case, only 1/3 of the dibromo monomer was

mixed with the cross-linker at the beginning of the coupling reaction, and the other parts were added after a time interval of 24 h each.

In Table 4.3 the synthetic and morphological properties are summarized.
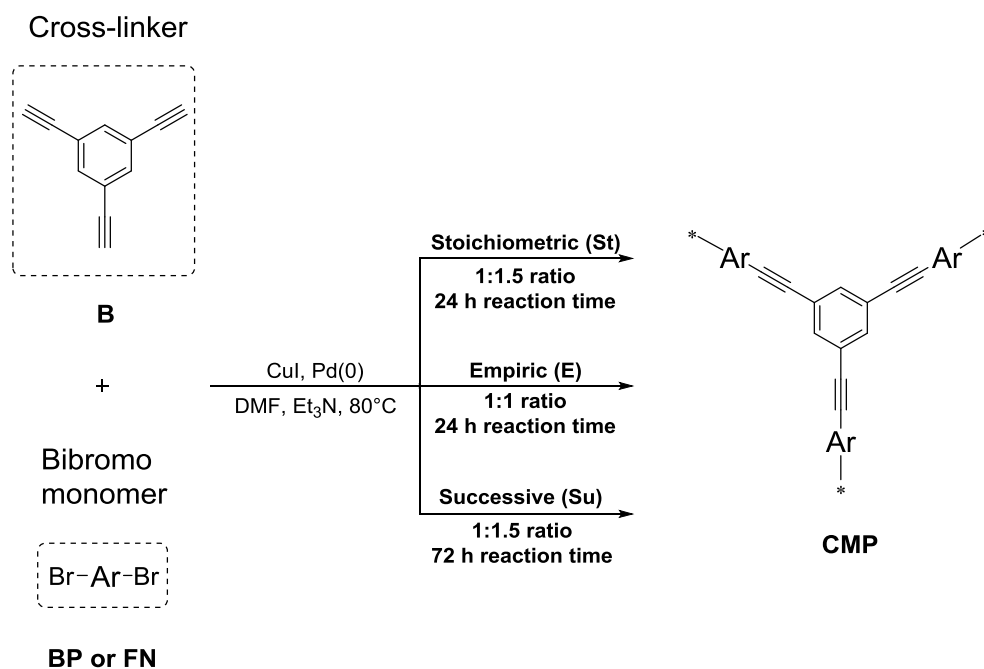
Scheme 4.1 Porosity control of CMPs via synthetic methods.

Table 4.3 Synthetic and morphological properties of the synthesized CMPs.

CMPs	Yield [%]	Surface area S_{BET} [m²/g]	Pore size [nm]	Pore volume [cm³/g]
CMP-B-BP$_{1.5}$-FN$_{1.5}$ (St)	88	8	2.6	0.025
CMP-B-BP$_{1,5}$-FN$_{1.5}$ (E)	61	24	1.4	0.217
CMP-B-BP$_{1.5}$-FN$_{1.5}$ (Su)	73	829	1.5	0.709

St: stoichiometric cross-linker:monomer ratio; E: empiric cross-linker:monomer ratio; Su: succsessive monomer addition.

The stoichiometric method gave the highest yield compared to the others. This is probably due to the step-growth nature of the reaction where exact stoichiometry is the key to high conversions. The next best yield is for the successive method where also an overall 1:1.5 ratio is used, while the 1:1 ratio gave the lowest yields.

With the stoichiometric ratio though only a surface area of 8 m^{2}g^{-1} and poor porosity was reached. However, the same synthetic procedure but with an empiric crosslinker:monomer ratio lead only to a slightly increase of the surface area (24 m^{2}g^{-1}). In comparison, an enormous

increase of the BET surface area was achieved upon the successive addition of comonomers. CMP-B-BP$_{1,5}$-FN$_{1,5}$ (Su) exhibited a surface area of 829 m^{2}g^{-1}, which is a factor 100 higher than the surface area gained by the empiric method.

To the best of knowledge this is the first time the successive method was used for the CMP synthesis via Sonogashira coupling. The high porosity could be a result of the monomer being dissolved better with a lower concentration in the reaction mixture in the beginning of the coupling. Also probably homo-coupling occurs between the alkyne groups since they are in excess in the reaction mixture for most of the reaction time.[117] So it is possible that the structures although they are more porous do not possess a low BG because the degree of acceptor units is not as high and the structure might be more block-like than alternating.

Nitrogen sorption isotherms of the samples and their corresponding pore size distributions are shown in Figure 4.13 to Figure 4.18. In general it can be said that the CMPs with a low surface area tend to have a larger hysteresis and their shape is mostly inconsistent.
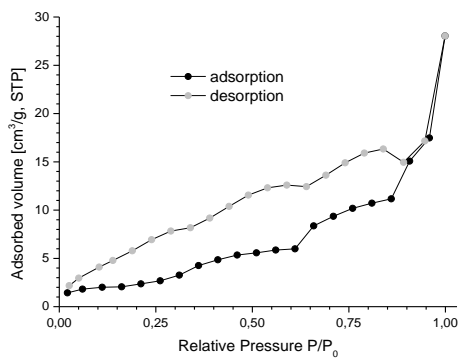
Figure 4.13 Adsorptionisotherm of CMP-B-BP$_{1.5}$-FN$_{1.5}$ (St).
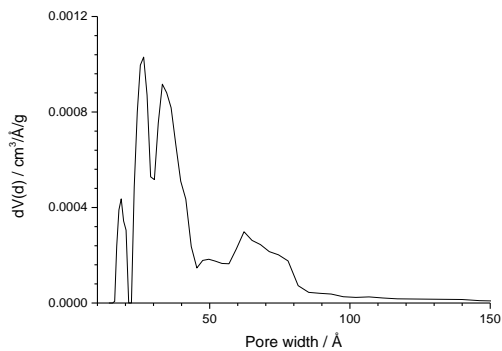
Figure 4.14 Pore size distribution of CMP-B-BP$_{1.5}$-FN$_{1.5}$ (St).
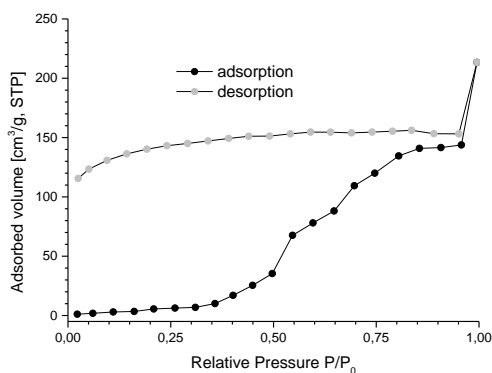
Figure 4.15 Adsorptionisotherm of CMP-B-BP$_{1.5}$-FN$_{1.5}$ (E).
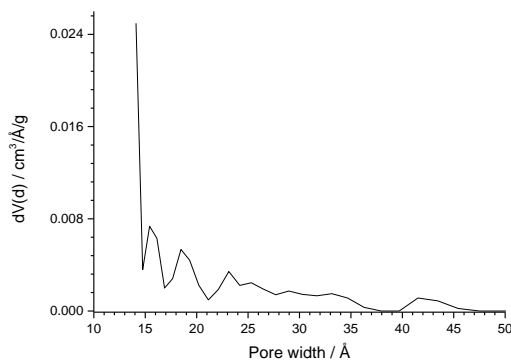
Figure 4.16 Pore size distribution of CMP-B-BP$_{1.5}$-FN$_{1.5}$ (E).
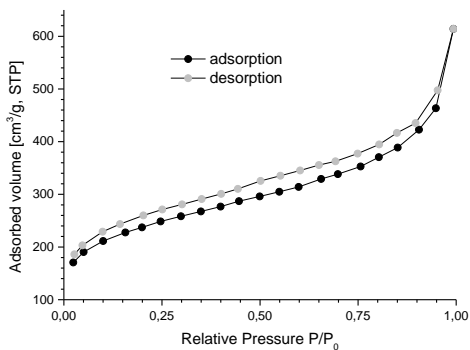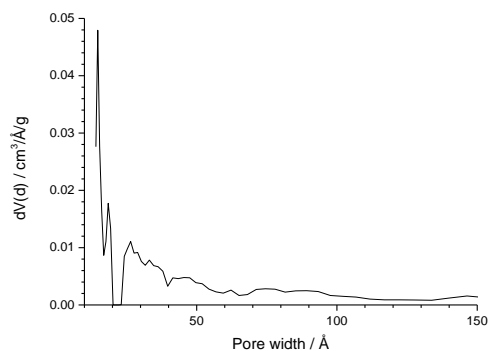

Figure 4.17 Adsorptionisotherm of CMP-B-BP$_{1.5}$-FN$_{1.5}$ (Su).

Figure 4.18 Pore size distribution of CMP-B-BP$_{1.5}$-FN$_{1.5}$ (Su).

CMP-B-BP$_{1.5}$-FN$_{1.5}$ (Su) has a type II isotherm which means non-porous or macroporous character. The pore size distribution however shows that the material has a higher content of micropores and some mesopores and also the SA (829 m^2g^{-1}) is the highest of all CMPs synthesized which argues for microporous material.

CMP-B-BP$_{1.5}$-FN$_{1.5}$ (St) and CMP-B-BP$_{1.5}$-FN$_{1.5}$ (E) do not show a specific type of isotherm and a big variation of desorption to adsorption. The pore size distributions of CMP-B-BP$_{1.5}$-FN$_{1.5}$ (St) and CMP-B-BP$_{1.5}$-FN$_{1.5}$ (E) show a low degree of micro- and mesoporosity and the low surface areas also speak for low porosity.

It can be observed that the successive method overall gave the highest nanoporosity and therefore the highest surface areas. The empiric method as well gave good results regarding microporosity, while the stoichiometric method gave the poorest porosity.

SEM images of the CMPs showed different morphologies. In particular, CMP-B-BP$_{1.5}$-FN$_{1.5}$ (St) and CMP-B-BP$_{1.5}$-FN$_{1.5}$ (E) appeared as fused particles, while CMP-B-BP$_{1,5}$-FN$_{1,5}$ (Su), as high surface area polymer, showed a rather porous morphology (Figure 4.19 to Figure 4.21). This indicates that the porosity and thus the surface area can be adumbrated from an image of the surface.
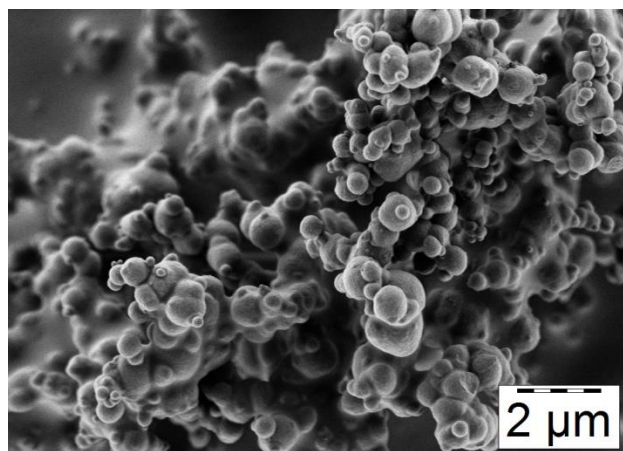
Figure 4.19 SEM image of CMP-B-BP$_{1.5}$-FN$_{1.5}$ (St).
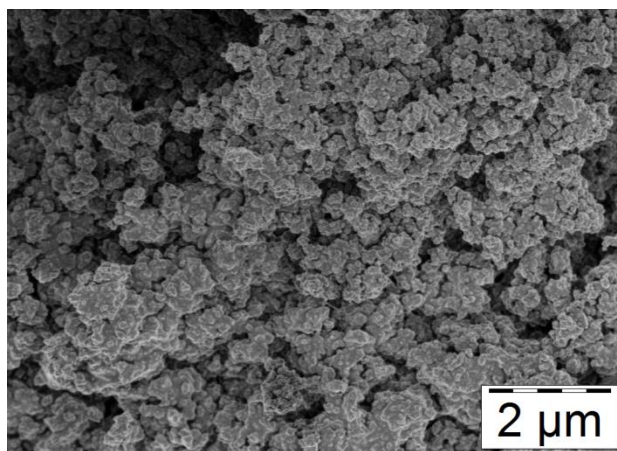
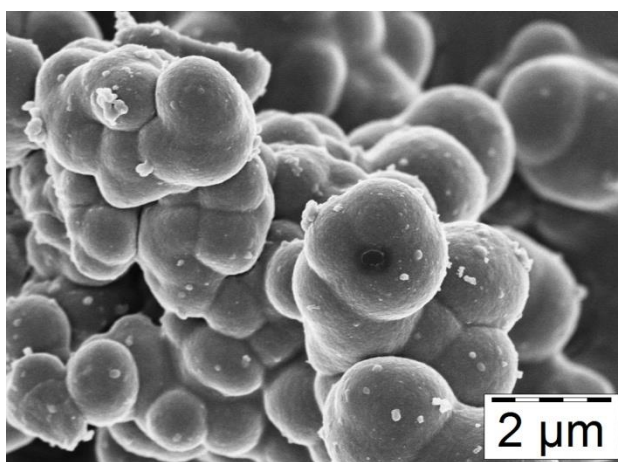**Figure 4.20 SEM image of CMP-B-BP$_{1.5}$-FN$_{1.5}$ (Su).**

Figure 4.21 SEM image of CMP-B-BP$_{1.5}$-FN$_{1.5}$ (E).

Although the three CMPs showed different morphologies and porosities, their FT-IR and ss-NMR spectra confirmed the same polymer backbone structures.

As shown in Figure 4.22, all three CMPs showed typical infrared signals at 1700 cm^{-1} for -C=O, and a weak signal at around 2250 cm^{-1} indicating internal -C≡C- alkyne bonds. Also some unreacted alkynyl groups can be seen at 3300 cm^{-1}, which indicate that if homo-coupling occurred it was not finished even for the long reaction time of the successive method. The presence of -C-Br vibrations cannot be easily allocated with IR-spectroscopy. As can be seen all methods yield similar spectra so it can be stated that there is only little difference in the structure by using different synthesis methods. The spectrum of CMP-B-BP$_{1.5}$-FN$_{1.5}$ (Su) has a slightly more intense fingerprint area which could be due to its enhanced surface area.
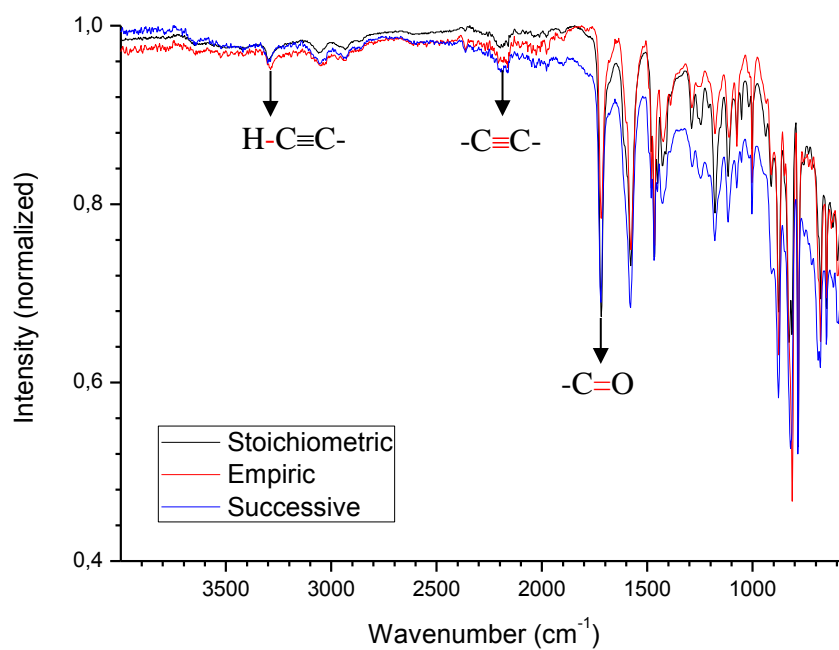
Figure 4.22 Superimposed IR spectra of CMP-B-BP$_{1.5}$-FN$_{1.5}$ (St) (black), CMP-B-BP$_{1.5}$-FN$_{1.5}$ (E) (red) and CMP-B-BP$_{1.5}$-FN$_{1.5}$ (Su) (blue).

The ss-^{13}C-NMR spectra (Figure 4.23) are in good agreement with the IR results. All three spectra nearly align with each other so that actually no difference between the single structures can be distinguished.
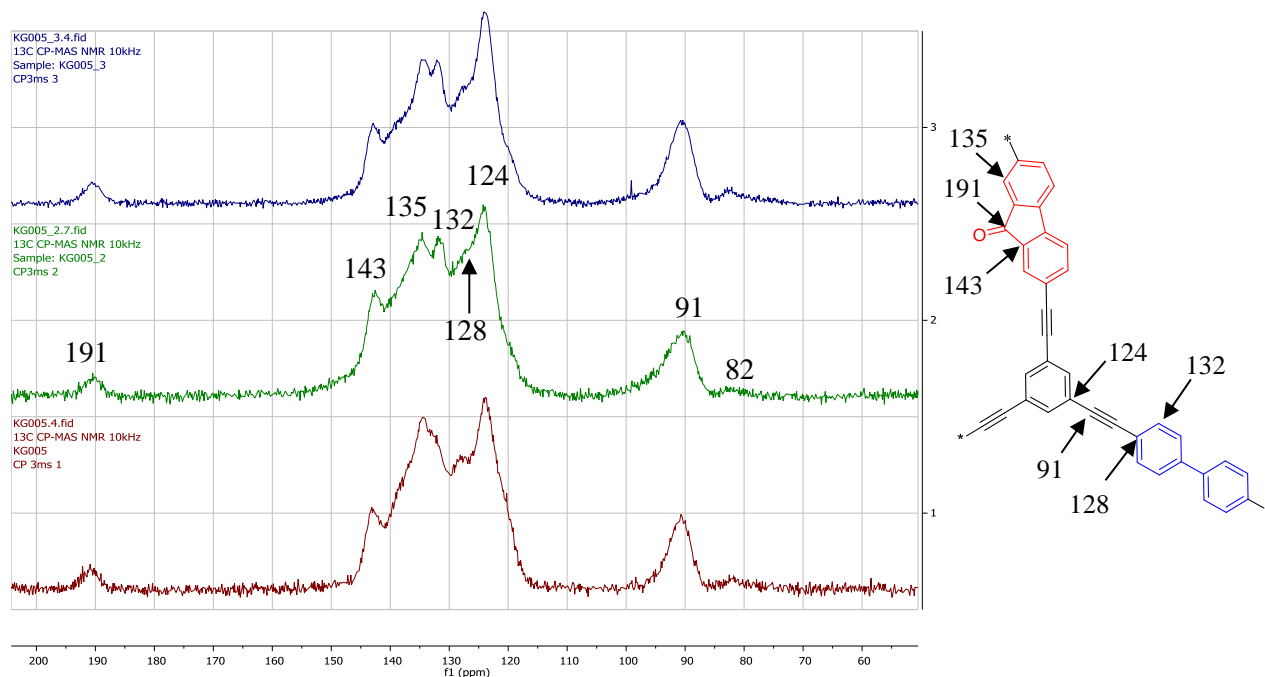
Figure 4.23 Stacked ss-^{13}C-NMR spectra of CMP-B-BP$_{1.5}$-FN$_{1.5}$ (St) (red), CMP-B-BP$_{1.5}$-FN$_{1.5}$ (E) (blue) and CMP-B-BP$_{1.5}$-FN$_{1.5}$ (Su) (green).

The signal at 91 ppm can be ascribed to the -C≡C- groups, and signals between 143 – 124 ppm can be ascribed to the various aromatic carbons. All three spectra possess relative to the internal alkyne signal a small terminal alkyne signal at around 82 ppm. This argues for homo-coupling during the formation process since nearly all terminal groups are employed. An aromatic C-Br cannot be seen.

Overall it can be said that the polymer backbone structure was not affected by using different synthesis methods. This is also supported by the TGA results which show that the same CMP with different porosities exhibit very similar thermal stabilities (Figure 4.24).
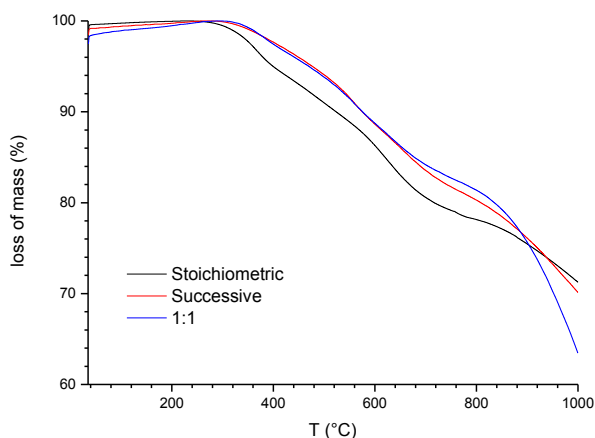
Figure 4.24 TGA curves of CMP-B-BP$_{1.5}$-FN$_{1.5}$ (St) (black), CMP-B-BP$_{1.5}$-FN$_{1.5}$ (E) (blue) and CMP-B-BP$_{1.5}$-FN$_{1.5}$ (Su) (red).

They were stable to about 300°C. CMP-B-BP$_{1.5}$-FN$_{1.5}$ (E) and CMP-B-BP$_{1.5}$-FN$_{1.5}$ (Su) have very similar decomposition behavior, while CMP-B-BP$_{1.5}$-FN$_{1.5}$ (St) decomposed slightly quicker, but not significantly than the other two CMPs.

To get a better understanding of how the structure is influenced by the synthesis method ^{13}C-ss-NMR could be used to measure samples after different reaction times and see how the ratio of terminal to internal alkyne groups changes. This should be especially interesting for the successive method as the co-monomer gets added day by day. Also energy-dispersive X-ray spectroscopy could be used to determine the bromine content and therefore the amount of endgroups. This could further indicate homo-coupling.

The optical properties of the series of CMP-B-BP$_{1.5}$-FN$_{1.5}$ were determined by recording the UV/Vis DRS spectra (Figure 4.25).
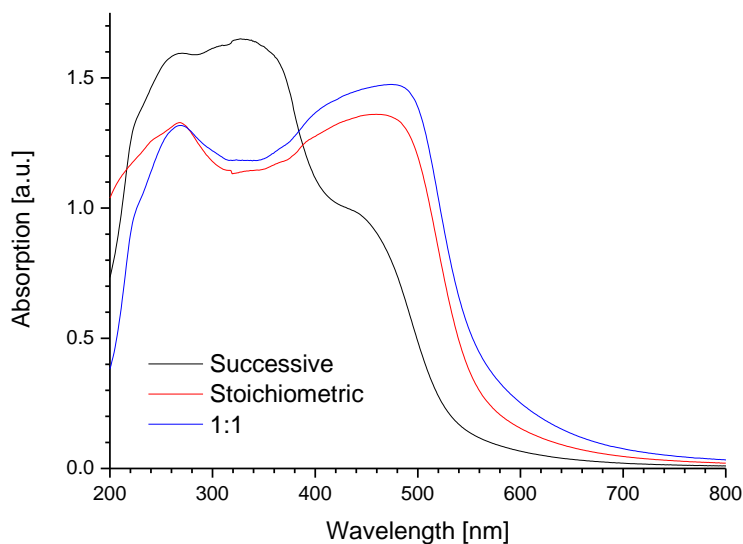
Figure 4.25 UV/Vis DRS spectra of CMP-B-BP$_{1.5}$-FN$_{1.5}$ synthesized via stoichiometric (red), successive (black) and empiric (blue) method.

It can be seen that the CMPs with lower surface areas are more bathochromically shifted compared to CMP-B-BP$_{1.5}$-FN$_{1.5}$ (Su) with the highest surface area (829 m²g^{-1}). But interestingly, the lowest surface area CMP (CMP-B-BP$_{1.5}$-FN$_{1.5}$ (St)) is not the most bathochromically shifted one. This might be because of a lower acceptor content in the stoichiometric CMP compared to the empiric one. From the absorption edge, the optical band gaps could be calculated (Table 4.4).

Table 4.4 Band gaps of CMP-B-BP$_{1.5}$-FN$_{1.5}$ series.

CMP	BG / eV
CMP-B-BP$_{1.5}$-FN$_{1.5}$ (St)	2.24
CMP-B-BP$_{1.5}$-FN$_{1.5}$ (E)	2.19
CMP-B-BP$_{1.5}$-FN$_{1.5}$ (Su)	2.31

In theory, a high degree of conjugation in CPs would lead to lower BGs. It seems like the CMP with the highest SA and porosity though has the highest BG. This result supports the hypothesis that via the successive method, the cross-linking degree of the donor-acceptor building blocks is high, but rather more twisted and has a defined three dimensional (3-D) geometry character.

We suggest that inside the low surface area CMPs, the polymer backbone structure should have a less 3-D, but more plate-like character according to a strong π–π stacking effect between the comonomers. This effect would lead to less cross-linking degree and therefor more linear polymer domains. And from the conjugation point of view, the less 3-D structure would cause larger extended π-system and therefore narrower HOMO/LUMO band gaps.
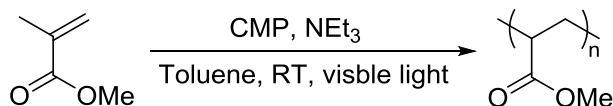
4.2. Photocatalytic experiments

In this part of the work, the feasibility of the CMPs as visible light photocatalysts was tested. A number of photocatalytic reactions were conducted. Additionally, the influence of the surface area on the photocatalytic activity was also studied. At last, the obtained knowledge of the crucial parameters of the polymer properties were investigated for designing new CMPs for specific catalytic reactions.

As shown in the literature[26,156], conjugated polymers could function as photosensitizer to initiate free radicals. Here, the ability of the CMPs as visible light photoinitiators was investigated in a similar manner.

4.2.1. Photopolymerization of MMA

A series of the free radical polymerization reaction of MMA with CMP-B-FN$_3$, CMP-B-BP$_3$ and CMP-B-BP$_{1.5}$-FN$_{1.5}$ via visible light was conducted (Scheme 4.2).

Scheme 4.2 Photopolymerization of MMA catalyzed by CMP under visible light.

The activity of the three CMPs as photoinitiators is listed in Table 4.5.

Table 4.5 Screening experiments for the photopolymerization of MMA.

CMP	Precipitated PMMA
CMP-B-FN$_3$	✓
CMP-B-BP$_{1.5}$-FN$_{1.5}$	✓
CMP-B-BP$_3$	–

Reaction conditions: 1 mL MMA, 25 mg CMP and 41 μL triethylamine were mixed together and sparged with N$_2$ for 5 min. Irradiation with the table lamp for 20 h. Formed PMMA was precipitated in methanol.

The reactions catalyzed with CMP-B-FN$_3$ and CMP-B-BP$_{1.5}$-FN$_{1.5}$ yielded PMMA under light irradiation, while no product was obtained by using CMP-B-BP$_3$ as photoinitiator. This is expected due to the polymer structure of CMP-B-BP$_3$, which only contains a weak electron donor, i.e. benzene units. Under light irradiation, the electron-hole-pair charge separation is insufficient and the excited electron is therefor rather short-living. In this case, CMP-B-BP$_3$ is not able to generate long-living excited electrons, which is mandatory for the free radical polymerization of MMA.

To study the kinetics of the photopolymerization using CMP-B-FN$_3$ and CMP-B-BP$_{1.5}$-FN$_{1.5}$ (Su) as initiators, the conversion was plotted against time (Figure 4.26).
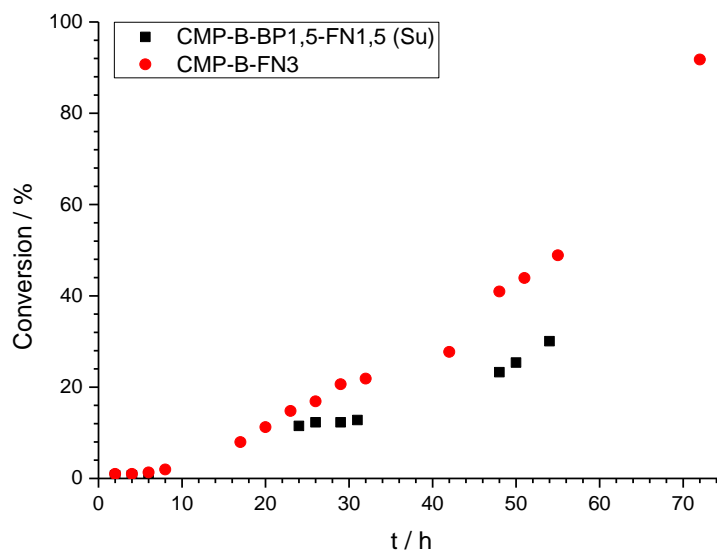
Figure 4.26 Conversion (determined via ^{1}H-NMR) vs time plot for the polymerization of PMMA with CMP-B-FN$_3$ and CMP-B-BP$_{1.5}$-FN$_{1.5}$ (Su).

The conversion of the photopolymerization of MMA using both CMPs increased exponentially with the time. A quantitative conversion could be reached only after 3 days. As photoinitiator,

CMP-B-FN$_3$ is more effective than CMP-B-BP$_{1.5}$-FN$_{1.5}$ (Su). This is probably due to its higher acceptor ratio. It is to note that although the surface area of CMP-B-BP$_{1.5}$-FN$_{1.5}$ (Su) is significantly higher than the one of CMP-B-FN$_3$, its ability to convert MMA into PMMA was even lower.

To study the reaction mechanism, the reaction was conducted without CMP, without triethylamine or without light irradiation. In all three cases no polymerization occurred, showing that every single compound is needed in order to ensure a successful reaction.

Based on the observed findings during the control experiments, a mechanism for the free radical polymerization of PMMA using the CMPs as visible light photoinitiator is suggested in Figure 4.27.
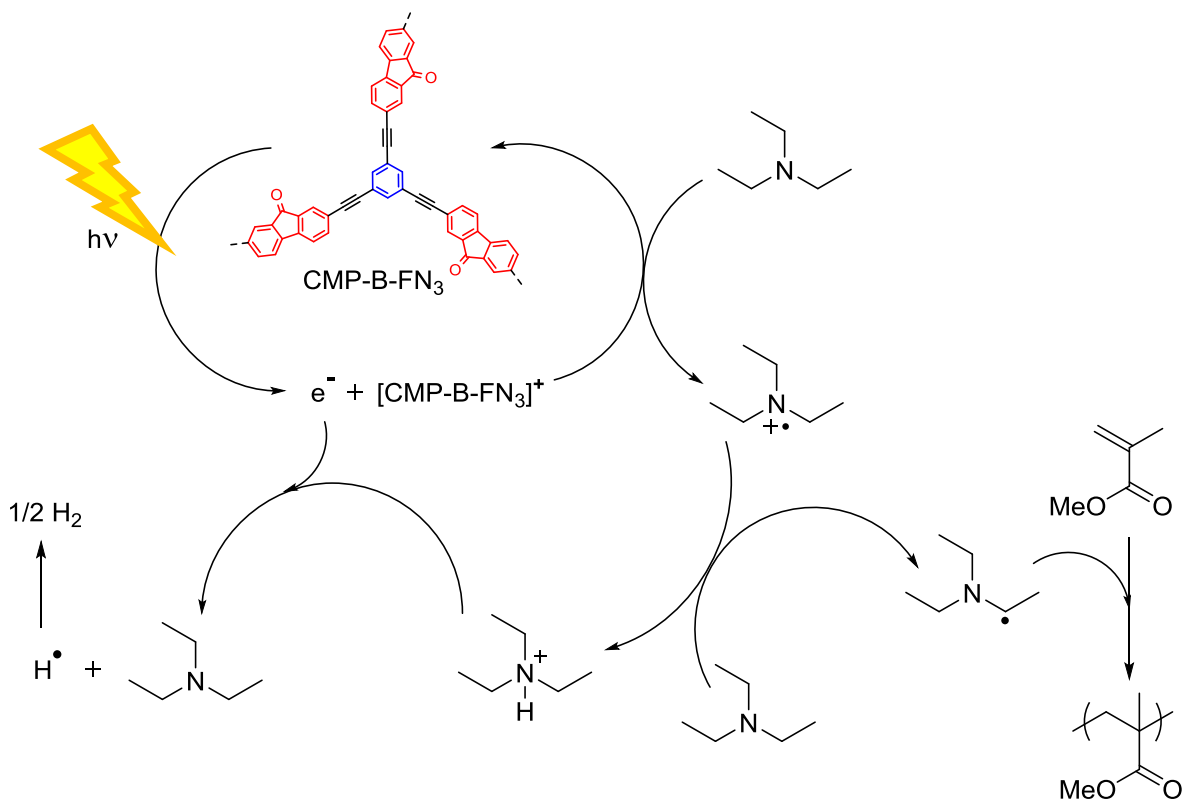
Figure 4.27 Suggested mechanism for the Photopolymerization of MMA via CMPs.

An additional experiment using 9H-fluorenone as a homogeneous photoinitiator lead to a conversion of 15% after 72 h, indicating the own photocatalytic activity of 9H-fluorenone as building block. The molecular weight M_n and the polydispersity Đ of formed PMMA are listed in Table 4.6.

Table 4.6 Properties of the PMMA samples produced with the different catalysts.

Catalyst used	Reaction time / h	Conversion /%	M_n / g mol^{-1}	Đ
CMP-B-FN$_3$	72	91	110 900	1.99
CMP-B-BP$_{1.5}$-FN$_{1.5}$ (Su)	92	95	201 600	3.03
9H-fluorenone	72	15	5 000	2.07

4.2.2. Fluorination via C-H activation

Direct fluorination of $C(sp^3)$-H bonds is still a major challenge in organic chemistry and for this purpose mostly metal-based catalysts were utilized.[157-159] Xia *et al.* reported that 9H-fluorenone could catalyze the selective fluorination of benzylic C-H bonds under visible light irradiation, with yields of over 90% (Scheme 4.3).[27]
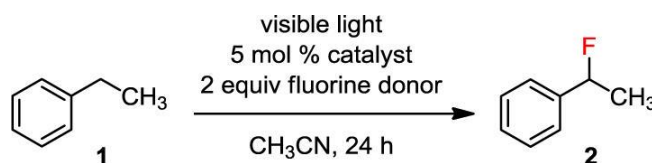
Scheme 4.3 Fluorination of ethylbenzene with 9H-fluorenone as selective, visible-light photocatalyst.[27]

Inspired by this finding, we further tested the FN-containing CMPs for the photofluorination reaction via C-H activation. Since the polymerization of MMA did work best with CMP-B-FN$_3$ a couple of experiments were conducted using that particular CMP.

To find out the optimal reaction conditions, a similar experiment was carried out according to Xia *et al.*, using 9H-fluorenone as a homogeneous catalyst.[27] By using the directly purchased solvent, the reaction did not yield the same product. However, by using dried solvent, the product was obtained with a yield of 49%. This indicates that the fluorination reaction has a sensitive nature and requires dry reaction conditions.

Further reactions were carried out using the optimized reaction conditions. Different reaction parameters for the CMP and co-reactants were tested. The results are listed in Table 4.7.

.

Table 4.7 Yields of fluorination experiments varying different reaction parameters.

#	Catalyst	Light source	CMP concentration	Solvent amount	Substrate amount	Inert gas	Yield
1a	CMP-B-FN$_3$	Blue LED	1 mg mL^{-1}	3 mL	100 mg	N$_2$	39%
1b	CMP-B-FN$_3$	Blue LED	1 mg mL^{-1}	3 mL	50 mg	N$_2$	-
2	CMP-B-FN$_3$	White LED	1 mg mL^{-1}	3 mL	50 mg	N$_2$	-
3	CMP-B-FN$_3$	White LED	1 mg mL^{-1}	3 mL	50 mg	Ar	-
4	CMP-B-FN$_3$	White LED	3 mg mL^{-1}	3 mL	50 mg	Ar	-
5	CMP-B-FN$_3$	White LED	5 mg mL^{-1}	3 mL	50 mg	Ar	-
6	CMP-B-FN$_3$	Blue LED	1 mg mL^{-1}	10 mL	50 mg	Ar	18%
7	CMP-B-FN$_3$	White LED	1 mg mL^{-1}	10 mL	50 mg	Ar	-

Further reaction conditions: 1 eq ethylbenzene, 1.5 eq Selectfluor and 1 eq fluorobenzene as internal standard. All yields were determined via ^{19}F-NMR against the internal standard.

The fluorinated product was obtained with a yield of 39% by using CMP-B-FN$_3$. However, other screening experiments, as listed in Table 4.7 (entry 1a), did not result into a clear observation. Plotting the same reaction for the kinetic study could not be carried out either.

The fluorination via C-H activation by using the FN containing CMPs did not lead to a satisfactory observation. The results could not be followed in a consistent way. The reasons are still unclear and need to be further investigated in the future.

Based on the provided mechanism of Xia *et al.*[27], the suggested mechanism for the CMP catalyzed fluorination is given in Figure 4.28. As stated before, CMPs can create radicals by using the energy of light to create an electron-hole pair, which can split the C-H bond. To further investigate the mechanism also CMPs without FN units were tested (Chapter 4.4).
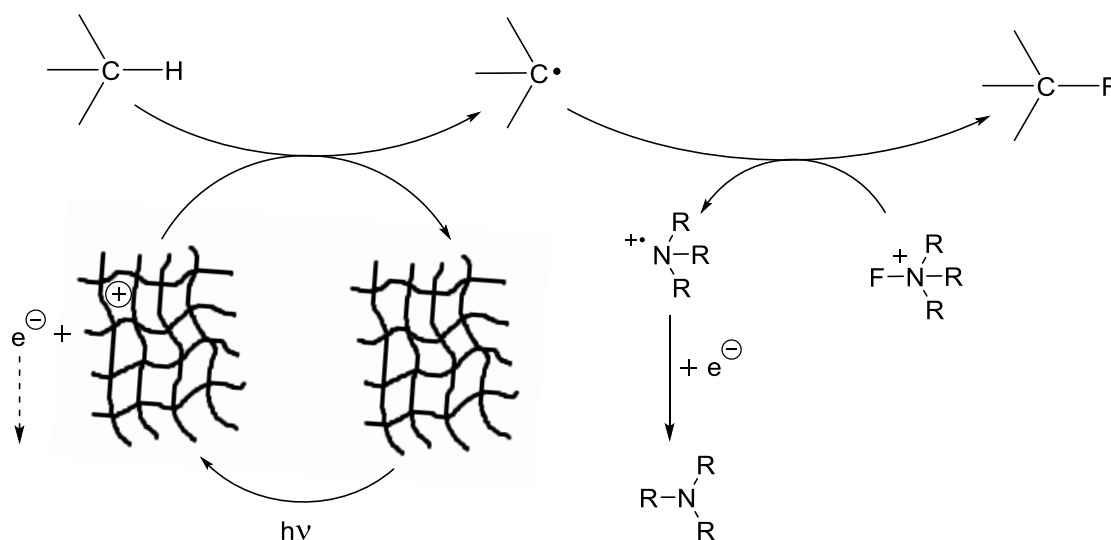
Figure 4.28 Suggested mechanism for the fluorination catalyzed by CMPs.

4.3. Molecular design of CMPs for enhanced photocatalytic efficiency

In this part of the thesis, a series of an A_2+B_3-type CMPs were designed and their energetic levels are investigated. The structures of the CMP series are displayed in Figure 4.29.
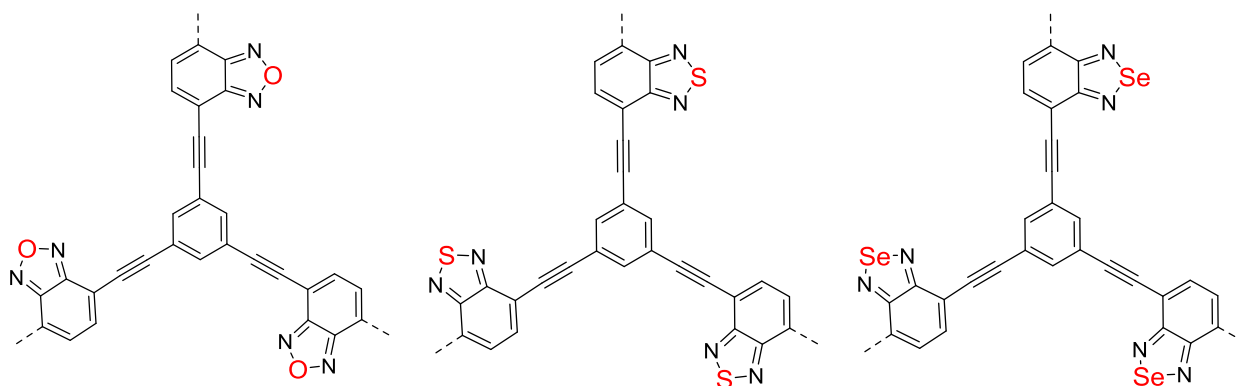

Figure 4.29 Structures of CMP-B-BO$_3$, CMP-B-BT$_3$ and CMP-B-BS$_3$.

The three CMPs were compared regarding their porosity, chemical and electrochemical structure using multiple techniques (Nitrogen sorption, TGA, FT-IR, ss-NMR, UV/Vis DRS, CV, EPR). Their photocatalytic activity was tested by the photo-oxidation of benzylamines and partially the Aza-Henry reaction.

The CMPs were synthesized by the three methods stated earlier (Chapter 4.1). The empiric method displayed comparable morphological properties, which are shown in the table below (Table 4.8), so they were used for photocatalytic experiments.

Table 4.8 Synthetic and morphological properties of the synthesized CMPs.

CMPs	Yield [%]	Surface area S_{BET} [m²/g]	Pore size [nm]	Pore volume [cm³/g]
CMP-B-BO$_3$	75	516	1.5	0.375
CMP-B-BT$_3$	94	244	1.5	0.207
CMP-B-BS$_3$	22	411	5.0	0.417

The low yield for the synthesis of CMP-B-BS$_3$ is probably due to the poor solubility of 4,7-dibromobenzo[c]-1,2,5-selenadiazole in DMF. It was tried to increase the solubility via sonication and heating prior triethylamine addition without any effect on the yield or the SA.

CMP-B-BO$_3$ possesses with 516 m^2g^{-1} the highest surface area, while CMP-B-BT$_3$ has the lowest SA with 244 m^2g^{-1}. CMP-B-BS$_3$ features the highest pore volume of 0.417 cm^3g^{-1} although it has the largest average pore size with 5 nm and the mediocre surface area of 411 m^2g^{-1}.

Nitrogen sorption isotherms and corresponding pore size distributions of CMP-B-BO$_3$, CMP-B-BT$_3$ and CMP-B-BS$_3$ are represented in Figure 4.30 to Figure 4.35.
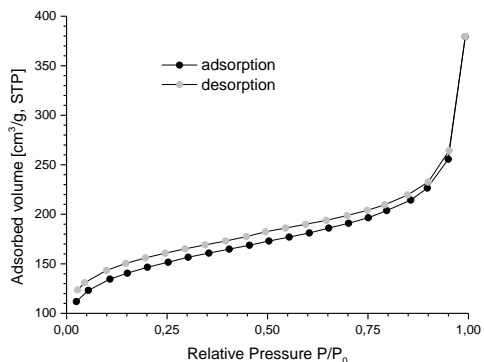
Figure 4.30 Adsorptionisotherm of CMP-B-BO$_3$.
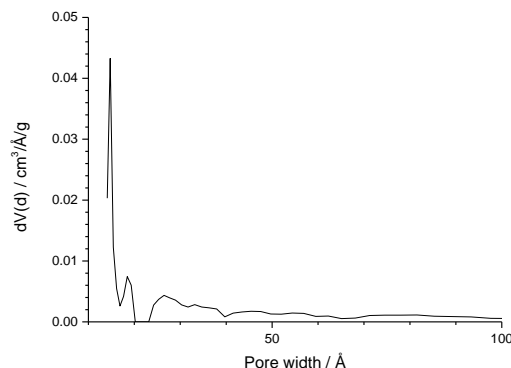
Figure 4.31 Pore size distribution of CMP-B-BO$_3$.
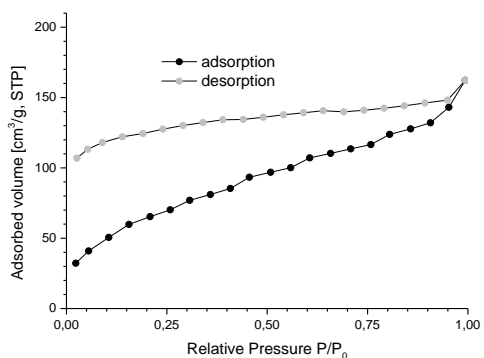
Figure 4.32 Adsorptionisotherm of CMP-B-BT$_3$.
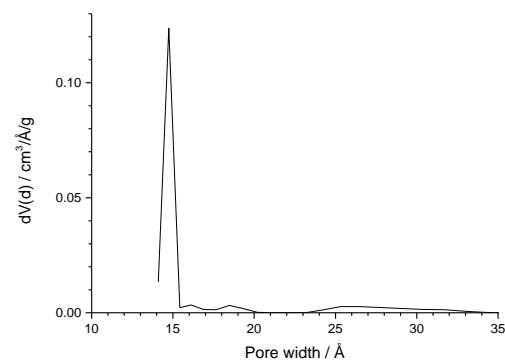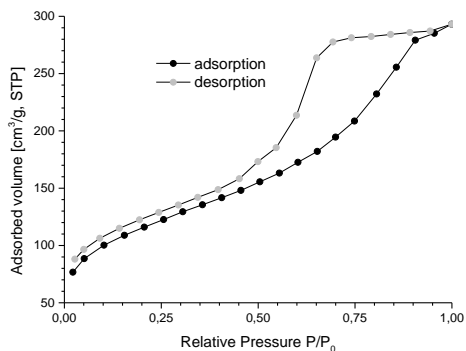

Figure 4.33 Pore size distribution of CMP-B-BT$_3$.

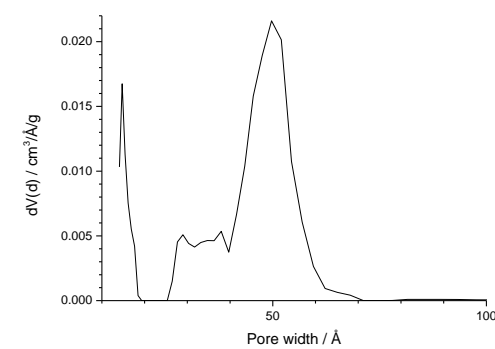**Figure 4.34 Adsorptionisotherm of CMP-B-BS$_3$.**

Figure 4.35 Pore size distribution of CMP-B-BS$_3$.

CMP-B-BO$_3$ isotherm clearly exhibits type II behavior. Together with the pore size distribution this states mostly microporous character since the average pore size is at 1.5 nm. The isotherm has no hysteresis which means there are nearly no mesopores.

The isotherm of CMP-B-BT$_3$ as well displays type II behavior but the desorption part differs heavily from the adsorption part. This is most likely due to poor outgassing or other mistakes

made during sample preparation. In the pore size distribution a comparably large quantity of micropores are detected with the average at 1.5 nm as well.

CMP-B-BS$_3$ has a mostly mesoporous structure which is displayed by the type IV shaped isotherm with an H1 hysteresis loop indicating capillary condensation. With the pore size distribution having its maximum at 5 nm the mesoporous character is supported.

TGA curves are presented in Figure 4.36. CMP-B-BO$_3$ and CMP-B-BS$_3$ are stable until they start decomposing at about 300 °C, while CMP-B-BT$_3$ is stable until 400 °C. The chalcogenes inside the building blocks seem to be able to change the thermal stability of the CMPs.
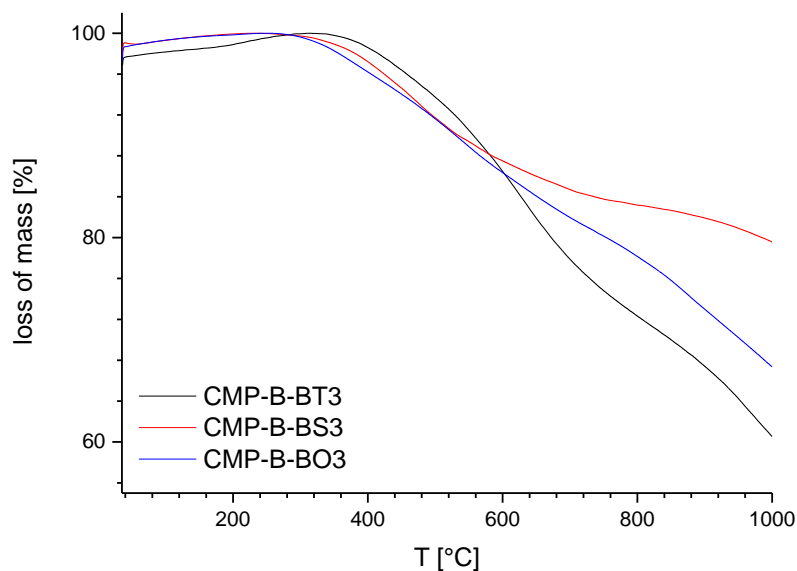
Figure 4.36 TGA curves of CMP-B-BO$_3$ (blue), CMP-B-BT$_3$ (black), and CMP-B-BS$_3$ (red).

The CMP structures were analyzed with FT-IR spectroscopy (Figure 4.37).
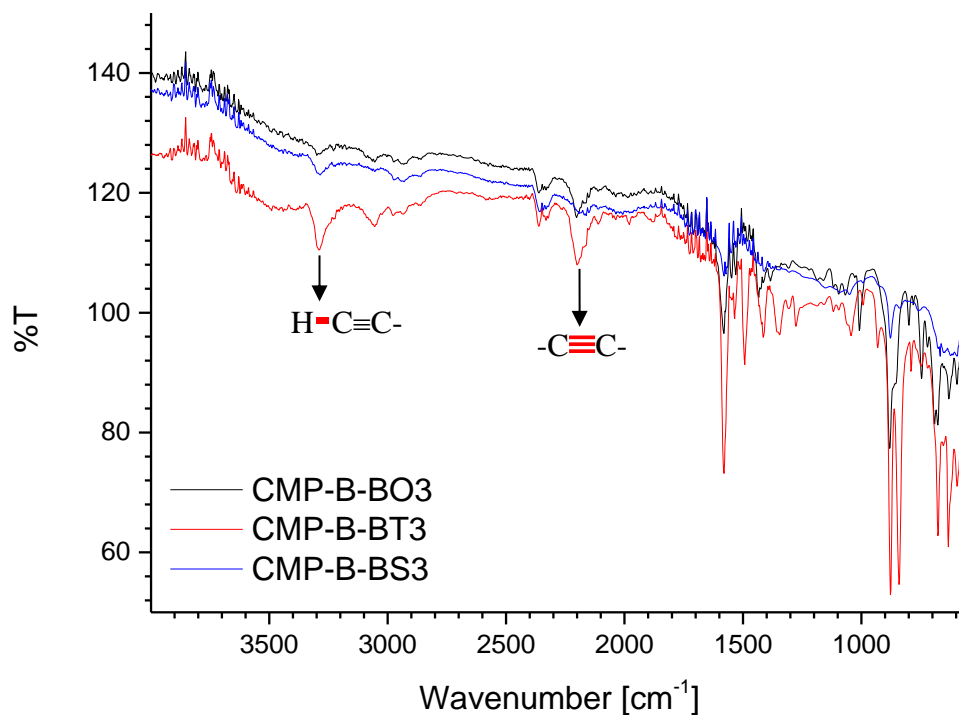
Figure 4.37 FT-IR spectra of CMP-B-BO$_3$ (black), CMP-B-BT$_3$ (red), and CMP-B-BS$_3$ (blue).

The typical alkyne vibrations at ~3300 cm^{-1} and ~2200 cm^{-1} can be ascribed for all three CMPs. Besides from that not a lot of information can be gained from the IR spectra. The fingerprint area shows some similarities but differs in most cases from each other.

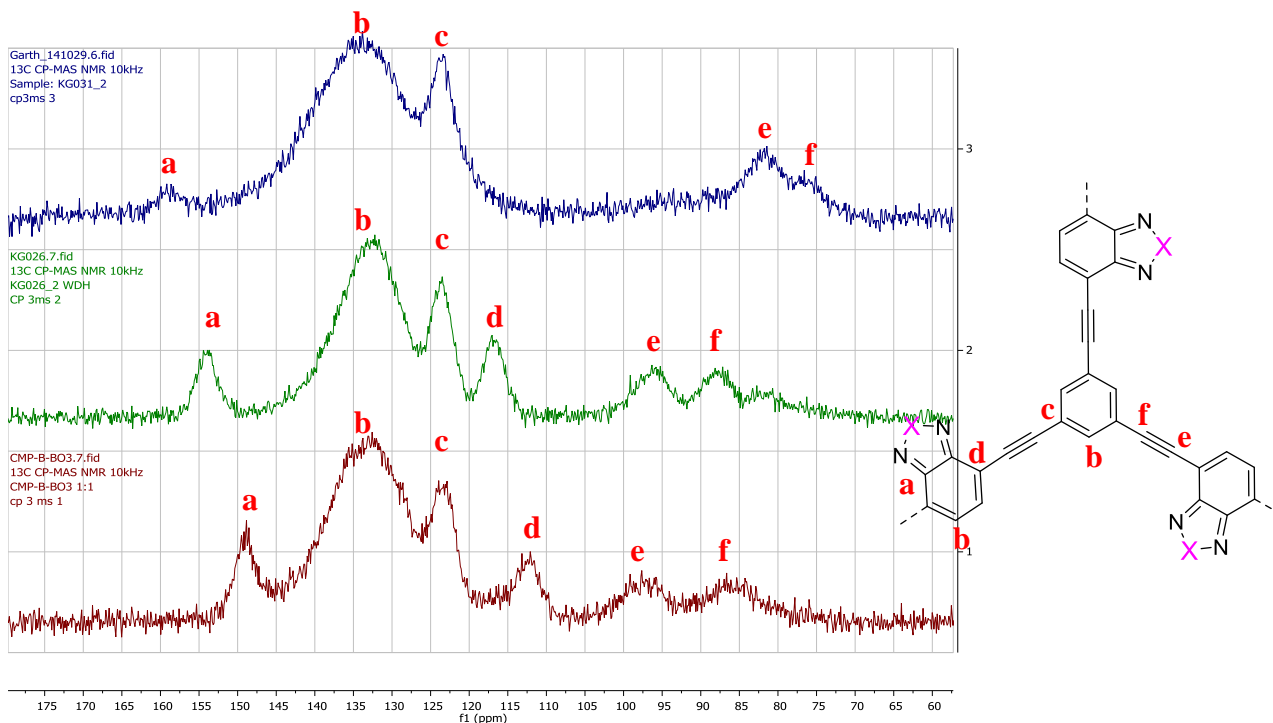For further structural characterization ss-^{13}C-NMR spectra were recorded (Figure 4.38).

Figure 4.38 Ss-^{13}C-NMR spectra with assigned peaks of CMP-B-BO$_3$ (red), CMP-B-BT$_3$ (green) and CMP-B-BS$_3$ (blue).

Corresponding to the measurement of CMP-B-BT$_3$ of Zhang *et al.*[135] the signals can be assigned, which indicates a successful synthesis in all three cases. Signal **a** and **d** shift downfield as the atomic number goes up. Peak **d** of CMP-B-BS$_3$ is probably merged with signal **c** resulting in a higher intensity of **c**. The peaks **e** and **f** of CMP-B-BS$_3$ are moved upfield though and are closer together. This and the low intensity of **a** could support the theory that not as many BS units are incorporated and homo-coupling occurred.

To get a ratio of acceptor units in each CMP, elemental analysis could be conducted. This would yield a percentage of nitrogen in the polymer from which the amount of diazole units could be determined.

UV/Vis DRS spectra were recorded (Figure 4.39) and corresponding optical BGs were calculated from the absorption edges (Table 4.9).
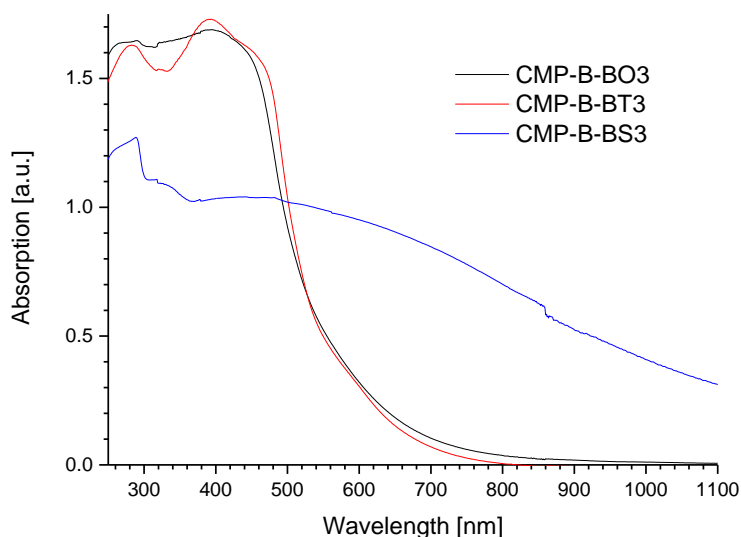
Figure 4.39 UV/Vis DRS absorption spectra of CMP-B-BO$_3$ (black), CMP-B-BT$_3$ (red), and CMP-B-BS$_3$ (blue).

Table 4.9 Calculated optical BGs for the stated CMPs.

CMP	Optical BG / eV
CMP-B-BO$_3$	2.24
CMP-B-BT$_3$	2.21
CMP-B-BS$_3$	1.21*

*Broad absorption band, approximated value.

CMP-B-BO$_3$ and CMP-B-BT$_3$ showed nearly the same absorption range, while CMP-BT-BS$_3$ had a much broader absorption band. The optical band gaps of CMP-B-BO$_3$ and CMP-B-BT$_3$, as expected, are also similar with 2.24 and 2.21 eV, respectively. The optical band gap of 1.21 eV could only be calculated approximated for CMP-B-BS$_3$, since the curve has a very broad absorption band and it is therefore not easy to determine the wavelength of the absorption edge. But is seems clear that in comparison CMP-B-BS$_3$ has the lowest optical BG and should hence have the best conjugation in the network.

To determine the HOMO and LUMO levels of the CMPs, cyclic voltammetry was performed. The results are listed in Table 4.10. The corresponding cyclic voltammograms are shown in Figure 4.40 to Figure 4.45.

Table 4.10 Electrochemical BGs and determined HOMO and LUMO levels for the CMPs.

CMP	HOMO / eV	LUMO / eV	Electrochemical BG / eV
CMP-B-BO$_3$ (E)	-5.14	-3.87	1.27
CMP-B-BT$_3$ (E)	-5.13	-3.75	1.38
CMP-B-BS$_3$ (E)	-5.09	-3.59	1.50

Compared to the optical band gaps calculated from the UV/vis absorption edge, the electrochemical BGs of the CMPs appeared different. In particular, CMP-B-BS$_3$ showed the highest BG of the three CMPs with approximately 1.50 eV. CMP-B-BO3 and CMP-B-BT3 exhibited electrochemical band gaps of 1.27 and 1.38 eV, respectively. These values lay nearly 1 eV underneath the optical band gaps. In literature the electrochemical BG for a similar CMP-B-BT$_3$ is found to be 2.10 eV,[135] which also differs a lot from the determined electrochemical BG in this work but is closer to the optical one.
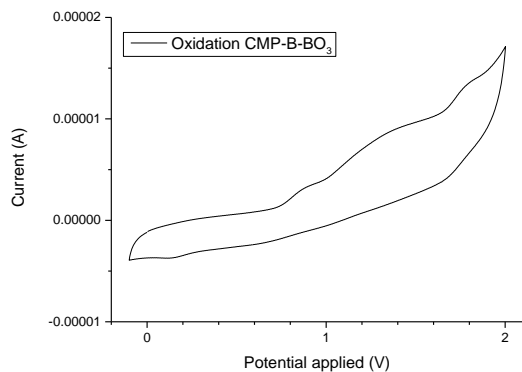
Figure 4.40 Oxidation cycle of CMP-B-BO$_3$.
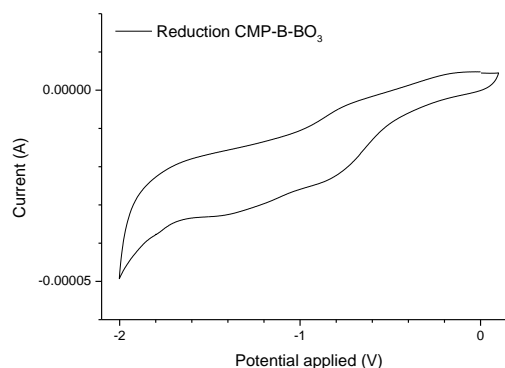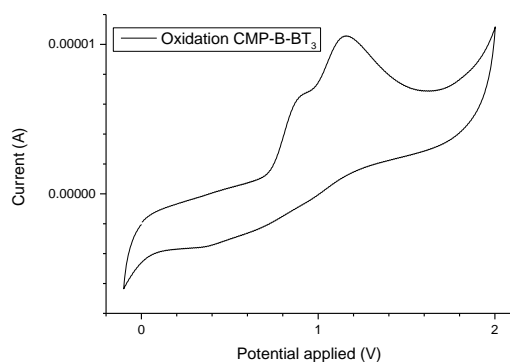

Figure 4.41 Reduction cycle of CMP-B-BO$_3$.

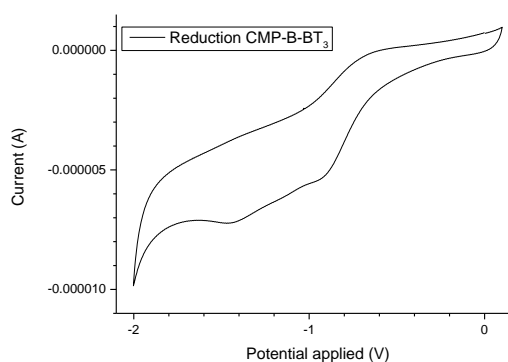**Figure 4.42 Oxidation cycle of CMP-B-BT$_3$.**

Figure 4.43 Reduction cycle of CMP-B-BT$_3$.
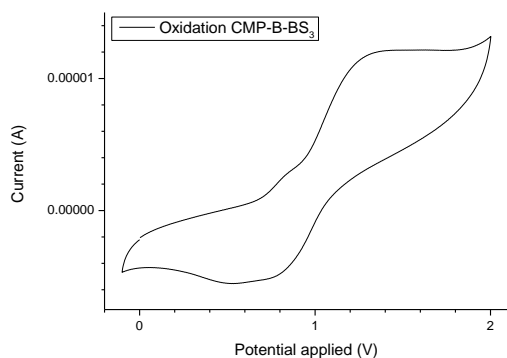

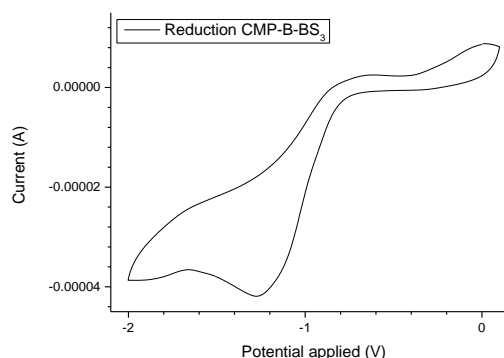**Figure 4.44 Oxidation cycle of CMP-B-BS$_3$.**

Figure 4.45 Reduction cycle of CMP-B-BS$_3$.

The energy diagram (Figure 4.46) of the HOMO and LUMO levels shows an interesting trend. The HOMO levels of the CMPs lie very close together, which is expected since they are influenced by the donor unit, in all the cases the benzene ring. The LUMO levels, on the other hand are affected by the acceptor character of the comonomer, here BO, BT and BS units. However, the variation of the acceptor characters of these building blocks and therefore their influence on the LUMO level are not tremendous.
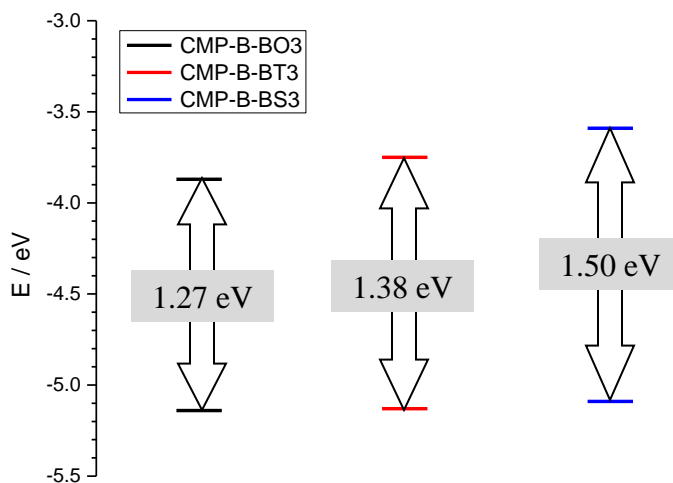
Figure 4.46 Energy diagram of the HOMO and LUMO levels of CMP-B-BO$_3$ (black), CMP-B-BT$_3$ (red), and CMP-B-BS$_3$ (blue).

The huge difference between the band gaps derived from the UV/Vis spectroscopy and cyclic voltammetry could probably be explained as the following:

The narrow HOMO−LUMO band gaps arise from localized donor and acceptor sites within the polymer domains through the donor and acceptor units, in this case phenyl and BO, BT and BS units respectively. This is similar to a previously published work, where even in conjugated polythiophenes containing strongly redox-active components the donor and acceptor units can exhibit independent electroactivity.[160]

To investigate the ability of the CMPs to generate long-living electron-hole pairs, electron paramagnetic resonance (EPR) spectroscopy was performed. As shown in Figure 4.47 to Figure 4.49, EPR spectra of CMP-B-BO$_3$, CMP-B-BT$_3$, and CMP-B-BS$_3$ were recorded in dark and under light irradiation. It can be clearly seen that all three CMPs exhibited enhanced EPR signals under light irradiation, compared to the signals taken in dark.
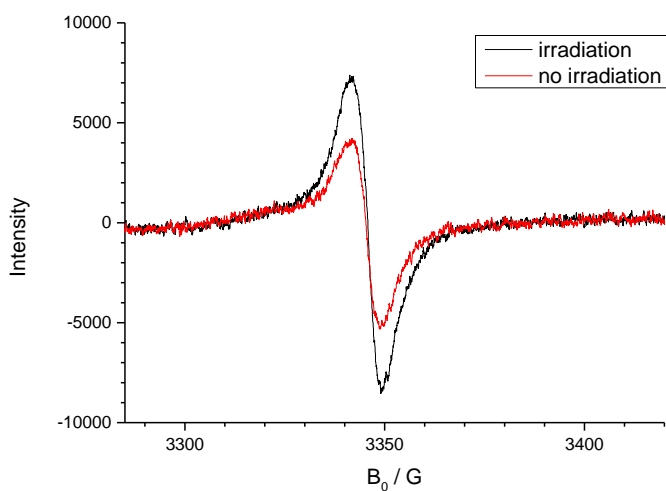
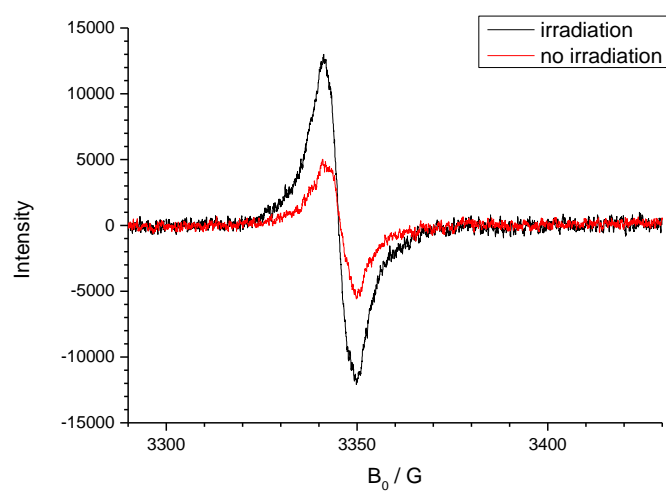**Figure 4.47 EPR spectra of CMP-B-BO3 with irradiation (black) and in the dark (red).**

Figure 4.48 EPR spectra of CMP-B-BT$_3$ with irradiation (black) and in the dark (red).
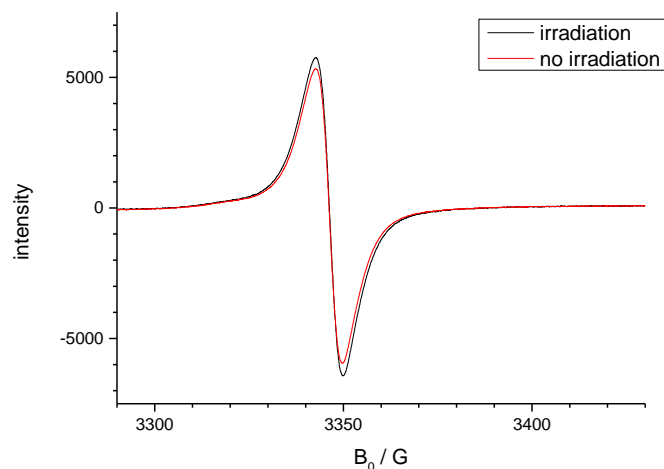
Figure 4.49 EPR spectra of CMP-B-BS$_3$ with irradiation (black) and in the dark (red).

When comparing the intensities of the signals of the CMPs in the dark (Figure 4.50), all three CMPs exhibited very similar signal intensities. However, under light irradiation (Figure 4.51), CMP-B-BT$_3$ showed the highest intensity, followed by CMP-B-BO$_3$ and CMP-B-BS$_3$. This result implies that CMP-B-BT$_3$ could generate the highest amount of stable electron-hole pairs under light irradiation, and therefore could be considered as a good candidate for light-induced catalytic reactions. Hence it can be expected that CMP-B-BT$_3$ could be the most efficient photocatalyst within the series for catalytic reactions.
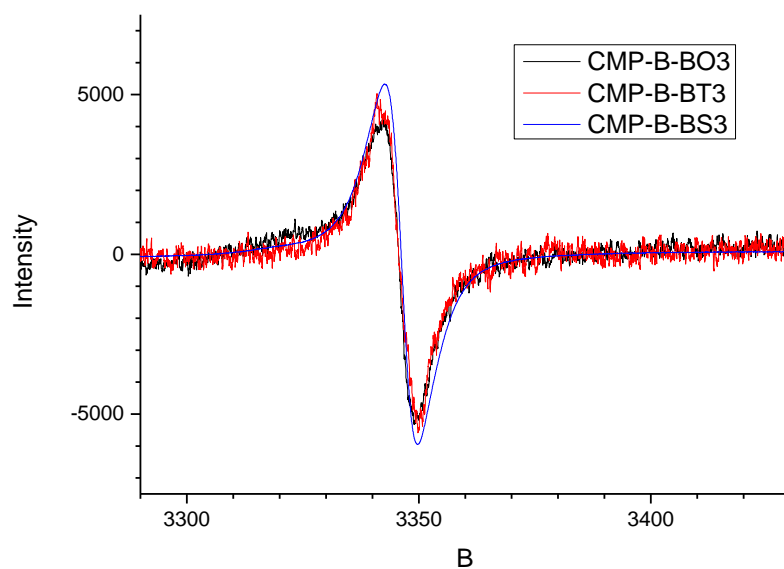
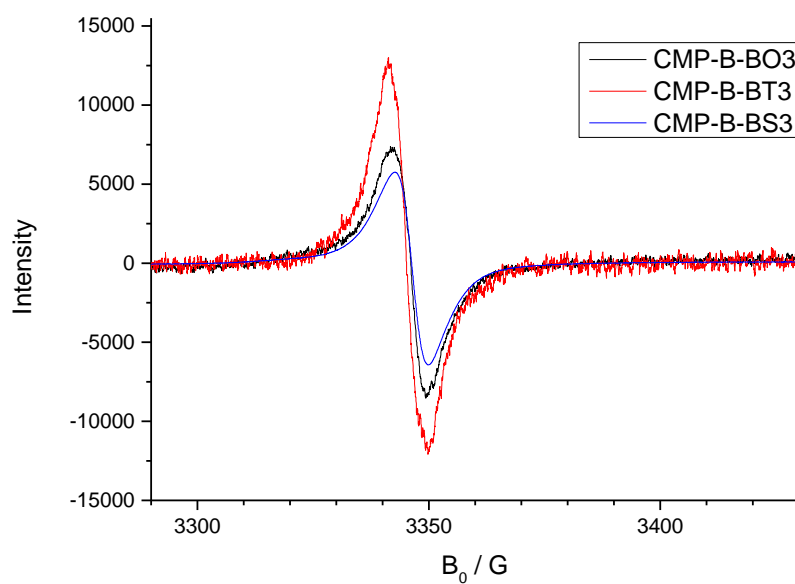**Figure 4.50 EPR spectra without irradiation of CMP-B-BO$_3$ (black), CMP-B-BT$_3$ (red), and CMP-B-BS$_3$ (blue).**

Figure 4.51 EPR spectra under irradiation of CMP-B-BO$_3$ (black), CMP-B-BT$_3$ (red), and CMP-B-BS$_3$ (blue).

4.3.1. Photo-oxidation of benzylamines

The selective oxidation reaction of benzylamines (Scheme 4.4) is of great importance in organic chemistry. As product, the imine containing compounds are widely used as precursors in pharmaceutical industries. So far, this reaction was able to be catalyzed using metal-containing catalysts[161-164], organic photocatalysts[165,166], organic salts[167,168], MOFs[94], and CMPs[29].
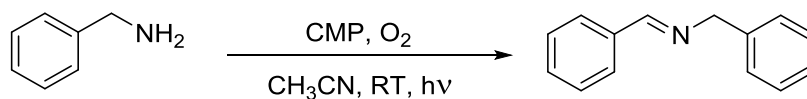
Scheme 4.4 Photo-oxidation of benzylamine catalyzed by a CMP.

The CMPs of the so-called chalcogene series were investigated. The first tests with CMP-B-BT$_3$ yielded full conversions according to ^{1}H-NMR spectra. Compared to the CMPs reported by Kang *et al.*,[29] CMP-B-BT$_3$ was used in a much lower concentration (1 mg mL^{-1}). Additionally to achieve the full conversion, much less reaction time was needed. A conversion versus time plot was recorded to study the kinetics and to optimize the reaction conditions (Figure 4.52). The tests using the other two CMPs are listed in Table 4.11.
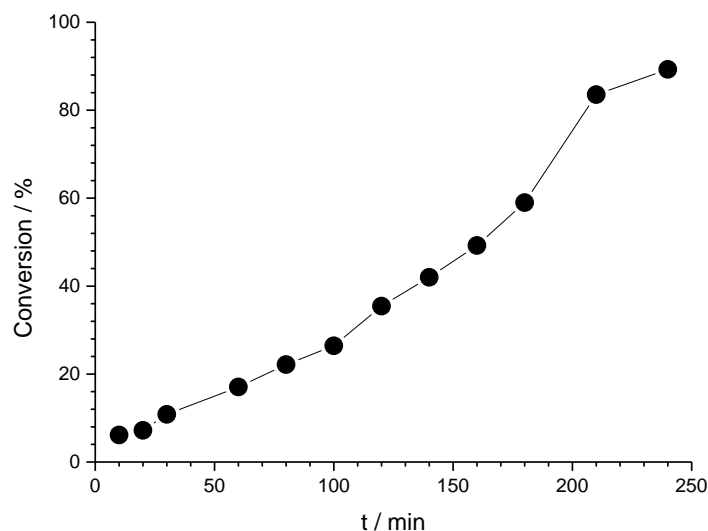
Figure 4.52 Conversion (determined via ^{1}H-NMR) vs time plot for the dimerization of benzylamine with CMP-B-BT$_3$.

A smooth exponential growth was recorded and after 4 h nearly 90% conversion was reached. To study the structural effect of the CMPs on the catalytic efficiency CMP-B-BO$_3$ and CMP-B-BS$_3$ were also investigated under the same reaction conditions.

Three different benzyl amine derivatives, i.e. benzylamine, 4-fluorobenzylamine (with the electron-withdrawing fluoro group) and 4-methoxybenzylamine (with the electron-donating methoxy group), were used for the screening experiments. The results are listed in Table 4.11.

Table 4.11 Conversions for the shown reaction catalyzed by the stated CMPs.

CMP	Conversion		
	R = H	**R = F**	**R = OCH3**
CMP-B-BO$_3$ (E)	23%	20%	7%
CMP-B-BT$_3$ (E)	74%	50%	12%
CMP-B-BS$_3$ (E)	8%	3%	2%

Reaction conditions: 1 mmol substrate, 3 mg CMP in 3 mL CH$_3$CN under the irradiation of the blue LED for 3 h in O$_2$ atmosphere at RT.

CMP-B-BT$_3$ clearly showed the highest conversions after the same reaction time. This can be confirmed by the EPR results (Chapter 4.3), where CMP-B-BT$_3$ can generate more stable

electron-hole pairs and therefore more radicals under light irradiation compared to the other two CMPs. CMP-B-BS$_3$, on the other hand, produced a minimal amount of enhanced electron-hole pairs upon irradiation and hence yields the lowest conversions. Both electron-withdrawing as well as the electron-donating substrates gave a worse conversion than the naked benzylamine. It would be expected that the more electron-donating compound would lead to higher conversions, in the assumption that the deprotonated benzylamine radical cation could be stabilized. The opposite results here could be likely explained that the formed cation radical is stabilized in the way so that it cannot react quickly with the activated and therefore lower the total oxidation reaction of the benzylamine.

Inspired by the suggested mechanism of Kang *et al.*[29] for the photo-oxidation of benzylamines using a CMP network, the following mechanism is proposed (Figure 4.53).
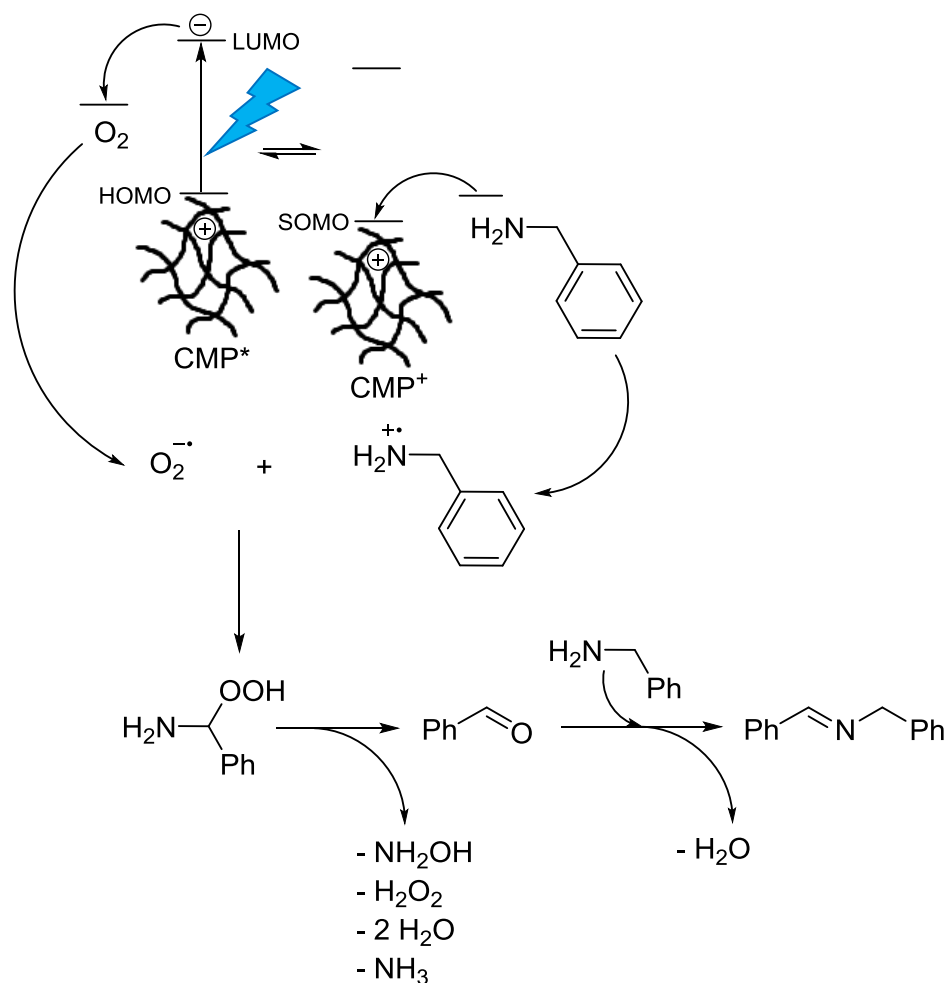
Figure 4.53 Suggested mechanism for the photo-oxidation of benzylamines catalyzed by a CMP network using blue light.

Under light irradiation, an electron-hole pair is generated. If the excited electron is on a higher energy level than singlet oxygen it can be transferred and produce the radical anion of oxygen. This causes a drop of the energy level of the HOMO to form the singly occupied molecular orbital (SOMO) which can on the other hand reduce the benzylamine. That leads towards its radical cation. Both radical ions can be combined for the peroxide which decomposes to form the benzaldehyde. Finally, it can react with another benzylamine to yield the final product.

For verifying the mechanism, different control experiments were conducted similar to the free radical polymerization of MMA (Table 4.12). The reaction was stirred in the dark or without a CMP as catalyst for 24 h. Only very small yields were reached compared to the relatively long reaction time, indicating that both light and CMP is mandatory for a successful reaction. Also another control reaction was carried out for 3 h with the all donor based CMP-B-BP$_3$ and gave a 7% conversion, which is nearly the same value as for the reaction with CMP-B-BS$_3$.

Table 4.12 Control experiments for the photo-oxidation of benzylamines.

Experiment #	Conversion
Blank[a]	2%
Blank[b]	3%
Blank[c]	7%

Reaction conditions: 1 mmol benzylamine in 3 mL CH$_3$CN under O$_2$ atmosphere at RT; Reaction time: 24 h.
[a]3 mg CMP-B-BT$_3$, no irradiation. [b]Irradiation with the white LED, no CMP. [c]3 mg CMP-B-BP$_3$ as catalyst.

In addition, an extra experiment was performed to verify the necessity of light to maintain the photo-oxidation reaction of benzylamine. The same reaction using CMP-B-BT$_3$ was carried out, alternating between 1 h periods of visible light irradiation and 1 h periods of complete lack of visible light irradiation (Figure 4.54). As shown in the graph, no conversion was determined during the reaction time in the dark, proving the importance of light for this catalytic reaction.
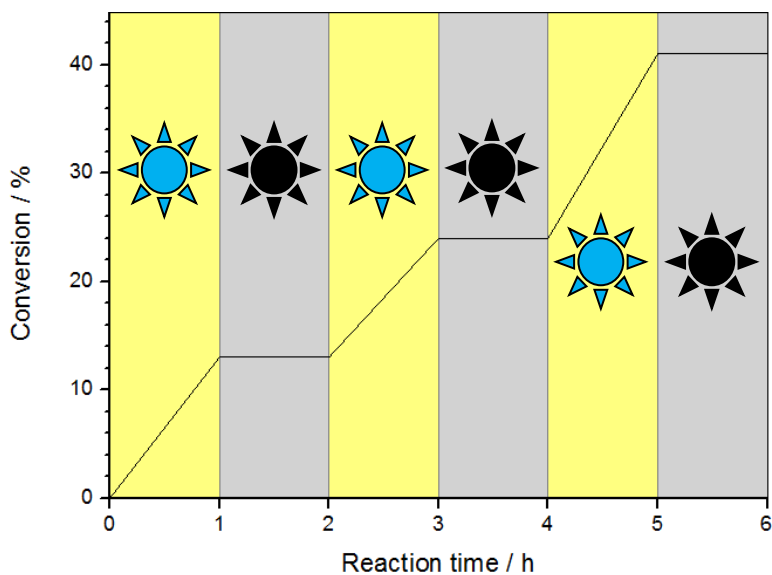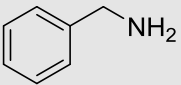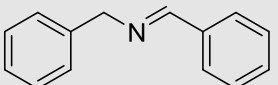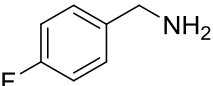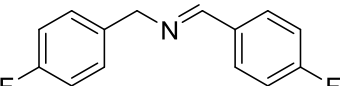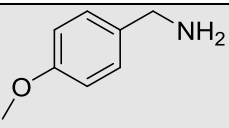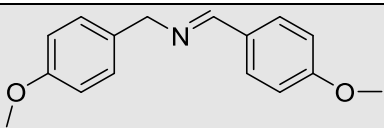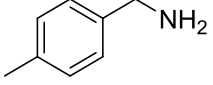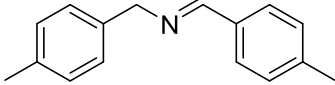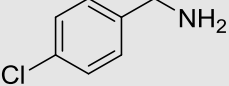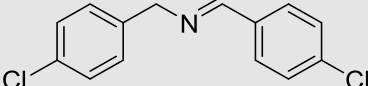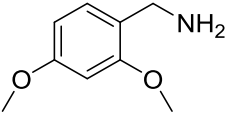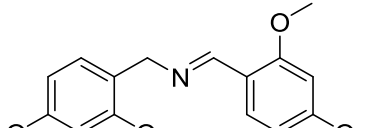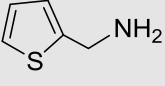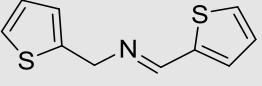
Figure 4.54 Conversion (determined via ^{1}H-NMR) vs reaction time plot. The yellow area indicates irradiation with the blue LED, while there was no irradiation during the grey marked reaction times.

Furthermore, various substrates of benzylamines were tested using CMP-B-BT$_3$ as photocatalyst (Table 4.13). The oxidative potentials of the compounds were determined using cyclic voltammetry. Corresponding curves are shown in the appendix (Chapter 7).

Table 4.13 Series of different substrates with CMP-B-BT$_3$ as photocatalyst.

	Substrate	Product	Conversion (%)	E$_{ox}$ vs SCE (eV)
1			74	1.099
2			50	0.992
3			12	0.927
5			55	0.974
6			43	0.899
7			-	1.027
8			10	0.867

Reaction conditions: CMP-B-BT$_3$ (3 mg), substrate (1 mmol), 1 atm O$_2$, 3 mL CH$_3$CN, blue LED, 3 h, room temperature. Conversion data were determined by ^{1}H NMR. E$_{ox}$ values were determined via cyclic voltammetry.

Plain benzylamine (entry 1) was successfully converted into the desired product in the highest yield of all derivatives. The derivatives with electron-withdrawing and electron-donating groups were less successfully converted into the products. This cannot be easily explained by the different oxidation potentials of the benzylamine derivatives, where benzylamine (entry 1) showed the highest oxidation potential than other derivatives (Figure 4.55). If only the oxidation potential played the crucial role for the deprotonation step and the C-N coupling reaction afterwards, the naked benzyl amine would only achieve a very low conversion into the overall final product. Here, most likely, a stabilizing effect of the deprotonated intermediates of the

different benzylamine derivatives would affect the overall C-N coupling reaction to the final product.
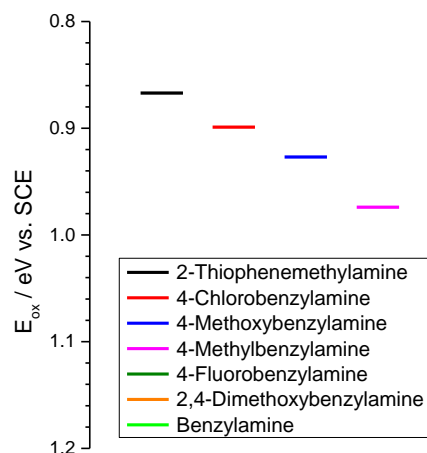
Figure 4.55 Energy diagram of the oxidation potentials E_{ox} of the used benzylamines.

In the literature, a variation of trends is found for the conversions of the same amines used as in this work and the effect of electron-donating or -withdrawing compounds on the reaction is not clear yet.[94,162-164,166]

In addition, also the prior used CMP-B-BP$_{1.5}$-FN$_{1.5}$ (St) and (Su) were utilized by this reaction to further investigate the influence of porosity on the photocatalytic activity.

Table 4.14 Conversions for the photo-oxidation of benzylamine catalyzed by CMPs.

CMP	Conversion
CMP-B-BP$_{1.5}$-FN$_{1.5}$ (St)	32%
CMP-B-BP$_{1.5}$-FN$_{1.5}$ (Su)	31%

Reaction conditions: CMP (3 mg), substrate (1 mmol), 1 atm O_2, 3 mL CH_3CN, blue LED, 3 h, room temperature. Conversion data were determined by ^{1}H NMR.

It can be seen here (Table 4.14), that the surface area has no influence on the reactions efficiencies. Interestingly, it seems that also the BG difference between CMP-B-BP$_{1.5}$-FN$_{1.5}$ (St) and CMP-B-BP$_{1.5}$-FN$_{1.5}$ (Su) do not change photocatalytic activity as well. Further investigations and more repeating experiments are necessary to prove these investigations.

At last, the reaction was conducted under energy saving conditions with the energy saving table lamp, where after 24 h a conversion of 33% was reached. This result shows that CMP-B-

BT$_3$ has potential as an economical catalyst and that the reaction can be optimized to energy- and cost-saving conditions.

4.3.2. Aza-Henry reaction

To further examine the photocatalytic activity of this series of CMPs and our prediction, that CMP-B-BT$_3$ could be the most efficient photocatalyst, the so-called Aza-Henry reaction, a C-C bond formation reaction, was also investigated (Scheme 4.5).
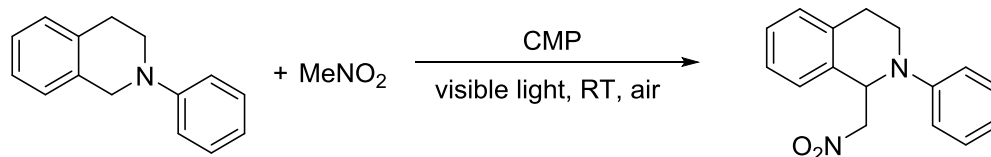
Scheme 4.5 General reaction scheme of the Aza-Henry reaction catalyzed by a CMP.

Similar reactions were reported by Jiang *et al*., where they used CMPs containing a well-known organophotocatalyst, Rose Bengal dye, in the polymer backbone.[28]

In this work the chalcogene-containing CMPs were used here to function as an entire polymer-based catalyst. The reaction was carried out overnight using CMP-B-BT$_3$ and a white LED lamp. The product 1-(nitromethyl)-2-phenyl-1,2,3,4-tetrahydroisoquinoline was obtained with a yield of 57%. This experiment confirmed the photocatalytic activity of CMP-B-BT$_3$. Due to the limited time period of the thesis, further screening experiments are planned as following up future plan.

4.3.3. Conclusion

The results within this series showed that CMP-B-BT$_3$ is the most efficient photocatalyst. Although the HOMO/LUMO levels and the resulting band gaps of the three CMPs did not differ tremendously, the building block BT containing sulfur appeared as the most promising building block to generate long-living electron-hole pairs under visible light irradiation according to the EPR experiments. This should be the main factor for the photocatalytic efficiency.

Compared to the CMPs reported in the literature, CMP-B-BT$_3$ and CMP-B-BO$_3$ gave better yields within much shorter reaction times. The proposed mechanism was proven indirectly by various control experiments.

The Aza-Henry reaction using CMP-B-BT$_3$ gave a promising outlook on the scope of this new class of conjugated porous polymer based photocatalysts.

4.4. Geometrical influences

A CMP with an A_4+B_2 geometry was synthesized via the stoichiometric method (Scheme 4.6). The synthetic and morphological properties are shown in Table 4.15.
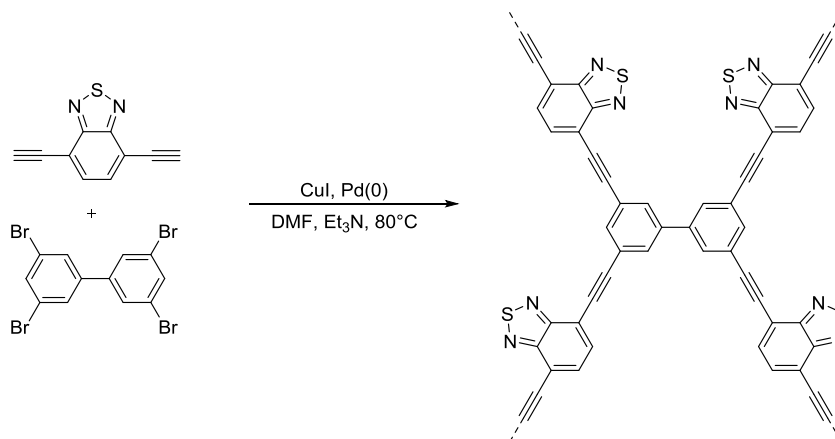
Scheme 4.6 Reaction scheme for the synthesis of CMP-BP-BT$_4$.

Table 4.15 Synthetic and morphological properties of the synthesized CMPs.

CMPs	Yield [%]	Surface area S_{BET} [m²/g]	Pore size [nm]	Pore volume [cm³/g]
CMP-BP-BT$_4$	31	50	1.5	0.120

The low yield of 31% also results from the poor solubility of the diazole compound in DMF. The corresponding nitrogen sorption isotherm and pore size distribution is shown in Figure 4.56 and Figure 4.57.
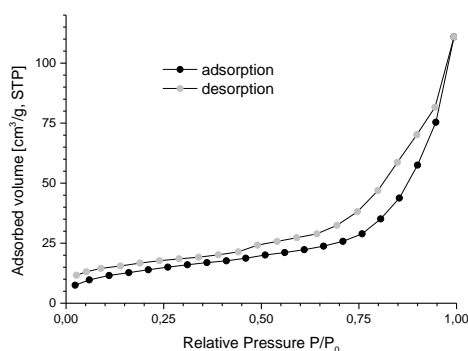
Figure 4.56 Adsorptionisotherm of CMP-BP-BT$_4$.
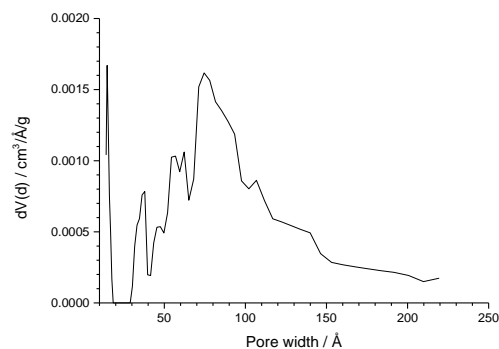
Figure 4.57 Pore size distribution of CMP-BP-BT$_4$.

CMP-BP-BT$_4$ shows type II behavior with a small hysteresis, which could be caused by a slightly mesoporosity. The pore size distribution of the material only showed a low amount of micropores, and BET surface was rather low with 50 m² g^{-1}.

SEM images showed a porous morphology. Similar to the A_3+B_2 type CMPs, CMP-BP-BT$_4$ appeared as fused particles (Figure 4.58).
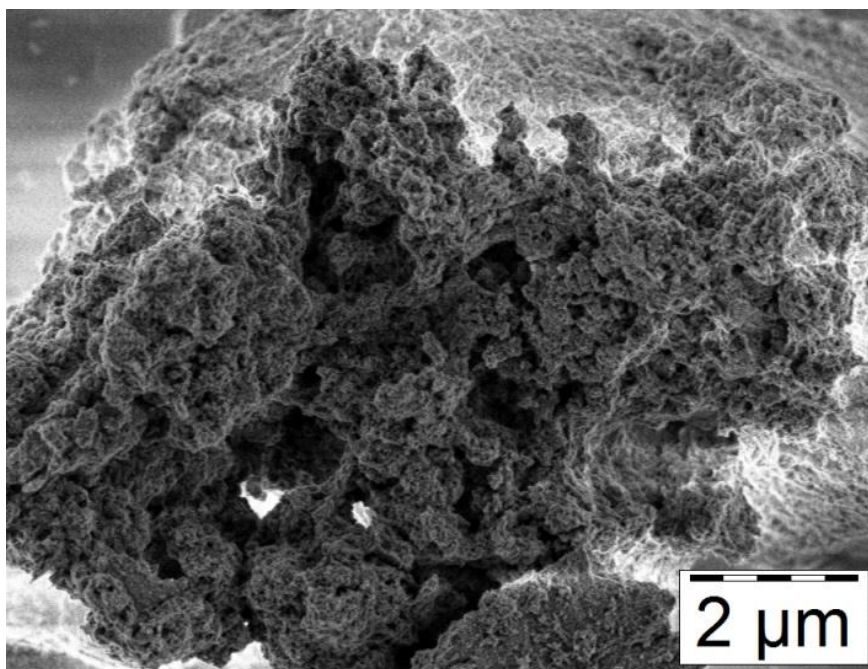
Figure 4.58 SEM image of CMP-BP-BT$_4$.

As shown in the TGA curve (Figure 4.59) the CMP is stable until 250 °C, with the thermal stability being slightly lower than the A_3+B_2 type polymer mentioned before.
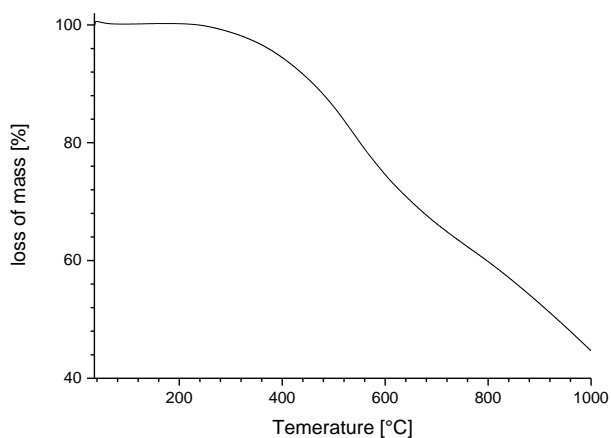
Figure 4.59 TGA curve of CMP-BP-BT$_4$.

The FT-IR spectrum also shows the typical vibration of internal alkyne bonds at 2250 cm^{-1} (Figure 4.60). The signal of terminal triple bonds at 3300 cm^{-1} is nearly overlaid by a broad signal at 3500 cm^{-1}. This signal could be caused by residual water in the structure.
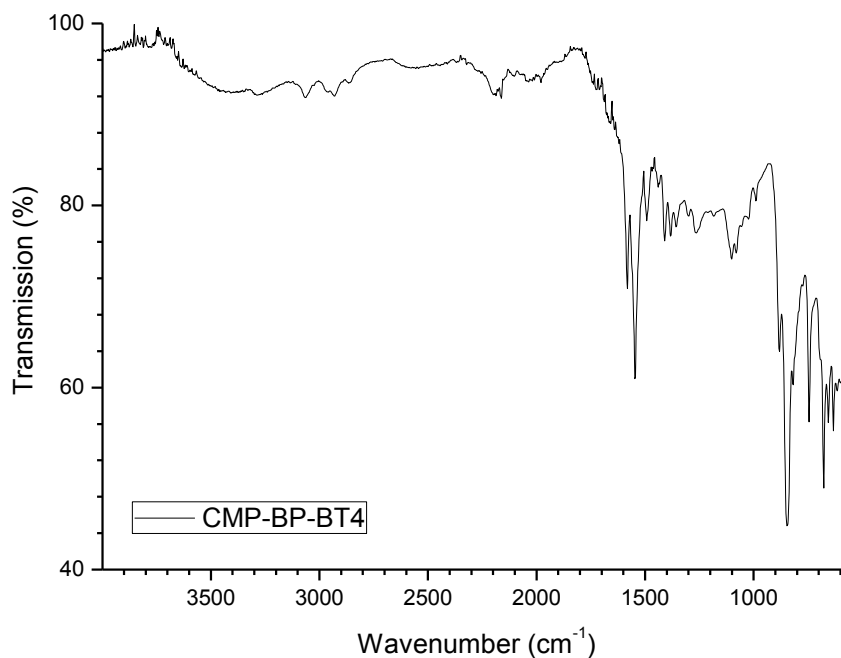
Figure 4.60 FT-IR spectrum of CMP-BP-BT$_4$.

The UV/Vis DRS absorption spectrum is shown in Figure 4.61. The calculated band gap from the absorption edge is 1.36 eV. This is the lowest optical BG of all the CMPs synthesized in this work. That is probably a result of the high acceptor content, and therefore a highly lowered LUMO level of the conjugated system.
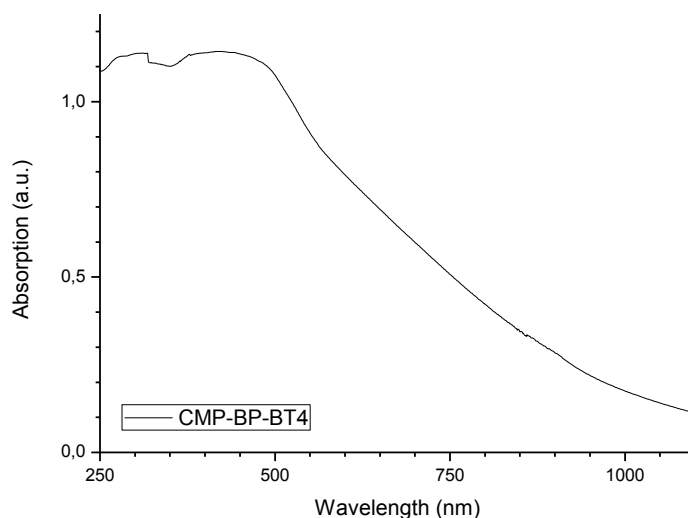
Figure 4.61 UV/Vis DRS spectrum of CMP-BP-BT$_4$.

CMP-BP-BT$_4$ was also utilized as a photocatalyst for the photo-fluorination reaction and yielded the mono fluorinated product in a yield of 19% by using the table lamp. The exact reaction conditions are shown in Table 4.16.

Table 4.16 Photo-fluorination catalyzed by CMP-BP-BT$_4$.

Catalyst	Light source	CMP concentration	Solvent amount	Substrate amount	Inert gas	Yield
CMP-BP-BT$_4$	Table lamp	1 mg mL^{-1}	3 mL	100 mg	N$_2$	19%

Reaction conditions: 1 eq ethylbenzene, 1.5 eq Selectfluor and 1 eq fluorobenzene as internal standard, 72 h irradiation time. All yields were determined via ^{19}F-NMR against the internal standard.

Due to the limited time for this thesis, no further studies on this CMP were conducted. The positive result for the fluorination shows that this geometry is a possible photocatalyst for C-H activation. Further detailed studies should be performed.

5. Conclusion and Outlook

In this work, synthesis and characterization of new conjugated microporous polymers (CMPs) are described. Different synthetic methods are developed in order to control the porosity of the CMPs. Furthermore, the photocatalytic activity of the CMPs is tested. A special emphasis is paid to the influence of the energetic levels and the HOMO/LUMO band gap of the CMPs, in order to gain the insights of the design principle for a high photocatalytic efficiency.

At first, a series of CMPs with an A_2+B_3 geometry was synthesized via stoichiometric, empiric and successive method. The best results regarding high surface area and porosity were achieved by using the successive synthetic method. The empiric method also yielded CMPs with high microporous content, while the CMPs obtained by the stoichiometric method showed the lowest porosity.

The photocatalytic free radical polymerization of MMA using the CMPs as visible light photoinitiator showed that the catalytic efficiency was not influenced by the surface area of the CMPs, but rather by the donor-acceptor combination of the polymer backbone, i.e. the ratio of acceptor units. With a higher acceptor content, the CMPs observed a high catalytic activity. Better conversions were obtained than with the homogeneous catalytic counterpart 9H-fluorenone.

Fluorenone-based CMPs were successfully used for the direct fluorination reaction of ethylbenzene via C-H activation. Further studies are needed to ensure repeatability of the photocatalysis.

To study the design principle for the CMPs with high photocatalytic activity, the influence of the energetic levels and the HOMO/LUMO band gaps of the CMPs on the catalytic reactions were investigated by incorporating a series of chalcogene-containing acceptor units, i.e. benzooxa- (BO), benzothia- (BT) and benzoselenadiazole (BS) comonomers into the backbone of the CMPs. The three CMPs were used for the photo-oxidation of benzylamines. The sulfur containing polymer CMP-B-BT$_3$ was found to be the most efficient catalyst. EPR measurements implied that CMP-B-BT$_3$ generates the highest amount of stable radicals under visible light irradiation, while CMP-B-BO$_3$ could generate less and CMP-B-BS$_3$ produced nearly no stable radicals upon light irradiation. The reaction mechanism was examined by various control experiments. It was shown, that both CMP and light were mandatory to achieve a successful reaction. The HOMO levels of the CMPs were determined to be energetically higher than the oxidation potentials of benzylamines tested, which should not lead to an oxidation. The fact that

the catalytic reaction was still carried out could be probably explained by the so-called singly occupied molecular orbital (SOMO) theory, according to which the HOMO level of the CMPs could be shifted to energetically lower position than the oxidation potential of the benzylamines, so that the oxidation reaction occurred. Further studies are considered in the future.

6. Experimental Section

6.1. Instruments and methods

For TGA measurements the temperature was raised from 35 °C to 1000 °C with a rate of 10°C/min under nitrogen atmosphere.

All SEM images were recorded with a LEO Gemini 1530 (Carl Zeiss AG, Germany) using an in lens SE detector.

The FT-IR spectra were measured with a Varian 1000 FT-IR spectrometer.

Liquid state NMR spectra were obtained with a Bruker AVANCE 250, 300 or 500 spectrometer, while ss-NMR measurements were obtained at 300 MHz Larmor frequency equipped with a standard 4mm magic angle spinning (MAS) double resonance probe head using a Bruker Avance II solid state NMR spectrometer.

Nitrogen sorption data was recorded at 77.3 K on an Autosorb 1 (Quantachrome Instruments) and exploited with the QuadraWin software from Quantachrome Instruments. The BET surface areas were calculated using the data points from $0 < P/P_0 < 0.25$ and the nonlinear density functional theory (NLDFT) equilibrium model for the BET model fitting while the pore size distributions were determined with Quenched Solid Density Functional Theory (QSDFT, N_2, assuming carbon adsorbent with slit pores) using the adsorption branches of the isotherms.

For the UV/Vis DRS adsorption spectra a Perkin Elmer Lambda 100 spectrophotometer was used.

Electron paramagnetic resonance (EPR) was conducted on a Magnettech Miniscope MS200 spectrometer.

Cyclic voltammetry experiments were conducted on an Autolab Potentiostat PGSTAT204 (metronohm). To create measurable CMP films the CMP was mixed and grinded with Nafion, few drops of the mixture were dropped on top of a glassy carbon working electrode and the solvents were evaporated in a vacuum oven for at least 30 min. For determination of the HOMO and LUMO levels always the second cycle of a measurement was taken. The measurements were carried out in a 0.1 molar solution of tetrabutylammonium phosphate in acetonitrile. A Pt-counter electrode and a SCE reference electrode were used.

For photocatalytic experiments three different light sources were used. If it is referred to white LED, blue LED or table lamp in this work, the following data applies:

- White LED: white LED light source (1.2 W cm^{-2}) (OSA Opto Lights)

- Blue LED: single wavelength blue LED light source (4.5 W cm^{-2}, 460 nm) (OSA Opto Lights)

- Table lamp: 23 W household energy saving fluorescent light bulb (Osram)

If not further stated all chemicals were used without further purification.

6.2. CMP synthesis via Sonogashira coupling
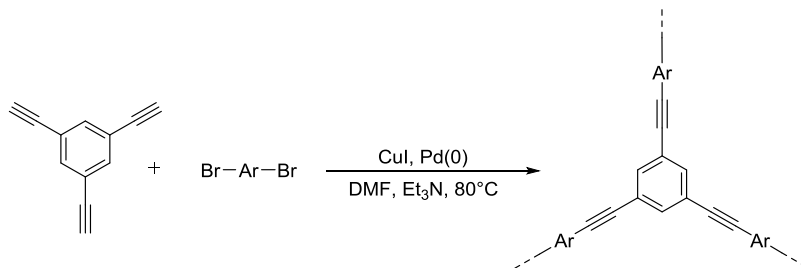
Scheme 6.1 Synthesis of CMPs with a 1,3,5-geometry via Sonogashira coupling.

General procedure:

The Monomer (1 or 1.5 eq), the cross-linker (triethynylbenzene) (1 eq), copper(I)iodide (0.03 eq), tetrakis(triphenylphosphine)palladium(0) (0.03 eq) were dissolved in 10 mL DMF and the solution was degassed for 5 min. 10 mL dry triethylamine were added and the reaction mixture was heated at 80 °C overnight under nitrogen atmosphere. After cooling, methanol was added and the precipitated powder was filtered and washed with water. The crude product was washed in a Soxhlet-Extractor with methanol and DCM for 24 h. The final product was obtained after drying for at least 24 h at RT in air.

For the successive monomer addition 1.5 eq of the monomer was added to the reaction mixture over 3 d in three 0.5 eq portions.

For CMP-BP-BT$_4$ the stoichiometric ratio used was 1:2 of cross-linker:monomer. The general procedure stayed the same.

6.3. Polymerization of MMA
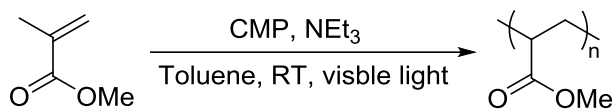
Scheme 6.2 Reaction scheme of the Polymerization of MMA with CMPs.

6.3.1. Screening experiments

General procedure:

  25 mg CMP, 1 mL MMA and 30 mg triethylamine were mixed together in clear vial. The vial was sealed with a septum and the solution was sparged with nitrogen for 5 min. It was irradiated with the table lamp overnight. THF was added to dissolve the formed polymer. The synthesized PMMA was precipitated in methanol after filtration with a syringe filter (Teflon, pore size: 0.45 µm).

6.3.2. Kinetic experiments

General procedure:

  To remove the stabilizer, MMA was purified through a small column of aluminum oxide. 6 mg (1 mg/mL) CMP-B-FN$_3$ or CMP-B-BP$_{1.5}$-FN$_{1.5}$ (Su), 2.8 g MMA (3 mL, 28.1 mmol), 90 mg triethylamine (0.888 mmol) and 3 mL toluene were mixed together in a Schlenk flask. The flask was sealed with a septum and the solution was sparged with nitrogen for 5 min. It was irradiated with the table lamp. Samples were taken after different times and it was checked for the conversion via ^{1}H-NMR of the crude reaction mixture.

6.4. Fluorination
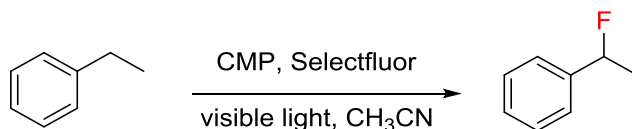
Scheme 6.3 Reaction scheme for the CMP catalyzed fluorination of ethylbenzene.

First screening experiments:

  1 eq (50 or 100 mg) ethylbenzene, 1 mg/mL CMP-B-FN$_3$, 2 or 1.5 eq Selectfluor and 1 eq fluorobenzene (as internal standard) were dissolved in 5 mL acetonitrile in a clear vial and the vial was sealed. The solution was sparged with nitrogen for 5 min. The mixture was irradiated

with the table lamp for at least 1 d. The crude yield was determined via ^{19}F-NMR spectroscopy. Variations of the catalysts and amounts are given in Table 6.1.

In experiment #1 acetonitrile-d3 was used. In experiment #4 and #5 the acetonitrile was dried over molecular sieves 4A prior to use.

Table 6.1 Variation of reaction conditions for screening experiments.

#	Catalyst	CMP concentration	Substrate amount	Selectfluor equivalents	Yield
1	CMP-B-FN$_3$	1 mg/mL	100 mg	2	1%
2a	CMP-B-FN$_3$	1 mg/mL	100 mg	1.5	-
2b	CMP-B-FN$_3$	1 mg/mL	100 mg	1.5	-
3[a]	9H-Fluorenone	-	50 mg	1.5	-
4[a,b]	9H-Fluorenone	-	50 mg	1.5	49%
5[b]	CMP-B-FN$_3$	1 mg/mL	100 mg	1.5	-

Reaction conditions: 1 eq ethylbenzene, 1.5 or 2 eq Selectfluor and 1 eq fluorobenzene as internal standard. Irradiation over 1 d with the table lamp. All yields were determined via ^{19}F-NMR against the internal standard. [a]0.05 eq of 9H-fluorenone as catalyst, no CMP was used. [b]Dried acetonitrile was used.

General procedure:

1 eq (50 or 100 mg) ethylbenzene, CMP-B-FN$_3$, 1.5 eq Selectfluor and 1 eq fluorobenzene (as internal standard) were mixed together in a clear vial and the vial was set under inert gas atmosphere. Dried acetonitrile was added as solvent via syringe. The mixture was stirred under irradiation for at least 3 d. A sample of the crude mixture was taken and the CMP was filtered of through a syringe filter (Teflon, pore size: 0.45 µm). The crude yield was determined via ^{19}F-NMR spectroscopy.

The variation of reaction conditions is shown in Table 6.2

Table 6.2 Variation of reaction conditions.

#	Catalyst	Light source	CMP concentration	Solvent amount	Substrate amount	Inert gas	Yield
1a	CMP-B-FN$_3$	Blue LED	1 mg mL^{-1}	3 mL	100 mg	N$_2$	39%
1b	CMP-B-FN$_3$	Blue LED	1 mg mL^{-1}	3 mL	50 mg	N$_2$	-
2	CMP-BP-BT$_4$	Table lamp	1 mg mL^{-1}	3 mL	100 mg	N$_2$	19%
3	CMP-B-FN$_3$	White LED	1 mg mL^{-1}	3 mL	50 mg	N$_2$	-
4	CMP-B-FN$_3$	White LED	1 mg mL^{-1}	3 mL	50 mg	Ar	-
5	CMP-B-FN$_3$	White LED	3 mg mL^{-1}	3 mL	50 mg	Ar	-
6	CMP-B-FN$_3$	White LED	5 mg mL^{-1}	3 mL	50 mg	Ar	-
7	CMP-B-FN$_3$	Blue LED	1 mg mL^{-1}	10 mL	50 mg	Ar	18%
8	CMP-B-FN$_3$	White LED	1 mg mL^{-1}	10 mL	50 mg	Ar	-

Further reaction conditions: 1 eq ethylbenzene, 1.5 eq Selectfluor and 1 eq fluorobenzene as internal standard. Irradiation over 3 d at least. All yields were determined via ^{19}F-NMR against the internal standard. ^{a}0.05 eq of 9H-fluorenone as catalyst, no CMP was used.

6.5. Aza-Henry reaction

6.5.1. Synthesis of 2-phenyl-1,2,3,4-tetrahydroisoquinoline
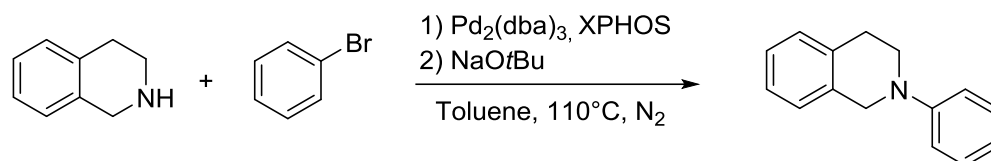
Scheme 6.4 Synthesis of 2-phenyl-1,2,3,4-tetrahydroisoquinoline.

Reaction conditions:

A two-necked round bottom flask equipped with a stir bar was dried in the vacuum oven. It was set under N$_2$ atmosphere. After cooling down 115 mg (0.2 mmol) Pd$_2$(dba)$_3$ and 249 mg (0.4 mmol) Xphos were filled in the flask and were dissolved in 15 mL of dry toluene. It was heated to 110 °C for 30 min while stirring. After cooling down 912 mg (9.5 mmol) NaO*t*Bu, 781 mg (5.0 mmol) bromobenzene and 1330 mg (10 mmol) 1,2,3,4-tetrahydroisoquinoline were added. The reaction mixture was refluxed overnight. After cooling down the reaction mixture was filtered through silica and the silica was washed with DCM. The solvent was evaporated and the crude product was purified via column chromatography (hexane/EtOAc: 9/1).

<u>Yield</u>: 750 mg (3.6 mmol, 72%)
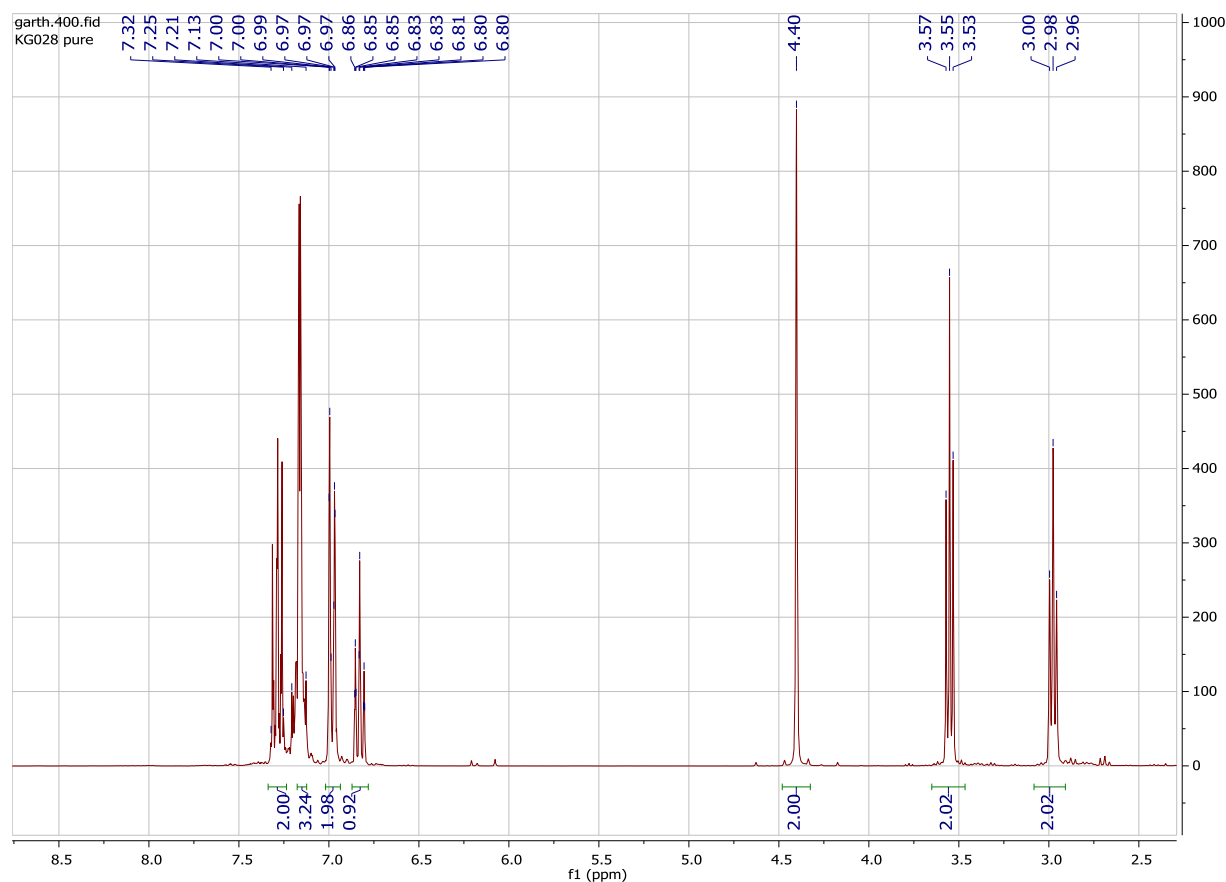
Figure 6.1 ^{1}H-NMR spectrum of the purified product 2-phenyl-1,2,3,4-tetrahydroisoquinoline

6.5.2. Synthesis of 1-(nitromethyl)-2-phenyl-1,2,3,4-tetrahydroisoquinoline
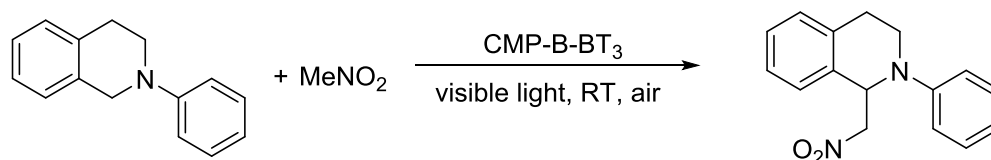
Scheme 6.5 Synthesis of 1-(nitromethyl)-2-phenyl-1,2,3,4-tetrahydroisoquinoline.

<u>Reaction conditions</u>:

Nitromethane was dried over molecular sieves 4A. 105 mg (0.5 mmol) 2-phenyl-1,2,3,4-tetrahydroisoquinoline, 2 mg of CMP-B-BT$_3$ and 2 mL nitromethane were mixed together in a clear vial and the vial was sealed. The reaction was exposed to air through a needle. The mixture was irradiated with the white LED for 21 h 30 min. The mixture was extracted with DCM and

water. It was filtrated and the solvent was evaporated. The yield was checked via ^{1}H-NMR of the crude mixture.

Yield: 57%

6.6. Photo-oxidation of benzylamines (C-N linkage)

Scheme 6.6 Photo-oxidation of benzylamine catalyzed by CMPs.

General procedure:

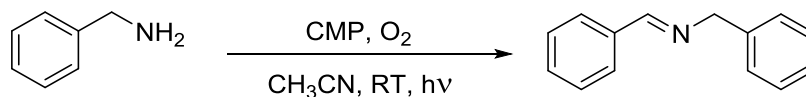Benzylamine (1 mmol), the CMP (1 mg/mL) and 3 mL acetonitrile were mixed together in a clear vial. The vial was set under O_2-atmosphere and it was sealed. It was equipped with an O_2-baloon. The reaction mixture was stirred and irradiated with the blue LED lamp for 3 h. To determine the conversion a ^{1}H-NMR of the crude mixture was taken after the CMP was filtered off.

An example spectrum of the crude mixture of the photo-oxidation of benzylamine with CMP-B-BT$_3$ as catalyst can be seen in Figure 6.2.
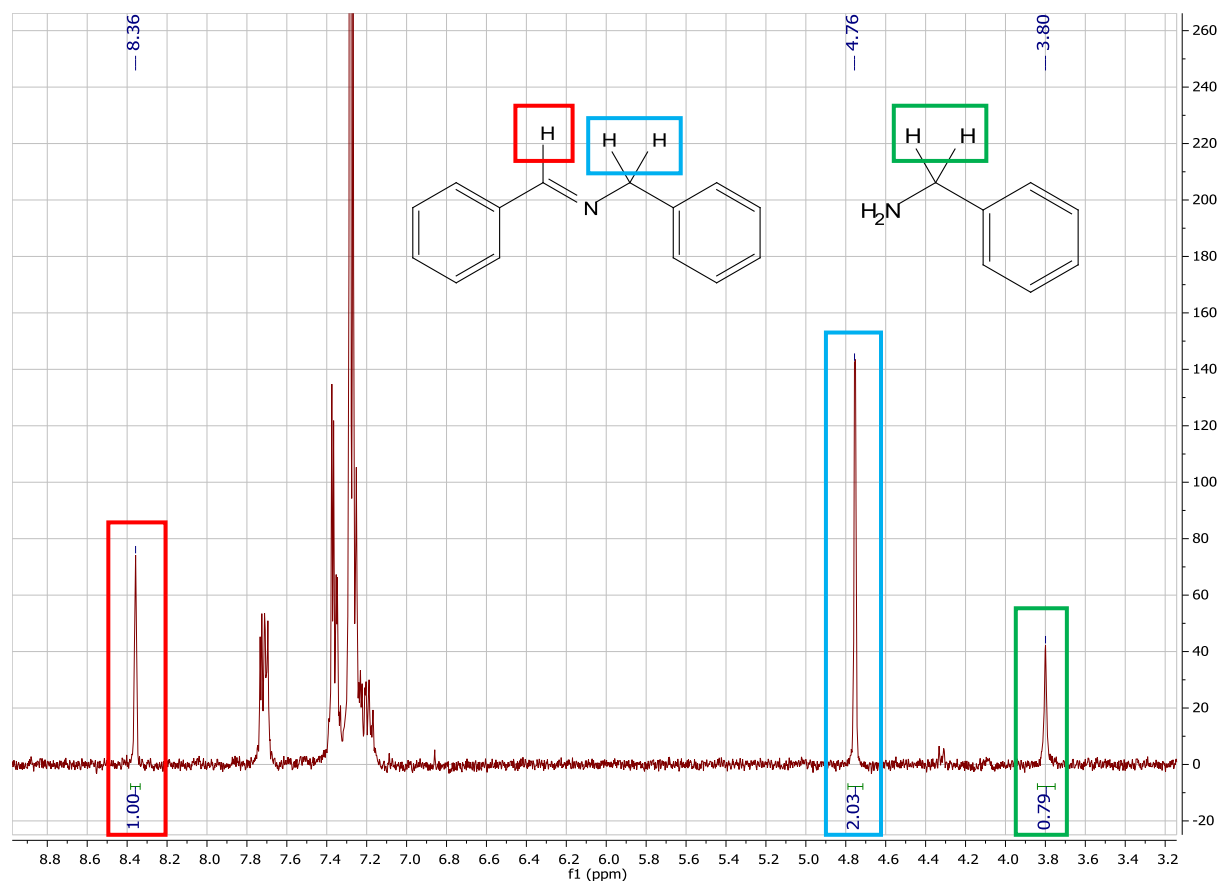
Figure 6.2 ^{1}H-NMR spectrum of the crude reaction mixture of the photo-oxidation of benzylamine with CMP-B-BT$_3$ as catalys. Red highlight: internal standard peak. Blue highlight: product peak. Green highlight: starting compound peak.

Control experiments:

Control experiments were conducted under the same conditions as the general procedure but the reaction time was extended to 24 h. For sample Blank[a] no CMP was added, the vial of sample Blank[b] was wrapped in aluminum foil and for sample Blank[c] 3 mg of CMP-B-BP$_3$ were used instead of CMP-B-BT$_3$.

Conversion vs. time plot:

The conversion versus time measurement was conducted under the same conditions as the general procedure. A ^{1}H-NMR sample was taken via syringe after 10, 20, 30 and 60 min and then after every 20 min up to 240 min.

<u>Light on-off graph</u>:

   For recording the conversion versus time plot with irradiation being switched off the same reaction conditions as in the general procedure were used. The blue LED was turned off after 1 h and the sample was wrapped in aluminum foil for the next hour. A ^{1}H-NMR spectrum was taken after every irradiated and darkened phase.

7. Appendix

Figure 7.1 Cyclic voltammogram of benzylamine.
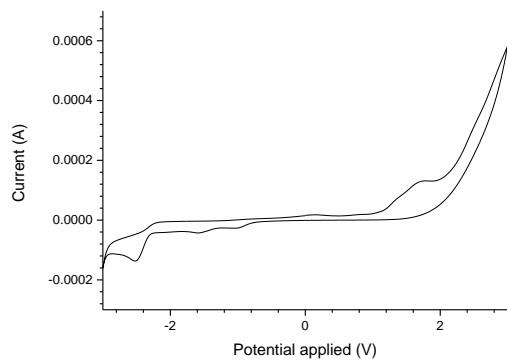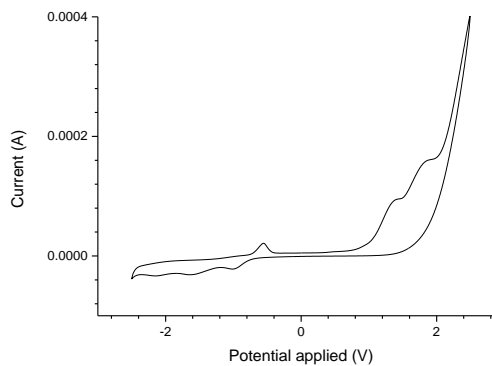

Figure 7.2 Cyclic voltammogram of 4-fluorobenzylamine.
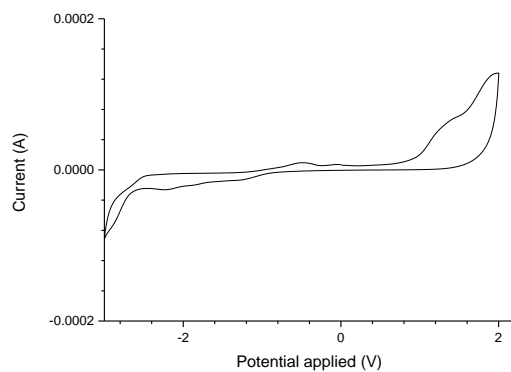

Figure 7.3 Cyclic voltammogram of 4-methoxybenzylamine.
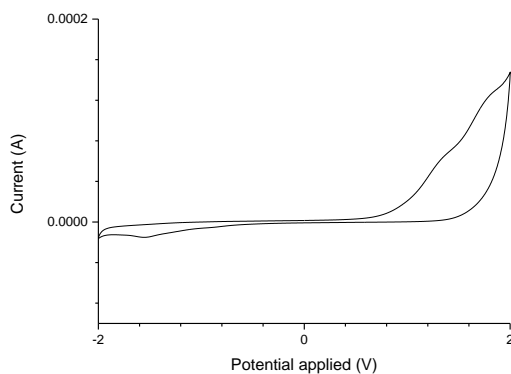

Figure 7.4 Cyclic voltammogram of 4-chlorobenzylamine.
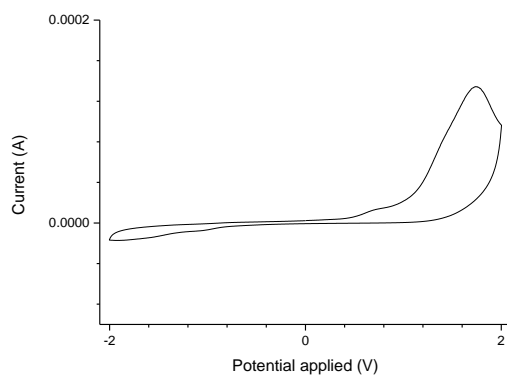

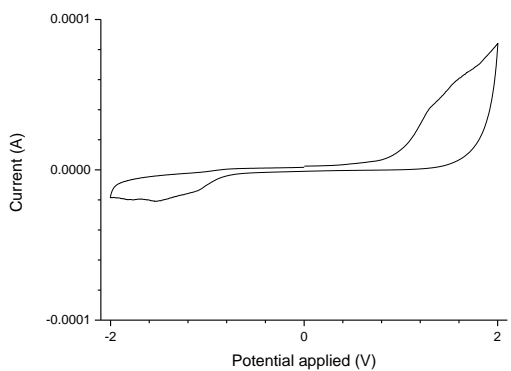**Figure 7.5 Cyclic voltammogram of 2,4-dimethoxybenzylamine.**

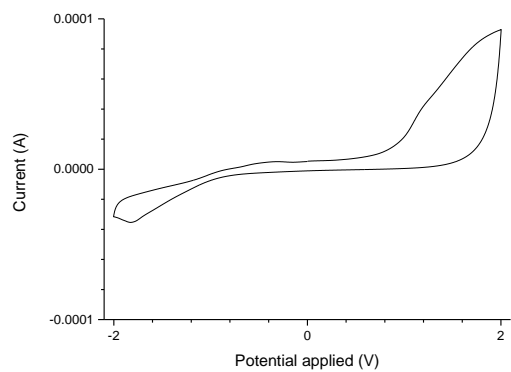**Figure 7.6 Cyclic voltammogram of 4-methylbenzylamine.**

Figure 7.7 Cyclic voltammogram of 2-thiophenemethylamine.

8. Bibliography

[1]: Gust, D.; Moore, T. A. *Science (Washington, D. C., 1883-)* **1989**, *244*, 35.

[2]: Gust, D.; Moore, T. A.; Moore, A. L. *Acc. Chem. Res.* **1993**, *26*, 198.

[3]: Meyer, T. J. *Acc. Chem. Res.* **1989**, *22*, 163.

[4]: Hoffmann, N. *Chem. Rev. (Washington, DC, U. S.)* **2008**, *108*, 1052.

[5]: Fagnoni, M.; Dondi, D.; Ravelli, D.; Albini, A. *Chem. Rev. (Washington, DC, U. S.)* **2007**, *107*, 2725.

[6]: Ravelli, D.; Fagnoni, M.; Albini, A. *Chem. Soc. Rev.* **2013**, *42*, 97.

[7]: Narayanam, J. M. R.; Stephenson, C. R. J. *Chem. Soc. Rev.* **2011**, *40*, 102.

[8]: Gambarotti, C.; Melone, L.; Punta, C.; InTech: 2012, p 79.

[9]: Inagaki, A.; Akita, M. *Coord. Chem. Rev.* **2010**, *254*, 1220.

[10]: Moriya, Y.; Takata, T.; Domen, K. *Coord. Chem. Rev.* **2013**, *257*, 1957.

[11]: Juris, A.; Balzani, V.; Barigelletti, F.; Campagna, S.; Belser, P.; Von Zelewsky, A. *Coord. Chem. Rev.* **1988**, *84*, 85.

[12]: Kalyanasundaram, K. *Coord. Chem. Rev.* **1982**, *46*, 159.

[13]: Chen, Z.; Dong, X.; Lin, W. *Gongye Cuihua* **2009**, *17*, 1.

[14]: Liu, H.; Feng, W.; Kee, C. W.; Zhao, Y.; Leow, D.; Pan, Y.; Tan, C.-H. *Green Chem.* **2010**, *12*, 953.

[15]: Marin, M. L.; Santos-Juanes, L.; Arques, A.; Amat, A. M.; Miranda, M. A. *Chem. Rev. (Washington, DC, U. S.)* **2012**, *112*, 1710.

[16]: Neumann, M.; Fueldner, S.; Koenig, B.; Zeitler, K. *Angew. Chem., Int. Ed.* **2011**, *50*, 951.

[17]: Nicewicz, D. A.; Nguyen, T. M. *ACS Catalysis* **2014**, *4*, 355.

[18]: Teoh, W. Y.; Scott, J. A.; Amal, R. *J. Phys. Chem. Lett.* **2012**, *3*, 629.

[19]: Cooper, A. I. *Adv. Mater.* **2009**, *21*, 1291.

[20]: Dawson, R.; Cooper, A. I.; Adams, D. J. *Prog. Polym. Sci.* **2012**, *37*, 530.

[21]: Kaur, P.; Hupp, J. T.; Nguyen, S. T. *ACS Catal.* **2011**, *1*, 819.

[22]: Liu, Q.; Tang, Z.; Wu, M.; Zhou, Z. *Polym. Int.* **2014**, *63*, 381.

[23]: McKeown, N. B.; Budd, P. M. *Macromolecules (Washington, DC, U. S.)* **2010**, *43*, 5163.

[24]: Thomas, A. *Angew. Chem., Int. Ed.* **2010**, *49*, 8328.

[25]: Xu, Y.; Jin, S.; Xu, H.; Nagai, A.; Jiang, D. *Chem. Soc. Rev.* **2013**, *42*, 8012.

[26]: Wang, Z. J.; Landfester, K.; Zhang, K. *Polymer Chemistry* **2014**, *5*, 3559.

[27]: Xia, J. B.; Zhu, C.; Chen, C. *J. Am. Chem. Soc.* **2013**, *135*, 17494.

[28]: Jiang, J.-X.; Li, Y.; Wu, X.; Xiao, J.; Adams, D. J.; Cooper, A. I. *Macromolecules* **2013**, *46*, 8779.

[29]: Kang, N.; Park, J. H.; Ko, K. C.; Chun, J.; Kim, E.; Shin, H. W.; Lee, S. M.; Kim, H. J.; Ahn, T. K.; Lee, J. Y.; Son, S. U. *Angew. Chem. Int. Ed. Engl.* **2013**, *52*, 6228.

[30]: Sing, K. S. W.; Everett, D. H.; Haul, R. A. W.; Moscou, L.; Pierotti, R. A.; Rouquerol, J.; Siemieniewska, T. *Pure Appl. Chem.* **1985**, *57*, 603.

[31]: Dawson, R.; Adams, D. J.; Cooper, A. I. *Chem. Sci.* **2011**, *2*, 1173.

[32]: Garberoglio, G. *Langmuir* **2007**, *23*, 12154.

[33]: Ghanem, B. S.; Msayib, K. J.; McKeown, N. B.; Harris, K. D. M.; Pan, Z.; Budd, P. M.; Butler, A.; Selbie, J.; Book, D.; Walton, A. *Chem. Commun. (Cambridge, U. K.)* **2007**, 67.

[34]: Jiang, S.; Bacsa, J.; Wu, X.; Jones, J. T. A.; Dawson, R.; Trewin, A.; Adams, D. J.; Cooper, A. I. *Chem. Commun. (Cambridge, U. K.)* **2011**, *47*, 8919.

[35]: Jin, Y.; Voss, B. A.; Noble, R. D.; Zhang, W. *Angew. Chem., Int. Ed.* **2010**, *49*, 6348.

[36]: Lee, J.-Y.; Wood, C. D.; Bradshaw, D.; Rosseinsky, M. J.; Cooper, A. I. *Chem. Commun. (Cambridge, U. K.)* **2006**, 2670.

[37]: Makhseed, S.; Samuel, J. *Chem. Commun. (Cambridge, U. K.)* **2008**, 4342.

[38]: Mason, J. A.; Sumida, K.; Herm, Z. R.; Krishna, R.; Long, J. R. *Energy Environ. Sci.* **2011**, *4*, 3030.

[39]: Rao, K. V.; Mohapatra, S.; Kulkarni, C.; Maji, T. K.; George, S. J. *J. Mater. Chem.* **2011**, *21*, 12958.

[40]: Torrisi, A.; Bell, R. G.; Mellot-Draznieks, C. *Cryst. Growth Des.* **2010**, *10*, 2839.

[41]: Xu, C.; Hedin, N. *J. Mater. Chem. A* **2013**, *1*, 3406.

[42]: Budd, P. M.; Butler, A.; Selbie, J.; Mahmood, K.; McKeown, N. B.; Ghanem, B.; Msayib, K.; Book, D.; Walton, A. *Phys. Chem. Chem. Phys.* **2007**, *9*, 1802.

[43]: Celzard, A.; Albiniak, A.; Jasienko-Halat, M.; Mareche, J. F.; Furdin, G. *Carbon* **2005**, *43*, 1990.

[44]: Collins, D. J.; Zhou, H.-C. *J. Mater. Chem.* **2007**, *17*, 3154.

[45]: Dinca, M.; Long, J. R. *Angew. Chem., Int. Ed.* **2008**, *47*, 6766.

[46]: Murray, L. J.; Dinca, M.; Long, J. R. *Chem. Soc. Rev.* **2009**, *38*, 1294.

[47]: Xiao, B.; Yuan, Q. *Particuology* **2009**, *7*, 129.

[48]: Germain, J.; Frechet, J. M. J.; Svec, F. *Small* **2009**, *5*, 1098.

[49]: Furukawa, H.; Yaghi, O. M. *J. Am. Chem. Soc.* **2009**, *131*, 8875.

[50]: Germain, J.; Frechet, J. M. J.; Svec, F. *J. Mater. Chem.* **2007**, *17*, 4989.

[51]: Germain, J.; Svec, F.; Frechet, J. M. J. *Chem. Mater.* **2008**, *20*, 7069.

[52]: Han, S. S.; Furukawa, H.; Yaghi, O. M.; Goddard, W. A., III *J. Am. Chem. Soc.* **2008**, *130*, 11580.

[53]: Hirscher, M.; Panella, B.; Schmitz, B. *Microporous Mesoporous Mater.* **2009**, *129*, 335.

[54]: Klontzas, E.; Tylianakis, E.; Froudakis, G. E. *J. Phys. Chem. C* **2008**, *112*, 9095.

[55]: Li, A.; Lu, R.-F.; Wang, Y.; Wang, X.; Han, K.-L.; Deng, W.-Q. *Angew. Chem., Int. Ed.* **2010**, *49*, 3330.

[56]: Liu, X.; Li, H.; Zhang, Y.; Xu, B.; A, S.; Xia, H.; Mu, Y. *Polym. Chem.* **2013**, *4*, 2445.

[57]: Ma, S.; Sun, D.; Simmons, J. M.; Collier, C. D.; Yuan, D.; Zhou, H.-C. *J. Am. Chem. Soc.* **2008**, *130*, 1012.

[58]: McKeown, N. B.; Budd, P. M.; Book, D. *Macromol. Rapid Commun.* **2007**, *28*, 995.

[59]: Morris, R. E.; Wheatley, P. S. *Angew. Chem., Int. Ed.* **2008**, *47*, 4966.

[60]: Rosi, N. L.; Eckert, J.; Eddaoudi, M.; Vodak, D. T.; Kim, J.; O'Keeffe, M.; Yaghi, O. M. *Science (Washington, DC, U. S.)* **2003**, *300*, 1127.

[61]: Wood, C. D.; Tan, B.; Trewin, A.; Niu, H.; Bradshaw, D.; Rosseinsky, M. J.; Khimyak, Y. Z.; Campbell, N. L.; Kirk, R.; Stoeckel, E.; Cooper, A. I. *Chem. Mater.* **2007**, *19*, 2034.

[62]: Wood, C. D.; Tan, B.; Trewin, A.; Su, F.; Rosseinsky, M. J.; Bradshaw, D.; Sun, Y.; Zhou, L.; Cooper, A. I. *Adv. Mater. (Weinheim, Ger.)* **2008**, *20*, 1916.

[63]: Xiang, Z.; Cao, D.; Wang, W.; Yang, W.; Han, B.; Lu, J. *J. Phys. Chem. C* **2012**, *116*, 5974.

[64]: Yuan, S.; Dorney, B.; White, D.; Kirklin, S.; Zapol, P.; Yu, L.; Liu, D.-J. *Chem. Commun. (Cambridge, U. K.)* **2010**, *46*, 4547.

[65]: Yuan, S.; Kirklin, S.; Dorney, B.; Liu, D.-J.; Yu, L. *Macromolecules (Washington, DC, U. S.)* **2009**, *42*, 1554.

[66]: Cho, H. C.; Lee, H. S.; Chun, J.; Lee, S. M.; Kim, H. J.; Son, S. U. *Chem. Commun. (Cambridge, U. K.)* **2011**, *47*, 917.

[67]: Du, X.; Sun, Y.; Tan, B.; Teng, Q.; Yao, X.; Su, C.; Wang, W. *Chem. Commun. (Cambridge, U. K.)* **2010**, *46*, 970.

[68]: Schmidt, J.; Weber, J.; Epping, J. D.; Antonietti, M.; Thomas, A. *Adv. Mater. (Weinheim, Ger.)* **2009**, *21*, 702.

[69]: Bronstein, L. M.; Goerigk, G.; Kostylev, M.; Pink, M.; Khotina, I. A.; Valetsky, P. M.; Matveeva, V. G.; Sulman, E. M.; Sulman, M. G.; Bykov, A. V.; Lakina, N. V.; Spontak, R. J. *J. Phys. Chem. B* **2004**, *108*, 18234.

[70]: Roeser, J.; Kailasam, K.; Thomas, A. *ChemSusChem* **2012**, *5*, 1793.

[71]: Xu, H.; Chen, X.; Gao, J.; Lin, J.; Addicoat, M.; Irle, S.; Jiang, D. *Chem. Commun. (Cambridge, U. K.)* **2014**, *50*, 1292.

[72]: Kiskan, B.; Antonietti, M.; Weber, J. *Macromolecules (Washington, DC, U. S.)* **2012**, *45*, 1356.

[73]: Chan-Thaw, C. E.; Villa, A.; Katekomol, P.; Su, D.; Thomas, A.; Prati, L. *Nano Lett.* **2010**, *10*, 537.

[74]: Chen, L.; Yang, Y.; Guo, Z.-Q.; Jiang, D.-L. *Adv. Mater. (Weinheim, Ger.)* **2011**, *23*, 3149.

[75]: Chen, L.; Honsho, Y.; Seki, S.; Jiang, D. *J. Am. Chem. Soc.* **2010**, *132*, 6742.

[76]: Zhang, Y.; Zhang, Y.; Sun, Y. L.; Du, X.; Shi, J. Y.; Wang, W. D.; Wang, W. *Chem. - Eur. J.* **2012**, *18*, 6328.

[77]: Czaja, A. U.; Trukhan, N.; Muller, U. *Chem. Soc. Rev.* **2009**, *38*, 1284.

[78]: Eddaoudi, M.; Moler, D. B.; Li, H.; Chen, B.; Reineke, T. M.; O'Keeffe, M.; Yaghi, O. M. *Acc. Chem. Res.* **2001**, *34*, 319.

[79]: Yaghi, O. M.; Li, H.; Davis, C.; Richardson, D.; Groy, T. L. *Acc. Chem. Res.* **1998**, *31*, 474.

[80]: Cote, A. P.; Benin, A. I.; Ockwig, N. W.; O'Keeffe, M.; Matzger, A. J.; Yaghi, O. M. *Science (Washington, DC, U. S.)* **2005**, *310*, 1166.

[81]: El-Kaderi, H. M.; Hunt, J. R.; Mendoza-Cortes, J. L.; Cote, A. P.; Taylor, R. E.; O'Keeffe, M.; Yaghi, O. M. *Science (Washington, DC, U. S.)* **2007**, *316*, 268.

[82]: Urban, C.; McCord, E. F.; Webster, O. W.; Abrams, L.; Long, H. W.; Gaede, H.; Tang, P.; Pines, A. *Chem. Mater.* **1995**, *7*, 1325.

[83]: Webster, O. W.; Gentry, F. P.; Farlee, R. D.; Smart, B. E. *Polym. Prepr. (Am. Chem. Soc., Div. Polym. Chem.)* **1991**, *32*, 412.

[84]: Davankov, V. A.; Tsyurupa, M. P. *React. Polym.* **1990**, *13*, 27.

[85]: Budd, P. M.; Ghanem, B. S.; Makhseed, S.; McKeown, N. B.; Msayib, K. J.; Tattershall, C. E. *Chem. Commun. (Cambridge, U. K.)* **2004**, 230.

[86]: Budd, P. M.; McKeown, N. B.; Fritsch, D. *J. Mater. Chem.* **2005**, *15*, 1977.

[87]: Cheng, G.; Bonillo, B.; Sprick, R. S.; Adams, D. J.; Hasell, T.; Cooper, A. I. *Adv. Funct. Mater.* **2014**, *24*, 5219.

[88]: McKeown, N. B.; Budd, P. M. *Chem. Soc. Rev.* **2006**, *35*, 675.

[89]: McKeown, N. B.; Hanif, S.; Msayib, K.; Tattershall, C. E.; Budd, P. M. *Chem. Commun. (Cambridge, U. K.)* **2002**, 2782.

[90]: McKeown, N. B.; Makhseed, S.; Budd, P. M. *Chem. Commun. (Cambridge, U. K.)* **2002**, 2780.

[91]: Cheng, G.; Hasell, T.; Trewin, A.; Adams, D. J.; Cooper, A. I. *Angew. Chem., Int. Ed.* **2012**, *51*, 12727.

[92]: Dawson, R.; Laybourn, A.; Clowes, R.; Khimyak, Y. Z.; Adams, D. J.; Cooper, A. I. *Macromolecules (Washington, DC, U. S.)* **2009**, *42*, 8809.

[93]: Weder, C. *Angew. Chem., Int. Ed.* **2008**, *47*, 448.

[94]: Sun, D.; Ye, L.; Li, Z. *Appl. Catal., B* **2015**, *164*, 428.

[95]: Jiang, J.-X.; Wang, C.; Laybourn, A.; Hasell, T.; Clowes, R.; Khimyak, Y. Z.; Xiao, J.; Higgins, S. J.; Adams, D. J.; Cooper, A. I. *Angew. Chem., Int. Ed.* **2011**, *50*, 1072.

[96]: Kaye, S. S.; Dailly, A.; Yaghi, O. M.; Long, J. R. *J. Am. Chem. Soc.* **2007**, *129*, 14176.

[97]: Pachfule, P.; Kandambeth, S.; Diaz Diaz, D.; Banerjee, R. *Chem. Commun. (Cambridge, U. K.)* **2014**, *50*, 3169.

[98]: Xu, H.; Jiang, D.; American Chemical Society: 2014, p PMSE.

[99]: Xu, H.; Nagai, A.; Jiang, D. *PMSE Prepr.* **2013**, No pp. given.

[100]: Zhang, W.; Jiang, P.; Wang, Y.; Zhang, J.; Gao, Y.; Zhang, P. *RSC Adv.* **2014**, *4*, 51544.

[101]: Rose, M.; Palkovits, R. *RSC Catal. Ser.* **2013**, *12*, 384.

[102]: Budd, P. M.; Elabas, E. S.; Ghanem, B. S.; Makhseed, S.; McKeown, N. B.; Msayib, K. J.; Tattershall, C. E.; Wang, D. *Adv. Mater. (Weinheim, Ger.)* **2004**, *16*, 456.

[103]: Ritter, N.; Senkovska, I.; Kaskel, S.; Weber, J. *Macromolecules (Washington, DC, U. S.)* **2011**, *44*, 2025.

[104]: Chen, Q.; Wang, J.-X.; Yang, F.; Zhou, D.; Bian, N.; Zhang, X.-J.; Yan, C.-G.; Han, B.-H. *J. Mater. Chem.* **2011**, *21*, 13554.

[105]: Zhang, K.; Tieke, B.; Vilela, F.; Skabara, P. J. *Macromol. Rapid Commun.* **2011**, *32*, 825.

[106]: Chen, L.; Yang, Y.; Jiang, D. *J. Am. Chem. Soc.* **2010**, *132*, 9138.

[107]: Rao, K. V.; Mohapatra, S.; Maji, T. K.; George, S. J. *Chem. - Eur. J.* **2012**, *18*, 4505.

[108]: Zhang, P.; Weng, Z.; Guo, J.; Wang, C. *Chem. Mater.* **2011**, *23*, 5243.

[109]: Jiang, J.-X.; Trewin, A.; Adams, D. J.; Cooper, A. I. *Chem. Sci.* **2011**, *2*, 1777.

[110]: Xu, Y.-H.; Chen, L.; Guo, Z.-Q.; Nagai, A.; Jiang, D.-L. *J. Am. Chem. Soc.* **2011**, *133*, 17622.

[111]: Yuan, D.; Lu, W.; Zhao, D.; Zhou, H.-C. *Adv. Mater. (Weinheim, Ger.)* **2011**, *23*, 3723.

[112]: Liu, X.; Xu, Y.; Jiang, D. *J. Am. Chem. Soc.* **2012**, *134*, 8738.

[113]: Xiang, Z.; Cao, D. *Macromol. Rapid Commun.* **2012**, *33*, 1184.

[114]: Trewin, A.; Cooper, A. I. *Angew. Chem., Int. Ed.* **2010**, *49*, 1533.

[115]: Liu, X.; Xu, Y.; Guo, Z.; Nagai, A.; Jiang, D. *Chem. Commun. (Cambridge, U. K.)* **2013**, *49*, 3233.

[116]: Wang, X.-S.; Liu, J.; Bonefont, J. M.; Yuan, D.-Q.; Thallapally, P. K.; Ma, S. *Chem. Commun. (Cambridge, U. K.)* **2013**, *49*, 1533.

[117]: Laybourn, A.; Dawson, R.; Clowes, R.; Hasell, T.; Cooper, A. I.; Khimyak, Y. Z.; Adams, D. J. *Polymer Chemistry* **2014**.

[118]: Tan, D.; Fan, W.; Xiong, W.; Sun, H.; Cheng, Y.; Liu, X.; Meng, C.; Li, A.; Deng, W.-Q. *Macromol. Chem. Phys.* **2012**, *213*, 1435.

[119]: Jiang, J.-X.; Su, F.; Trewin, A.; Wood, C. D.; Niu, H.; Jones, J. T. A.; Khimyak, Y. Z.; Cooper, A. I. *J. Am. Chem. Soc.* **2008**, *130*, 7710.

[120]: Jiang, J.-X.; Su, F.; Wood, C. D.; Campbell, N. L.; Niu, H.; Dickinson, C.; Ganin, A. Y.; Rosseinsky, M. J.; Khimyak, Y. Z.; Cooper, A. I.; Trewin, A. *Angew. Chem., Int. Ed.* **2007**, *46*, 8574.

[121]: Stoeckel, E.; Wu, X.; Trewin, A.; Wood, C. D.; Clowes, R.; Campbell, N. L.; Jones, J. T. A.; Khimyak, Y. Z.; Adams, D. J.; Cooper, A. I. *Chem. Commun. (Cambridge, U. K.)* **2009**, 212.

[122]: Choi, J. H.; Choi, K. M.; Jeon, H. J.; Choi, Y. J.; Lee, Y.; Kang, J. K. *Macromolecules (Washington, DC, U. S.)* **2010**, *43*, 5508.

[123]: Chinchilla, R.; Najera, C. *Chem. Rev. (Washington, DC, U. S.)* **2007**, *107*, 874.

[124]: Jiang, J.-X.; Su, F.; Niu, H.; Wood, C. D.; Campbell, N. L.; Khimyak, Y. Z.; Cooper, A. I. *Chem. Commun. (Cambridge, U. K.)* **2008**, 486.

[125]: Li, A.; Sun, H.-X.; Tan, D.-Z.; Fan, W.-J.; Wen, S.-H.; Qing, X.-J.; Li, G.-X.; Li, S.-Y.; Deng, W.-Q. *Energy Environ. Sci.* **2011**, *4*, 2062.

[126]: Gu, C.; Huang, N.; Gao, J.; Xu, F.; Xu, Y.; Jiang, D. *Angew. Chem. Int. Ed. Engl.* **2014**, *53*, 4850.

[127]: Suresh, V. M.; Bonakala, S.; Roy, S.; Balasubramanian, S.; Maji, T. K. *J. Phys. Chem. C* **2014**, *118*, 24369.

[128]: Ren, S.; Dawson, R.; Laybourn, A.; Jiang, J.-x.; Khimyak, Y.; Adams, D. J.; Cooper, A. I. *Polym. Chem.* **2012**, *3*, 928.

[129]: Ma, L.; Wanderley, M. M.; Lin, W. *ACS Catal.* **2011**, *1*, 691.

[130]: Palkovits, R.; Antonietti, M.; Kuhn, P.; Thomas, A.; Schueth, F. *Angew. Chem., Int. Ed.* **2009**, *48*, 6909.

[131]: Urakami, H.; Zhang, K.; Vilela, F. *Chem. Commun. (Cambridge, U. K.)* **2013**, *49*, 2353.

[132]: Wang, Z. J.; Ghasimi, S.; Landfester, K.; Zhang, K. A. *Chem. Commun. (Camb.)* **2014**, *50*, 8177.

[133]: Wang, Z. J.; Ghasimi, S.; Landfester, K.; Zhang, K. A. I. *J. Mater. Chem. A* **2014**, *2*, 18720.

[134]: Xie, Z.; Wang, C.; de Krafft, K. E.; Lin, W. *J. Am. Chem. Soc.* **2011**, *133*, 2056.

[135]: Zhang, K.; Kopetzki, D.; Seeberger, P. H.; Antonietti, M.; Vilela, F. *Angew. Chem., Int. Ed.* **2013**, *52*, 1432.

[136]: Piok, T.; Gamerith, S.; Gadermaier, C.; Plank, H.; Wenzl, F. P.; Patil, S.; Montenegro, R.; Kietzke, T.; Neher, D.; Scherf, U.; Landfester, K.; List, E. J. W. *Adv. Mater. (Weinheim, Ger.)* **2003**, *15*, 800.

[137]: Vohra, V.; Giovanella, U.; Tubino, R.; Murata, H.; Botta, C. *ACS Nano* **2011**, *5*, 5572.

[138]: Heeger, A. J. *Rev. Mod. Phys.* **2001**, *73*, 681.

[139]: Yu, G.; Gao, J.; Hummelen, J. C.; Wudl, F.; Heeger, A. J. *Science (Washington, D. C.)* **1995**, *270*, 1789.

[140]: Stutzmann, N.; Friend, R. H.; Sirringhaus, H. *Science (Washington, DC, U. S.)* **2003**, *299*, 1881.

[141]: Deng, S.; Zhi, J.; Zhang, X.; Wu, Q.; Ding, Y.; Hu, A. *Angew. Chem. Int. Ed. Engl.* **2014**, *53*, 14144.

[142]: Mendez, J. D.; Schroeter, M.; Weder, C. *Macromol. Chem. Phys.* **2007**, *208*, 1625.

[143]: Jiang, J.-X.; Trewin, A.; Su, F.; Wood, C. D.; Niu, H.; Jones, J. T. A.; Khimyak, Y. Z.; Cooper, A. I. *Macromolecules (Washington, DC, U. S.)* **2009**, *42*, 2658.

[144]: Dawson, R.; Laybourn, A.; Khimyak, Y. Z.; Adams, D. J.; Cooper, A. I. *Macromolecules (Washington, DC, U. S.)* **2010**, *43*, 8524.

[145]: Ben, T.; Ren, H.; Ma, S.; Cao, D.; Lan, J.; Jing, X.; Wang, W.; Xu, J.; Deng, F.; Simmons, J. M.; Qiu, S.; Zhu, G. *Angew. Chem., Int. Ed.* **2009**, *48*, 9457.

[146]: Müllen, K.; Reynolds, J. R.; Masuda, T. *Conjugated Polymers*; RSC: Cambridge, UK, 2014.

[147]: Sonogashira, K.; Tohda, Y.; Hagihara, N. *Tetrahedron Lett.* **1975**, 4467.

[148]: Thorand, S.; Krause, N. *J. Org. Chem.* **1998**, *63*, 8551.

[149]: Xiao, P.; Hong, W.; Li, Y.; Dumur, F.; Graff, B.; Fouassier, J. P.; Gigmes, D.; Lalevée, J. *Polymer* **2014**, *55*, 746.

[150]: Yagci, Y.; Yilmaz, F.; Kiralp, S.; Toppare, L. *Macromol. Chem. Phys.* **2005**, *206*, 1178.

[151]: Xiao, P.; Dumur, F.; Thirion, D.; Fagour, S.; Vacher, A.; Sallenave, X.; Morlet-Savary, F.; Graff, B.; Fouassier, J. P.; Gigmes, D.; Lalevée, J. *Macromolecules* **2013**, *46*, 6786.

[152]: Havinga, E. E.; ten Hoeve, W.; Wynberg, H. *Synth. Met.* **1993**, *55*, 299.

[153]: Brunauer, S.; Emmett, P. H.; Teller, E. *J. Am. Chem. Soc.* **1938**, *60*, 309.

[154]: Landers, J.; Gor, G. Y.; Neimark, A. V. *Colloids Surf., A* **2013**, *437*, 3.

[155]: Sonar, P.; Williams, E. L.; Singh, S. P.; Manzhos, S.; Dodabalapur, A. *Phys. Chem. Chem. Phys.* **2013**, *15*, 17064.

[156]: Kiskan, B.; Zhang, J.; Wang, X.; Antonietti, M.; Yagci, Y. *ACS Macro Lett.* **2012**, *1*, 546.

[157]: Liu, W.; Huang, X.; Cheng, M.-J.; Nielsen, R. J.; Goddard, W. A., III; Groves, J. T. *Science (Washington, DC, U. S.)* **2012**, *337*, 1322.

[158]: Braun, M.-G.; Doyle, A. G. *J. Am. Chem. Soc.* **2013**, *135*, 12990.

[159]: Halperin, S. D.; Fan, H.; Chang, S.; Martin, R. E.; Britton, R. *Angew. Chem., Int. Ed.* **2014**, *53*, 4690.

[160]: Berridge, R.; Skabara, P. J.; Pozo-Gonzalo, C.; Kanibolotsky, A.; Lohr, J.; McDouall, J. J. W.; McInnes, E. J. L.; Wolowska, J.; Winder, C.; Sariciftci, N. S.; Harrington, R. W.; Clegg, W. *J. Phys. Chem. B* **2006**, *110*, 3140.

[161]: Zheng, Z.; Chen, C.; Bo, A.; Zavahir, F. S.; Waclawik, E. R.; Zhao, J.; Yang, D.; Zhu, H. *ChemCatChem* **2014**, *6*, 1210.

[162]: Ye, L.; Li, Z. *ChemCatChem* **2014**, *6*, 2540.

[163]: Yang, X.-J.; Chen, B.; Li, X.-B.; Zheng, L.-Q.; Wu, L.-Z.; Tung, C.-H. *Chem. Commun. (Cambridge, U. K.)* **2014**, *50*, 6664.

[164]: Rueping, M.; Vila, C.; Szadkowaska, A.; Koenigs, R. M.; Fronert, J. *ACS Catal.* **2012**, *2*, 2810.

[165]: Huang, L.; Zhao, J.; Guo, S.; Zhang, C.; Ma, J. *J. Org. Chem.* **2013**, *78*, 5627.

[166]: Berlicka, A.; Konig, B. *Photochem Photobiol Sci* **2010**, *9*, 1359.

[167]: Ohkubo, K.; Nanjo, T.; Fukuzumi, S. *Bull. Chem. Soc. Jpn.* **2006**, *79*, 1489.

[168]: Nicolas, C.; Herse, C.; Lacour, J. *Tetrahedron Lett.* **2005**, *46*, 4605.